Photocatalytic Oxidation of Emerging Pollutants by Nano TiO_2

By

Kireesan Sornalingam

A thesis submitted in partial fulfilment of the requirements for the degree of Doctor of Philosophy

School of Civil and Environmental Engineering

Faculty of Engineering and Information Technology

University of Technology Sydney

Australia

2018

Certificate of authorship

I certify that the work in this thesis has not previously been submitted for a degree nor has it been submitted as part of requirements for a degree except as fully acknowledged within the text.

I also certify that the thesis has been written by me. Any help that I have received in my research work and the preparation of the thesis itself has been acknowledged. In addition, I certify that all information sources and literature used are indicated in the thesis.

Signature of Student:

Production Note:
Signature removed prior to publication.

…….....

05/04/2018

Acknowledgements

First and foremost, I would like to express my sincere gratitude to my supervisors Assoc. Prof. Andrew McDonagh and Prof. John Zhou for their support and guidance throughout my candidature. I would like to thank Dr. Md Johir for his immense technical support and valuable advice in conducting experiments. Special thanks to Prof. John Canning and Dr. Kevin Cook for their excellent support for optical fibre related experiments.

My sincerest thanks to Mr. Alexander Angeloski, Dr. Verena Taudte, Ms. Katie McBean and Mr. Mark Berkahn for their assistance in material characterisation and chemical analysis. I would like to convey my gratitude to Prof. Saravanamuth Vigneswaran, Assoc. Prof. Ho Kyong Shon and Ms. Phyllis Agius for their guidance. I am thankful to Flow Systems for providing the wastewater required for the research experiments. I am grateful to Brinthapan and Thivakhar to whom I owe my life in Australia.

I would like to acknowledge the financial support received from the University of Technology and the faculty of engineering and information technology.

Last but not the least, I am indebted to my family and friends for their unconditional support.

Abbreviations

AOP: Advanced Oxidation Processes

BET: Brunauer, Emmet and Teller

C_o: Initial Concentration

CB: Conduction Band

COD: Chemical Oxygen Demand

DC: Direct Current

DP: Deposition-Precipitation

DO: Dissolved Oxygen

DOC: Dissolved Organic Carbon

DOM: Dissolved Organic Matter

E1: Estrone

E2: 17β-estradiol

E3: Estriol

EDC: Endocrine Disrupting Chemicals

EDS: Energy Dispersive X-ray Spectroscopy

EE2: 17α-ethynylestradiol

ESI: Electrospray Ionisation

e^-: electrons

HA: Humic Acid

HP: High Pressure

h^+: holes

I: Light Intensity

IC: Inorganic Carbon

ICP-MS: Inductively Coupled Plasma Mass Spectrometry

k: rate constant

LC-MS-QQQ: Liquid Chromatography - Mass Spectrometry - Triple Quadrupole

L-H: Langmuir-Hinshelwood

LP: Low Pressure

LSPR: Localised Surface Plasmon Resonance

MP: Medium Pressure

MPC: Midpolar Compounds

MP-AES: Microwave Plasma - Atomic Emission Spectroscopy

m/z: mass / charge

NPC: Nonpolar Compounds

PC: Polar Compounds

PPCPs: Pharmaceutical and Personal Care Products

PTFE: Polytetrafluoroethylene

PZC: Point of Zero Charge

QTOF-LC-MS: Quadrupole Time-Of-Flight Liquid Chromatography - Mass Spectrometry

r: reaction rate

RT: Retention Time

SEM: Scanning Electron Microscope

SIM: Selective Ion Monitoring

STP: Sewage Treatment Plant

SWW: Synthetic Wastewater

$t_{1/2}$: Half-life

TEM: Transmission Electron Microscope

TGA: Thermogravimetric analysis

TIC: Total Ion Chromatogram

TOC: Total Organic Carbon

UHPLC: Ultra-High Performance Liquid Chromatography

UPW: Ultrapure Water

UV: Ultra Violet

VB: Valence Band

WW: Waste Water effluent from membrane bio-reactor

XRD: X-ray Diffraction

YES: Yeast Estrogen Screen

λ: Wavelength

Table of contents

List of figures

List of tables

Publications and conference presentations

Publications included in this work

Sornalingam K, McDonagh A, Zhou JL. Photodegradation of estrogenic endocrine disrupting steroidal hormones in aqueous systems: Progress and future challenges. Sci. Total Environ. 2016; 550: 209-224.

Sornalingam K, McDonagh A, Zhou JL, Johir MAH, Ahmed MB. Photocatalysis of estrone in water and wastewater: Comparison between Au-TiO_2 nanocomposite and TiO_2, and degradation by-products. Sci. Total Environ. 2018; 610: 521-530.

Other publications

Ahmed MB, Johir MAH, Zhou JL, Ngo HH, Guo W, Sornalingam K. Photolytic and photocatalytic degradation of organic UV filters in contaminated water. Curr. Opin. Green. Sus. Chem. 2017a; 6: 85-92.

Ahmed MB, Zhou JL, Ngo HH, Guo W, Johir MA, Sornalingam K*, et al.* Nano-Fe^0 immobilized onto functionalized biochar gaining excellent stability during sorption and reduction of chloramphenicol via transforming to reusable magnetic composite. Chem. Eng. J. 2017b; 322: 571-581.

Ahmed MB, Zhou JL, Ngo HH, Guo W, Johir MAH, Sornalingam K. Single and competitive sorption properties and mechanism of functionalized biochar for removing sulfonamide antibiotics from water. Chem. Eng. J. 2017c; 311: 348-358.

Ahmed MB, Zhou JL, Ngo HH, Guo W, Johir MAH, Sornalingam K*, et al.* Chloramphenicol interaction with functionalized biochar in water: sorptive

mechanism, molecular imprinting effect and repeatable application. Sci. Total Environ. 2017d; 609: 885-895.

Ahmed MB, Zhou JL, Ngo HH, Johir MAH, Sornalingam K. Sorptive removal of phenolic endocrine disruptors by functionalized biochar: Competitive interaction mechanism, removal efficacy and application in wastewater. Chem. Eng. J. 2018; 335: 801-811.

Conference presentations

Sornalingam K, McDonagh A, Zhou JL. UVA and visible light photocatalysis of 17β-estradiol in different water matrices by Au-TiO_2 catalysts and the identification of degradation by-products. The International Conference on Water, Informatics, Sustainability and Environment, 3-5 July 2017, Ottawa, Canada.

Sornalingam K, McDonagh A, Zhou JL. Photocatalytic Oxidation of emerging pollutants by nano TiO_2. CEE Research Showcase 2017, UTS, Sydney, Australia, 28 August, 2017.

Sornalingam K, Canning J, Cook K, McDonagh A, Zhou JL. Air-clad optical fibres for the photocatalytic degradation of emerging contaminants. The 3rd Australian New Zealand Conference on Optics (ANZCOP), 4-7 December 2017, Queenstown, New Zealand.

Abstract

Emerging contaminants pose health threats to flora and fauna even at trace level concentrations. Among these pollutants, estrogenic steroidal hormones such as estrone (E1), 17β-estradiol (E2), estriol (E3) and 17α-ethynylestradiol (EE2) are known to cause endocrine disruption, especially in aquatic systems. The successful treatment of these chemicals in water requires advanced oxidation processes (AOPs) in addition to the conventional treatment methods. Photocatalysis by TiO_2 that utilises free radicals for the photodegradation of organic pollutants is an AOP that has attracted recent research interest.

TiO_2 photocatalysis face challenges such as its inability to degrade pollutants under visible light irradiation, the requirement for suitable immobilisation techniques for catalyst reuse and the need for appropriate methods to transmit light over long distances including under water. Each of the aforementioned shortcomings should be addressed for TiO_2 to be successfully applied.

This study focusses on addressing the challenges to effectively degrade estrogenic steroidal hormones using TiO_2 photocatalysis. Commercial Aeroxide P25 TiO_2 was modified with gold nanoparticles to achieve visible light photocatalytic activity. Au-TiO_2 photocatalysts were synthesised using deposition-precipitation (DP) method and characterised using thermogravimetric analysis (TGA), X-ray diffraction (XRD), Raman spectroscopy, UV-Vis spectroscopy, scanning electron microscopy (SEM), inductively coupled plasma mass spectrometer (ICP-MS), zeta potential and particle size analysis.

The performance of the new catalysts was compared to that of commercial P25 TiO_2 under different LED light sources: UVA, cool white and green. For the degradation of E1, E2, E3 and EE2, 0 – 8 *wt.*% gold loadings to P25 TiO_2 were studied, where 4 wt.% Au-TiO_2 was found to provide the fastest degradation rate of the pollutants. The catalysts' performance decreased for the light sources in the order, UVA > cool white > green light. Photocatalysis of E1 (1 mg l^{-1}) was found to follow pseudo 1st order kinetics. E1 degradation was significantly more efficient by using 4 *wt.%* Au-TiO_2 than P25 TiO_2 under UVA ($k = 0.28 \pm 0.01$ min^{-1} vs. 0.01 min^{-1}) and cool white light ($k = 2.44 \pm 0.36$ h^{-1} vs. 0.06 ± 0.01 h^{-1}). The photocatalytic activity under visible light decreased in the order: 4 *wt.%* Au-TiO_2 > 8 *wt.%* Au-TiO_2 > 2 *wt.%* Au-TiO_2 > 1 *wt.%* Au-TiO_2 > P25 TiO_2. The enhanced activity of the Au-TiO_2 catalysts was attributed to the gold nanoparticles acting as electron sinks to minimise electron-hole recombination under UVA and due to increased absorption of light in the 500-600 nm wavelength as a result of localised surface plasmon resonance (LSPR).

The stability of the catalysts for reuse is an important factor for consideration in photocatalysis. This was studied by reusing the catalysts over three cycles, for the photodegradation of E1. After three cycles of photocatalysis, the activity did not diminish by any significant amount (< 3%), showing the reusability of the photocatalysts. The detection and identification of photodegradation by products is important to understand the degradation mechanism of the pollutants. The photodegradation by-products of E1 were identified using QTOF-LC-MS and a possible degradation pathway was proposed. Four E1 by-products were identified, of which one was lumiestrone and the other three were hydroxylated forms of E1. In addition, the photoproducts were also degraded with further photocatalysis.

The constituents of water influence the rate of photodegradation of pollutants. The photocatalytic rate of E1 were studied using three different water matrices – ultrapure water (UPW), synthetic waste water (SWW) and wastewater effluent from membrane bio-reactor (WW). The photodegradation rate of E1 decreased for the water matrices in the order, UPW > SWW ≈ WW. This may be due to the negative effects of the constituents present in wastewater.

The recycling of photocatalysts is a major challenge faced by TiO_2 suspended catalysts, since the costs of separating the catalysts from the water is not economical. The immobilisation of the catalysts onto different substrates is considered as an alternative, in the expense of lost catalyst surface area. Here, the photocatalysts were coated onto glass beads using a simple dip coating technique followed by drying, calcination and washing with water to remove any loosely bonded catalysts. The immobilised catalysts proved to be capable of photodegrading EE2. The catalysts were easily reused by removing the glass beads, washing and drying them in furnace.

Transmitting light over long distances and underwater currently restricts the application of TiO_2 photocatalysis to the surface layer of water. This study addresses this limitation with: (i) a novel modified air-clad optical fibre and (ii) a flexible waterproof LED strip, reactor systems. The silica core of the air-clad fibres were capable of transmitting UVA and white light emission whilst the higher numerical aperture of the air-clad fibres compared to the conventional fibres enabled higher transmitted powers, effectively translating into significantly lower energy consumption. Efficient side emission of light from the optical fibres was obtained by collapsing the air-holes of an air-clad optical fibre using a fusion splicer. The optical fibre utilised photocatalytic reactor system efficiently removed the pollutants under

UVA, where 4 *wt.*% Au-TiO_2 showed enhanced activity compared to P25 TiO_2. The rate of photodegradation for both the catalysts was found to follow pseudo 1st order kinetics. EE2 $t_{1/2}$ under UVA were 1.26 h and 0.78 h, in the presence of P25 TiO_2 and the gold modified catalysts, respectively. The catalysts as well as the fibres were found to be stable for multiple reaction cycles with small loss of activity at the end of each cycle (6% decrease in degradation efficiency was noted after three cycles). A white light waterproof LED strip reactor showed good removal efficiency for the pollutant E3 in the presence of Au-TiO_2 photocatalysts, following pseudo 1st order kinetics with k = 0.13 h^{-1} and $t_{1/2}$ = 4.62 h. No degradation of the pollutants was observed in the absence of the catalysts (photolysis). There was no change in the E3 concentration after the initial adsorption under darkness in the presence of P25 TiO_2, since it is inactive under visible light. Thus, air-clad optical fibres and the flexible waterproof LED strips are promising modes of light transmittance for photocatalysis.

Chapter 1: Introduction

Chapter 1: Introduction

1.1 Research background

Endocrine disrupting chemicals (EDCs) are considered a threat to many living organisms. EDCs are exogenous chemicals that alter the functions of endogenous hormones to cause adverse effects, especially in reproductive health (Frontistis *et al.*, 2015; Roig *et al.*, 2013). EDCs can be present in the environment at trace concentrations but can still cause significant damage (Snyder *et al.*, 2003). Wastewater treatment plants remain the main mode through which EDCs reach the environment (Fredj *et al.*, 2015; Snyder *et al.*, 2003) and so aquatic life are particularly affected. EDCs consist of natural and synthetic hormones, pharmaceutical and personal care products (PPCPs), pesticides and some metals (Westerhoff *et al.*, 2005). EDCs are resistant to biodegradation, hence their complete removal by conventional water treatment facilities is difficult (Grover *et al.*, 2011; Johnson and Sumpter, 2001; Khanal *et al.*, 2006). Hence, the successful removal of EDCs from wastewater requires new biological, chemical and/or physical treatment techniques (Oller *et al.*, 2011).

1.1.1 Estrogenic steroidal hormones

Estrogenic steroidal hormones include E1, E2, E3 and EE2. The chemical structures of these hormones are depicted in Figure 1.1. They are known as major cause of endocrine activity in waterways (Onda *et al.*, 2003). The occurrence of these hormones in wastewater, ground water, surface water and in drinking water has been reported (D'Ascenzo *et al.*, 2003; Fine *et al.*, 2003; Klein, 2012; Wang *et al.*, 2008a). E1, E2 and E3 are naturally occurring (endogenous) estrogens, while EE2 is used as an active ingredient in oral contraceptive pills.

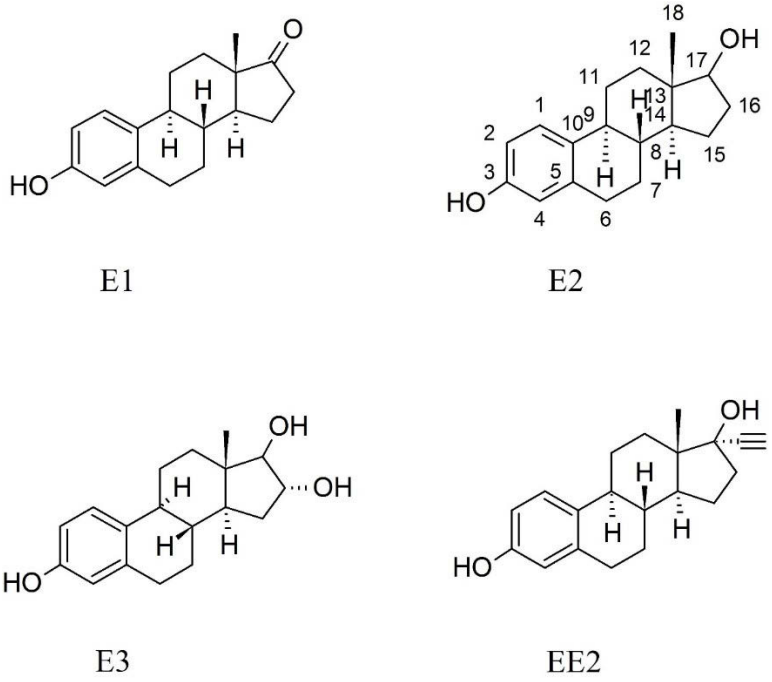

E1 E2

E3 EE2

Figure 1.1. Chemical structures of estrogenic steroidal hormones. The atomic numbering scheme is shown in the structure of E2.

1.1.2 Photodegradation

AOPs that degrade potent chemicals by free radical oxidation (Wang and Xu, 2012) have been implemented relatively recently. The main AOPs are photolysis, photocatalysis, ozonation (Qiang *et al.*, 2013), electrochemical oxidation (Murugananthan *et al.*, 2007), sonolysis (Suri *et al.*, 2007), ferrate (Jiang *et al.*, 2005) and fenton oxidation (Brienza *et al.*, 2014).

Photodegradation is a promising technology that uses light for the removal of EDCs and consists of photolysis where molecules undergo decomposition as a result of the absorption of light energy and photocatalysis which is the transformation of a compound by a catalyst that is activated by light energy (Macwan *et al.*, 2011). TiO_2, ZnO (Behnajady *et al.*, 2006; Subash *et al.*, 2013), WO_3 (Liu *et al.*, 2012b), ZnS

(Sharma *et al.*, 2012; Torres-Martínez *et al.*, 2001), SnO_2 (Wu *et al.*, 2009a; Zhang *et al.*, 2011a), $FeCl_3$ (Wang *et al.*, 2007), Fe_2O_3 (Niu *et al.*, 2010; Valenzuela *et al.*, 2002) and Bi_2WO_6 (Zhang and Zhu, 2012) are some of the commonly used photocatalysts.

TiO_2 is a particularly attractive photocatalyst due to its high activity, chemical and photo stability and commercial availability (Schneider *et al.*, 2014). The band gap energy of TiO_2 (3.2 eV for anatase) requires UV light for activation, which is only about 4% of the incident solar radiation (Dette *et al.*, 2014). Modification of TiO_2 to lower the band gap and enable visible light absorption are therefore attracting significant research interest.

1.1.3 Visible light photocatalysis

Noble metals (Ag, Au, Pt, Pd and Ru) can enhance the UV light activity of TiO_2 while introducing a notable visible light response (Yan *et al.*, 2013). Gold is favoured due to its non-toxicity, stability and biocompatibility (Ayati *et al.*, 2014). Though bulk gold has low activity, in nanoparticulate form gold absorbs visible light around 550 nm due to its localized surface plasmon resonance (LSPR) (Tanaka *et al.*, 2012). LSPR is the collective oscillations of the conduction electrons induced by electromagnetic irradiation (Wu *et al.*, 2008). Under UV irradiation, some electrons from the TiO_2 conduction band (CB) cross to gold nanoparticles on the TiO_2 surface; electron-hole recombination rates are reduced as a consequence (Chen *et al.*, 2012). Under visible light irradiation, electrons that gain sufficient energy to overcome the Schottky barrier can cross to the CB of TiO_2, hence leading to the visible light activity of the catalyst (Lin *et al.*, 2015b). In addition, some of the hot electrons in gold also move to the gold surface to form free radicals, which in turn degrade the pollutants (Lin *et al.*, 2015b).

Au-TiO_2 has been found to show photocatalytic activity for the production of H_2 (Priebe *et al.*, 2015), reduction of NO_X (Nguyen *et al.*, 2008), oxidation of CO (Li *et al.*, 2006) and for the removal of pollutants from water, for example, azo-dye degradation (Arabatzis *et al.*, 2003) and the removal of *p*-nitrophenol (Ismail *et al.*, 2012). A detailed review of the use of Au-TiO_2 for the removal of pollutants from water can be found elsewhere (Ayati *et al.*, 2014).

1.1.4 Immobilisation of photocatalysts

A significant issue with suspended photocatalyst particles is the difficulty of separating the catalyst from water once treatment is finished. Therefore, efficient catalyst immobilisation techniques are required if photocatalysis is to be applied in the commercial scale. Immobilisation of catalysts on different substrates such as glass (Liu *et al.*, 2012a), quartz (He *et al.*, 2016; Tanizaki *et al.*, 2002), ceramic (Zhao *et al.*, 2009a), alloy (Coleman *et al.*, 2000), inner wall of the reactor (Du *et al.*, 2008) or membranes (Dzinun *et al.*, 2015; Nakashima *et al.*, 2003; Zhao *et al.*, 2016) has been studied. Nevertheless, one of the major disadvantages of these methods is the inability of the light to penetrate throughout the reactor, restricting the placement of the catalysts to close to the surface of the water (Peill and Hoffmann, 1996).

1.1.5 Optical fibres for photocatalysis

Optical fibres allow light to be transmitted long distances with minimal loss, potentially making bench studies practical in real environments. Catalysts could either be immobilised onto the fibres (Lin *et al.*, 2015a; Lin *et al.*, 2017; Sun *et al.*, 2000) or the light emitted by the fibres could be cast to the catalysts coated on another surface (Denny *et al.*, 2009; Lin and Valsaraj, 2005). However, end emission from the fibres

is insufficient to activate large surface areas of the catalysts. A few studies have used side emitting optical fibres to address the aforementioned issues. On the other hand, most of the light in these fibres propagates in the forward direction, hence resulting in only a small portion of side emission, which may be insufficient for satisfactory photocatalytic activity. In addition, the light cannot be transmitted for long distances as a result of the loss due to side emission. Therefore, new techniques to attain selective side emission from optical fibres are required.

1.2 Research questions, objectives and scope

The major objective of this research is the development, characterisation and use of TiO_2 based visible light active photocatalysts (immobilised or in slurry form) for the abatement of the EDCs – E1, E2, E3 and EE2 under different light sources and water matrices and the identification of by-products.

In detail, the main research objectives of this study are to,

1. Synthesise Au-TiO_2 photocatalysts and examine their characteristics.
2. Develop detection techniques for EDCs using QTOF-LC-MS and LC-MS-QQQ.
3. Immobilise the photocatalysts onto glass beads and study their photocatalytic ability.
4. Measure the photocatalytic efficiency of the as prepared catalysts for the degradation of EDCs (e.g. E1, E2, E3 and EE2) under UVA, visible and green light.
5. Study the influence of different water matrices (UPW, SWW and WW) on the photodegradation of E1 and E2.

6. Identify the by-products of the pollutants and propose possible degradation pathways.
7. Modify air-clad optical fibres to achieve side emission of light and use the fibres to transmit light to underwater photocatalytic reactors for the abatement of EE2.
8. Utilise flexible waterproof white light LED strip for the successful light transmittance underwater enabling photocatalytic degradation of E3.

1.3 Overview of the thesis

To achieve the aforementioned objectives, the thesis is divided into seven chapters. A summary of these chapters is as follows:

Chapter 1 outlines the study, including a background of the research problem, the key objectives and the scope of this project.

Chapter 2 provides a comprehensive literature review describing the EDCs studied, the use of TiO_2 based visible light photocatalysts for the degradation of these EDCs, Au-TiO_2 photocatalyst synthesis techniques, the factors affecting photodegradation of estrogenic hormones and the formation of intermediates. Different catalyst immobilisation techniques as well as the use of optical fibres in photocatalysis are discussed.

Chapter 3 includes the chemicals and materials used in the experiments, the equipment used for photocatalyst characterisation, experimental setups utilised for photodegradation studies and the details of the techniques used to analyse the water matrices and the pollutants.

Chapter 4 describes the synthesis and characterisation of gold modified TiO_2 photocatalysts.

Chapter 5 investigates the use of P25 TiO_2 and Au-TiO_2 for the photocatalytic removal of E1 in different water matrices under UVA, cool white and green LEDs and elucidate possible degradation intermediates to propose possible degradation mechanism of E1.

Chapter 6 includes the use of modified air-clad optical fibres and flexible waterproof LED strips to enable underwater light transfer for the photocatalysis of E3 and EE2 in the presence of P25 TiO_2 and Au-TiO_2 photocatalysts.

Chapter 7 draws the major conclusions of this study and provides recommendations for future research.

Chapter 2: Literature Review

Chapter 2: Literature Review

This review provides an overview of TiO_2 based photocatalysts for the degradation of estrogenic hormones under different conditions together with an examination of the factors that influence the removal efficiency of the pollutants and the possible degradation mechanisms and pathways. Different methods of Au-TiO_2 preparation, immobilisation techniques and the use of optical fibres as a mode of light transfer for photocatalysis are discussed.

2.1 Introduction

The known EDCs, E1, E2, E3 and EE2 are major contributors of estrogenicity in aqueous systems (Onda *et al.*, 2003) and are the focus of this study. These hormones have similar chemical structures to each other (Figure 1.1) and are distinguished by their substitution at C16 and C17. E1, E2, and E3 have carbonyl or hydroxyl group substituents, while the synthetic EE2 contains an ethynyl substituent. The estrogens have low vapour pressures in the order of 9×10^{-13} to 3×10^{-8} Pa (Table 2.1) and have relatively low water solubility and are reasonably hydrophobic.

Table 2.1. Physicochemical properties of estrogenic endocrine disrupting steroidal hormones.

Compound	CAS number	Chemical Formula	MW (g mol^{-1})	Water solubility at 20 °C (mg l^{-1})	Vapour pressure (Pa)[c]	pK_a	log K_{ow}	log K_{oc}	Potency by YES assay[d]
E1	53-16-7	$C_{18}H_{22}O_2$	270.4	30[a]	$3x10^{-8}$	10.34±0.05	3.13-3.43[a]	3.1-3.5[a]	0.38
E2	50-28-2	$C_{18}H_{24}O_2$	272.4	13[a]	$3x10^{-8}$	10.46±0.03	2.69-4.0[a]	2.78-3.4[a]	1
E3	50-27-1	$C_{18}H_{24}O_3$	288.4	13[b]	$9x10^{-13}$	10.38±0.02	2.81[b]	3.5[b] (calc.)	0.0024
EE2	50-63-6	$C_{20}H_{24}O_2$	296.4	4.7-19[a]	$6x10^{-9}$	10.40±0.01	3.67-4.2[a]	3.8[a] (calc.)	1.19

[a]Johnson and Harvey (2002)

[b]Jürgens *et al.* (1999); Hanselman *et al.* (2003)

[c]Lai *et al.* (2000)

[d]Rutishauser *et al.* (2004)

K_{ow}: Octanol-water partition coefficient

K_{oc}: Organic carbon normalized partition coefficient

The yeast estrogen screen (YES) assay is widely used for measuring biological potencies of estrogenic chemicals (Table 2.1). EE2 and E2 are the most potent among the four hormones discussed here while E3 has the lowest estrogenicity (Rutishauser *et al.*, 2004). In comparison, bisphenol A, a well-known EDC, has a potency of estrogenic activity, as measured by YES, 1/15,000 that of E2 (Ying *et al.*, 2004). In the European Union's "first watch list for emerging water pollutants", E2 and EE2 have been included, to be monitored across the EU for up to four years (Directive, 2013). Table 2.2 shows concentration data for estrogenic steroidal hormones in the influents and effluents of STPs from various countries.

A few studies have been carried out on the endocrine disrupting effects of the estrogenic hormones E1, E2, E3 and EE2 among other EDCs in Australian waters (Gadd *et al.*, 2010; Game *et al.*, 2006; Scott *et al.*, 2014; Uraipong *et al.*, 2017). A survey by Uraipong *et al.* (2017) found EE2 concentrations between 15 and 29 ng l^{-1} EE2 in South Creek, NSW, at sites upstream and downstream of the municipal STPs. An assessment of endocrine activity in Australian rivers found that E1, E2 and EE2 exceeded their predicted no-effect concentration a number of times (Scott *et al.*, 2014).

Table 2.2. Concentrations and removal efficiency of major estrogenic hormones in different STPs.

Compound	Influent (ng l^{-1})	Effluent (ng l^{-1})	Removal (%)	STP	Reference
E1	44	17	61	6 STPs, Rome, Italy	D'Ascenzo *et al.* (2003)
	20.17-60	5.85-10.58	78-92	STP, Horsham, England	Zhang and Zhou (2008)
	64.51-116.06	8.6-22.4	81-86	4 STPs, Midlands, England	Ifelebuegu (2011)
	10.2-34.9	8.3-14.0	49.5	STP, Harbin, China	Zhang *et al.* (2011b)
	50-51	10-12	76.5-80	2 STPs, Sfax and Sousse, Tunisia	Belhaj *et al.* (2015)
		<5-7		2 STPS, QLD, Australia	Leusch *et al.* (2010)
E2	11	1.6	85	6 STPs, Rome, Italy	D'Ascenzo *et al.* (2003)
	26.4-51	2.05-8.92	69-90	STP, Horsham, England	Zhang and Zhou (2008)
	15.67-82.55	0.9-3.9	83-97	4 STPs, Midlands, England	Ifelebuegu (2011)
	46.6-93.0	8.7-32.4	69.3	STP, Harbin, China	Zhang *et al.* (2011b)
	10.8-19	n.d.-4	79-≥92	2 STPs, Sfax and Sousse, Tunisia	Belhaj *et al.* (2015)
		<5		2 STPS, QLD, Australia	Leusch *et al.* (2010)
E3	72	2.3	97	6 STPs, Rome, Italy	D'Ascenzo *et al.* (2003)
	49.8-216.9	n.d.-15.8	94.4	STP, Harbin, China	Zhang *et al.* (2011b)
	98-102	n.d.-15	85.5-≥97.5	2 STPs, Sfax and Sousse, Tunisia	Belhaj *et al.* (2015)
		<5		2 STPS, QLD, Australia	Leusch *et al.* (2010)
EE2	n.d.-10	n.d.	~100%	STP, Horsham, England	Zhang and Zhou (2008)
	n.d.-1.54	n.d.-0.5	41-58	4 STPs, Midlands, England	Ifelebuegu (2011)
	n.d.-11.53	n.d.	n.d.	STP, Harbin, China	Zhang *et al.* (2011b)
	25-45	n.d.-10	77.5-≥84	2 STPs, Sfax and Sousse, Tunisia	Belhaj *et al.* (2015)
		<5		2 STPS, QLD, Australia	Leusch *et al.* (2010)

n.d.: not detected.

Many conventional water treatment technologies may remove a proportion of EDCs (Grover *et al.*, 2011; Johnson and Sumpter, 2001). For instance, in a municipal STP in Galicia, Spain, Carballa *et al.* (2004) found that the overall removal efficiency of E2 was around 65%, while the concentration of E1 was increased due to the partial oxidation of E2. Similarly Liu *et al.* (2015) observed that around 38% of E1 and 75% of E2 and E3 were removed in municipal STPs. Hence new biological, chemical or physical treatment methods are needed to enhance wastewater EDCs removal (Oller *et al.*, 2011).

AOPs that degrade potent chemicals by free radical oxidation (Wang and Xu, 2012) have been implemented relatively recently. The main AOPs are photolysis, photocatalysis, ozonation (Qiang *et al.*, 2013), electrochemical oxidation (Murugananthan *et al.*, 2007), sonolysis (Suri *et al.*, 2007), ferrate (Jiang *et al.*, 2005) and fenton oxidation (Brienza *et al.*, 2014).

Photodegradation is a promising technology that uses light energy for the removal of EDCs and consists of photolysis and photocatalysis. TiO_2, ZnO (Behnajady *et al.*, 2006; Subash *et al.*, 2013), WO_3 (Liu *et al.*, 2012b), ZnS (Sharma *et al.*, 2012; Torres-Martínez *et al.*, 2001), SnO_2 (Wu *et al.*, 2009a; Zhang *et al.*, 2011a), $FeCl_3$ (Wang *et al.*, 2007), Fe_2O_3 (Niu *et al.*, 2010; Valenzuela *et al.*, 2002) and Bi_2WO_6 (Zhang and Zhu, 2012) are some of the common photocatalysts used. Though TiO_2 is an efficient catalyst under UV irradiation, it is inactive under visible light, which is only about 4 % of the sunlight. Therefore, there is a need to develop visible light active catalysts. Several methods have been used to modify TiO_2 with metal, non-metal or through the combination of both, to attain visible light activity. Modification with novel metals

have shown to introduce visible light activity in TiO_2, with gold emerging as an attractive option.

2.2 Photodegradation of estrogenic steroidal hormones

2.2.1 Photolysis

Photolysis is a process in which molecules undergo decomposition as a result of the absorption of light energy. Different sources of light may be utilised but UV disinfection lamps remain common. There are two types of photolysis, namely direct photolysis where the direct absorption of photons leads to degradation of pollutants, and indirect photolysis which occurs in the presence of photosensitisers. Photolysis is an economic mode of removing estrogenic steroidal hormones, especially under natural sunlight, but the removal rates are reported to be low. For instance 40-75 days were required for 50% degradation of E1, E2, E3 and EE2 (Fonseca *et al.*, 2011) under direct solar irradiation. Most of the bench scale studies showed an increase in photolysis efficiency in the order: sunlight, UVA, UVB and UVC. For example, 91.6% photodegradation of EE2 was achieved in 30 min under UVC light (Zhang *et al.*, 2010). Table 2.3 outlines the use of photolysis for the removal of estrogenic steroidal hormones under different light sources and conditions.

Table 2.3. Photolytic removal of estrogenic steroidal hormones.

Compound	Water type	Light source	C_o (mg l^{-1})	% Removal	Kinetic data	Reference
EE2	Distilled	30 W, λ = 254 nm	1.6-20.0	-	Pseudo 1st order, k = 0.03032-0.00864 min^{-1}	Liu *et al.* (2003a)
EE2	Distilled	250 W, λ ≥ 313 nm, 38000 Lux	2.5-15	-	k = 0.0726 min^{-1}	Liu *et al.* (2003b)
E1, E2	Distilled	30 W, λ = 254 nm, 1500 μW cm^{-2}	10	-	Pseudo 1st order, k_{E1} = 0.0119 min^{-1}, k_{E2} = 0.0173 min^{-1}	Liu and Liu (2004)
E2, EE2	Distilled	1 kW, λ = 200-300 nm; 4 x 15 W, λ = 254 nm	-	<5% with 15 W lamp; 17.7% (E2), 21.6% (EE2) with 1 kW	2nd order. k_{E2} = 1.41 ± 0.33 x 10^{10} M^{-1} s^{-1}, k_{EE2} = 1.08 ± 0.23 x 10^{10} M^{-1} s^{-1}	Rosenfeldt and Linden (2004)
E1, E2, E3, EE2	Milli-Q, river	1.1 kW, λ = 290-700 nm, 765 W m^{-2}	0.001-0.002	-	k_{E1} = 0.15 ± 0.005 h^{-1}, k_{E2} = 0.02 ± 0.002 h^{-1}, k_{E3} = 0.02 ± 0.003 h^{-1}, k_{EE2} = 0.02 ± 0.002 h^{-1}	Lin and Reinhard (2005)
EE2	Sea	16 x 25 W, λ = 300 nm; Sunlight	8.0	-	1st order, 0.019 h^{-1}	Zuo *et al.* (2006)
E2, EE2	Distilled	1 kW, λ = 200-300 nm, 4000-5000 mJ cm^{-2}	E2: 1362 EE2: 1482	Estrogenicity removal: E2: 99%, EE2: 95%	Pseudo 1st order	Rosenfeldt *et al.* (2007))
EE2	Distilled	150 W, λ = 238-579 nm	-	-	k = 7.1 ± 1.6 m^2 $einstein^{-1}$	Canonica *et al.* (2008)
EE2	River	Sunlight, 270 W m^{-2}	10-40	-	1st order, k = 0.007 h^{-1}	Matamoros *et al.* (2009)
E2	Distilled	λ = 290-720 nm, 650 W m^{-2}	0.272	47.6% (6 h)	Pseudo 1st order, k = 0.05 h^{-1}	Leech *et al.* (2009)
E1	Distilled	1000 W, λ = 290-700 nm, 100 mW cm^{-2},	5 ± 0.05	TOC removal (6 h) = 17%	Pseudo 1st order, k = 0.0132 min^{-1}	Chowdhury *et al.* (2010)
EE2	Distilled	30 W, λ = 254 nm	0.61	91.6% in 30 min	Pseudo 1st order, k = 0.091 min^{-1}	Zhang *et al.* (2010)
E2	Distilled	1000 W, λ = 300-400 nm, 100 mW cm^{-2}, 5.3 x 10^{-5} $einsteinm^{-2}$ s^{-1}	0.005	46% E2 in 10 h	1st order, k = 0.0652 ± 0.0033 h^{-1}	Chowdhury *et al.* (2011)

Compound	Water type	Light source	C_0 (mg l^{-1})	% Removal	Kinetic data	Reference
E1	Acetonitrile	7 UVC lamps	27.04	100% E1 to lumiestrone in 5 min	-	Trudeau *et al.* (2011)
E1	Distilled	1500 W, λ = 300-800 nm, 250 W m^{-2}	-	50% in 8 h	1st order, k = 0.090 ± 0.006 h^{-1}	Caupos *et al.* (2011)
E1, E2, E3, EE2	Distilled	Sunlight, 5.4 kWh m^{-2} day^{-1}	10	50% removal in days: E1 = 55, E2 = 60, E3 = 40, EE2 = 75	-	Fonseca *et al.* (2011)
E1, EE2	Distilled (a), river (b), lake (c)	UVB, 133 μW cm^{-2}	5 x 10^{-4}	-	Pseudo 1st order, a: k_{EE2} = 0.013 h^{-1}, k_{E1} = 0.208 h^{-1}; b: k_{EE2} = 0.001 h^{-1}, k_{E1} = 0.085 h^{-1}; c: k_{EE2} = 0.010 h^{-1}, k_{E1} = 0.004 h^{-1}	Atkinson *et al.* (2011)
E1, E2, EE2	Distilled	Solar simulator , λ < 300 nm, 765 W m^{-2}	0.01	53% net yield of lumiestrone from E1	k_{E1} = 29 x 10^{-5} s^{-1}, k_{E2} = 2.5 x 10^{-5} s^{-1}, k_{EE2} = 2.6 x 10^{-5} s^{-1}	Whidbey *et al.* (2012)
E1, E2, E3, EE2	STP effluent	UV	-	33.3%- 73.9%	-	Huang *et al.* (2013)
EE2	Lake	Sunlight	11.1 x 10^{-6}	-	Pseudo 1st order, k = 0.0301 h^{-1}	Zuo *et al.* (2013)
E3	Distilled	Sunlight; 150 W, λ > 300 nm	1.153	-	Pseudo 1st order, k = 0.187 h^{-1}	Chen *et al.* (2013)
EE2	Distilled (a), sea (b), river (c)	430 W, λ = 295-780 nm	3 x 10^{-4}	-	1st order, k_a = 0.04 ± 0.02 h^{-1}, k_b = 0.06 ± 0.02 h^{-1}, k_c = 0.11 ± 0.03 h^{-1}	Grzybowski and Szydlowski (2014)

2.2.2 Photocatalysis

Photocatalysis can be used to overcome the disadvantages of photolysis, especially the slow rate of degradation. Photocatalysis is the transformation of a compound by a catalyst that is activated by light energy (Macwan *et al.*, 2011). The catalyst takes part in the reaction to increase the rate of reaction but remains unchanged by the end (Ohtani, 2010). The photocatalysis material must be able to absorb light and have a surface capable of interacting with the substances to be catalysed. In most cases, the photocatalyst consists of small particles of a semiconductor material and thus have a reasonably large surface area and possess electrons occupying a valance band (VB) with unoccupied higher energy electronic states CB. The energy difference between these two bands (the band gap) must be appropriately tuned to allow absorption of visible or UV light by the photocatalyst. Figure 2.1 shows the UV-visible absorption spectrum to P25 TiO_2, which absorbs strongly in the UV region. In comparison, of E1, E2, E3 and EE2 absorb only in a narrow region at very short wavelengths (Figure 2.1) (also a region where there are very few solar photons at the Earth's surface).

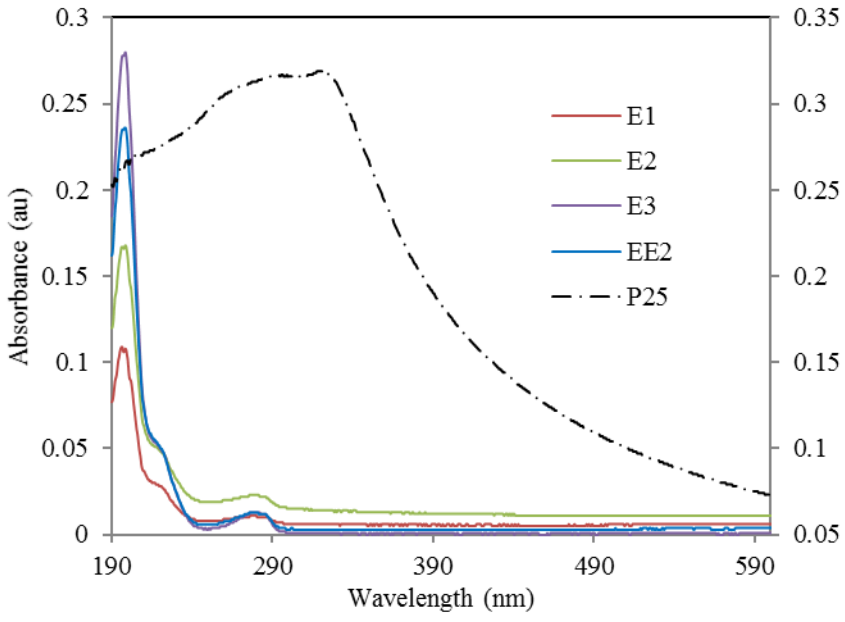

Figure 2.1. UV-visible absorbance spectra of E1, E2, E3 and EE2 (left axis) and P25 TiO_2 (right axis). Data collected by the authors.

Upon absorption of photons by the photocatalyst, electrons (e^-) are transferred from the VB to the CB leaving holes (h^+) in the VB (Eq. 1). Hydroxyl radicals are produced by the reaction between the h^+ and the H_2O molecules adsorbed on the catalyst surface (Eq. 2). The target compounds that are adsorbed on the catalyst surface can react with the e^- or the h^+ formed (Eq. 3), while recombination of these charged carriers is also possible. CB electrons also produce superoxide radical anions ($O_2^{\bullet-}$) by reacting with O_2 (Eq. 4).

2.2.2.1. Titanium dioxide

TiO_2 remains the best catalyst choice due to its chemical and photo stability, ability to degrade a diverse range of chemicals, cheap commercial availability, capacity to function at ambient conditions, and low toxicity (Xu *et al.*, 2014a). Among the mineral forms of TiO_2; anatase, rutile and brookite; the former is regarded as a better photocatalyst due to the bulk transport of excitons to the surface (Luttrell *et al.*, 2014). P25 (~85% anatase and 15% rutile; 21 nm average primary particle size) is the most commonly utilised commercial TiO_2 (Jovic *et al.*, 2015; Macwan *et al.*, 2011). However, only a small proportion of solar light has energy greater than the band gap energy of TiO_2 (anatase: 3.2 eV) (Fujishima *et al.*, 2008; Marschall and Wang, 2014). Therefore, doping procedures have been explored to lower the band gap, enabling visible wavelengths to be utilised. Table 2.4 outlines the use of TiO_2 photocatalysts for the removal of estrogenic steroidal hormones. TiO_2 photocatalytic reaction processes are as follows, where h^+ denotes a 'hole' formed by a missing electron and

P_{ad} is the pollutant adsorbed on the catalyst surface (Nakata and Fujishima, 2012; Ribeiro *et al.*, 2015):

$$TiO_2 + h\nu \longrightarrow TiO_2\,(e^- + h^+) \quad (1)$$

$$TiO_2\,(h^+) + H_2O \longrightarrow TiO_2 + {}^{\bullet}OH + H^+ \quad (2)$$

$$TiO_2\,(h^+) + P_{ad} \longrightarrow TiO_2 + P_{ad}^{\bullet +} \quad (3)$$

$$TiO_2\,(e^-) + O_2 \longrightarrow TiO_2 + O_2^{\bullet -} \quad (4)$$

Table 2.4. Photocatalytic removal of estrogenic steroidal hormones by TiO_2.

Compound	Catalyst	Light source	C_o (μg l^{-1})	% Removal	Kinetics	Reference
E2	P25 immobilised on Ti-6Al-4V alloy	150 W, λ < 300 nm, 8 x 10^{-8} einstein s^{-1} cm^{-2}	136.2-817.2	98% (3.5 h)	Pseudo 1st order, k = 0.0157 min^{-1}	Coleman *et al.* (2000)
E1, E2, EE2	TiO_2 film on quartz beads (d = 2 mm)	2 x 20 W, λ = 359 nm, 1.4 mW cm^{-2}	100	90% E1 and EE2 (30 min), 10% of E2 (2 h)	k_{E1} = 0.058 min^{-1}, k_{E2} = 0.015 min^{-1}, k_{EE2} = 0.05 min^{-1}	Tanizaki *et al.* (2002)
E2	TiO_2-PTFE mesh sheets	2 x 15 W, λ = 359 nm, 0.24 mW cm^{-2}	90	98% (1h)	1st order, k_{R1} = 0.033 min^{-1}; k_{R2} = 0.050 min^{-1}	Nakashima *et al.* (2002)
E2	P25	200 W, λ = 365 nm, 6 mW cm^{-2}	272.4	< 99% (30 min)	1st order	Ohko *et al.* (2002)
E1, E2	TiO_2 immobilized to PTFE mesh	8 x 15 W black-light (BL)	250	E1: 98% (distilled water, 16 min), 90% (sewage effluent, 4 min)	1st order, : k_{E1} = 0.12 min^{-1}, k_{E2} = 0.15 min^{-1}	Nakashima *et al.* (2003)
E1, E2, EE2	Coating of Ti with TiO_2	125 W UVA	10	100% removal: E1: 60 min, E2: 55 min, EE2: 50 min	1st order, k_{E1} = 0.086 min^{-1}, k_{E2} = 0.106 min^{-1}, k_{EE2} = 0.086 min^{-1}	Coleman *et al.* (2004)
E2, E3, EE2	P25, 2% Ag, Pt doping	15 W BL, λ = 300-400 nm	817.2, 865.2, 889.2	-	1st order, k = 0.12-0.18 min^{-1}	Coleman *et al.* (2005b)
E2, E3, EE2	P25 film in quartz coil	125 W MP Hg lamp	817.2, 865.2, 889.2	-	1st order, k_{E2} = 0.174 min^{-1}, k_{E3} = 0.156 min^{-1}, k_{EE2} = 0.231 min^{-1}	Coleman *et al.* (2005a)
E1, E2, EE2	TiO_2 immobilised on glass beads	4 W, λ = 365nm, 600 mW cm^{-2}	270.4, 272.4, 296.4	-	1st order, k_{E1} = 0.0043 min^{-1}, k_{E2} = 0.0042 min^{-1}, k_{EE2} = 0.0045 min^{-1}	Mizuguchi *et al.* (2006)

Compound	Catalyst	Light source	C_o (μg l^{-1})	% Removal	Kinetics	Reference
E2	P25 film in quartz coil	20 W, λ = 254 nm, 74 μ einstein s^{-1} l^{-1}	800	-	1st order, k = 0.218 min^{-1}	Coleman *et al.* (2007)
E2, EE2	P25	λ = 365 nm, 1.1 mW cm^{-2}	500	~100% (60 min)	k_{app} = ~10-70 min^{-1}	Karpova *et al.* (2007)
E1, E2	P25	R1: 150 W, λ = 238-579 nm; R2: 15 W, λ = 253 nm	0.5	R1: 72% E1, 95% E2 in 2 h; R2: 99% E1, E2 in 2h	Pseudo 1st order, R1: k_{E1} = 0.85 h^{-1}, k_{E2} = 0.82 h^{-1}; R2: k_{E1} = 2.7 h^{-1}, k_{E2} = 2.5 h^{-1}	Zhang *et al.* (2007)
E2	P25	8 W, λ = 365-370 nm	5000	-	-	Mai *et al.* (2008)
E1, E2, EE2	TiO_2	Sunlight	0.5-100	50% E1, 55% E2 in 2 h	1st order, k = 0.01 h^{-1}	Zhang and Zhou (2008)
E1, E2, E3, EE2	P25	8 W, λ = 300-420 nm, ; 8 W, λ = 253.7 nm	946.4, 953.4, 1009.4, 1037.4	UVA: E1, E2, E3, EE2 = 49, 20, 25, ~0% in 180 min. UVC: E1= 98%, E2, E3, EE2 = 60%	1st order	Puma *et al.* (2010)
E1, E2, E3	P25 immobilised by dip-coating	6 W, λ= 365 nm, 2.8 x 10^{-4} einstein m^{-2} s^{-1}	0.0276, 0.0147, 0.0134	95% (100 min)	1st order, k_{E1} = 0.0441 min^{-1}, k_{E2} = 0.0507 min^{-1}	Zhang *et al.* (2012c)
E1, E2, EE2	P25, Hombikat UV 100, Kronos vlp 7000, 7001, 7100, 7101	150 W, λ > 280 nm	85-300	EE2/P25: 95% (10 min), 95% (90 min- WW); EE2/ Kronos: 95% (25 min); EE2/Hombikat: 95% (120 min- WW); P25/E2: 100% (90 min- WW). Other/E2 maximum 80%	1st order	Frontistis *et al.* (2012b)

Compound	Catalyst	Light source	C_o (μg l^{-1})	% Removal	Kinetics	Reference
E1, E2, E3, EE2	P25	6W BL, λ = 365nm	0.100	-	1st order, k_{E1} = 0.0272 min^{-1}, k_{E2} = 0.0269 min^{-1}, k_{E3} = 0.0242 min^{-1}	Zhang *et al.* (2012b)
E2, EE2	P25, Hombikat UV 100, Tronox AK1	9 W, λ = 350-400 nm, 2.81 × 10^{-4} einstein min^{-1}	50-900	E2/P25: 95% (15 min). EE2/photolysis: 55% (90 min) EE2/sonophotocatalysis: 90% (4min)	-	Frontistis *et al.* (2012a)
EE2	P25	λ = 254 nm, 1.3 × 10^{-3} einstein min^{-1} l^{-1}	3500-5000	Photolysis: 60 ± 12% (30 min), P25: 92 ± 7% (30 min).	Pseudo 1st order, k_{UVC} = 0.03 min^{-1}, $k_{UVC/TiO2}$ = 0.106 min^{-1}	Nasuhoglu *et al.* (2012)
E1	P25, ZnO	18 W, λ: 320-400 nm, 0.2 W m^{-2}; Sunlight	27-600	95% (10 min)	1st order, ZnO: k = 0.362 min^{-1}, P25: k = 0.177 min^{-1}	Han *et al.* (2012)
EE2	A: P25, B: 0.5% Pt/TiO_2, J:0.5% Pt (0.12%Na)/TiO_2	150 W, λ> 280 nm, 13.1 × 10^{-3} W m^{-2}	100-300	Photolysis: 6% (60 min). 90% removal with A = 40-50 min, B = 30min , J = 30 min	-	Dimitroula *et al.* (2012)
E1	TiO_2-Tytanpol (T1), TiO_2-Sigma (T2), Hombikat (T3), TiO_2-S21 Sigma (T4)	700 W, λ = 254 nm, 2 mW cm^{-2}	50,000	-	1st order, k_{T1} = 0.0045 min^{-1}, k_{T2} = 0.0024 min^{-1}, k_{T3} = 0.0054 min^{-1}, k_{T4} = 0.0075 min^{-1}	Czech and Rubinowska (2013)
E1	TiO_2 hybridized magnetic Fe_3O_4	20 W, λ = 254 nm	-	-	1st order, k_{Fe} = 0.069 min^{-1}, k_{P25} = 0.029 min^{-1}	Xu *et al.* (2014b)
E2	P25	8 W, λ = 365 nm	1000	90% (64 W UV + PVDF)	-	Lopez Fernandez *et al.* (2014)
EE2	P25	8 W, λ = 365 nm, 475 μW cm^{-2}	1000	100% (30 min)	Pseudo 1st order, k = 0.151 min^{-1}	Li and Sun (2014)
E2	(i) P25, (ii) ECT-1023t, (iii) N-TiO_2, (iv) 4wt% (GO)- TiO_2	450 W, λ = 280-400 nm; λ = 200 nm - 30 μm	1000	UV/cat: (i) 98%, (ii) 77%, (iii) 27%, (iv) 48%, solar/cat: i) 86%,	-	Mboula *et al.* (2015)

Compound	Catalyst	Light source	C_o (μg l^{-1})	% Removal	Kinetics	Reference
				(ii) 40%, (iii) 23%, (iv) 59% in 60 min		
EE2	TiO_2/ WO_3 (W/Ti=12%) deposited on electrodes	400 W solar simulator, 130 mW cm^{-2}	10,000	TiO_2: 35% (4 h), TiO_2/WO_3: 45% (4 h)	Pseudo 1st order, k_{app} = 0.0059 min^{-1}	Oliveira *et al.* (2015)
E2, EE2	TiO_2 nanotubes	Sunlight	544.8, 592.8	~95% (180-240 min)	-	Kim *et al.* (2015)

2.2.2.2 Other photocatalysts

Some other commonly used photocatalysts for the abatement of E1, E2, E3 and EE2 are included in Table 2.5. ZnO is the second-most commonly studied photocatalyst after TiO_2. Some researchers observed increased activity for Zn-based catalysts compared to TiO_2 but these catalysts could lose their activity as a result of dissolution and contaminate water through the release of free Zn ions. For instance, Han *et al.* (2012) compared the efficiency of P25 and ZnO for the removal of E1 both under UVA and solar light (Table 2.4) and reported up to three times higher degradation rate in the presence of ZnO. On the other hand, 52% dissolution of ZnO in 60 min, calls into question its sustainability. A combination of $FeCl_3$ and $NaNO_2$ as photocatalyst resulted in intermediates that did not possess any estrogenicity, with an E2 degradation of 86.6% and 99.9% in a day and a month, respectively (Wang *et al.*, 2007). Li *et al.* (2010) found that Fe(III)-ethylenediamine-N,N′-disuccinic acid (Fe(III)-EDDS) exhibited good photoactivity for the degradation of E2 at higher pH values and suggested that this complex could be utilised in natural waters. Pan *et al.* (2014) tested a novel catalyst TiO_2-doped low-silica X zeolite for the degradation of EE2 (Table 2.5) and observed an enhancement factor of 2.3.

Table 2.5 Photocatalytic removal of estrogenic steroidal hormones by non-TiO_2 catalysts.

Compound	Catalyst	Light source	C_o (mg l^{-1})	% Removal	Kinetics	Reference
E2, E3, EE2	$FeCl_3/NaNO_2$, 18 μM $FeCl_3$ + 18 μM $NaNO_2$	Mimicked sunlight, 12000-15000 Lux	4.032	86.6% in 1 day, 99.9% in 30 days	-	Wang *et al.* (2007)
E2	Fe(III)-EDDS: $Fe(ClO_4)_3$ + S,S-ethylene diamine-N,N-disuccinic acid mixed in 1:1	4 x 15 W, λ = 300-500 nm	1.362	-	-	Li *et al.* (2010)
E1	ZnO coated on glass to form nanorod arrays	2 x 9 W, λ = 365 nm, 5.7 W m^{-2}	0.5	87% in 360 min	Pseudo 1st order, k = 0.58 min^{-1}	Liu *et al.* (2012a)
EE2	ZnO, 500 mg l^{-1}	150 W, λ > 280 nm, 0.0131 W m^{-2}.	0.5	100% EE2, 32% estrogenicity in 40 min	1st order, k = 0.41 min^{-1}	Frontistis *et al.* (2012c)
EE2	ZnO immobilized on glass, 4 g l^{-1}	150 W, λ > 280 nm	0.1	80% in 90 min	k_{app} = 0.0173 min^{-1}	Koutantou *et al.* (2013)
EE2	Ag/ZnO hollow sphere, 0.5 g l^{-1}, P25	8 W, λ = 254 nm, 145 W m^{-2}	2.7	~100% for Ag/ZnO, 53% for ZnO in 50 min	Pseudo 1st order, $k_{UV/ZnO}$ = 0.013 min^{-1}, $k_{Ag/ZnO}$ = 0.067 min^{-1}, $k_{UV/P25}$ = 0.017 min^{-1}	Li *et al.* (2014)
EE2	TiO_2-doped low-silica X zeolite (TiO_2-LSX), 0.1- 0.5 g l^{-1}	λ = 254 nm	10	UV: 60%, UV/TiO_2: 90% (60 min), TiO_2-LSX efficiency: 2.3 x TiO_2	Pseudo 1st order, k_{app} = 0.045 min^{-1} (0.1 g l^{-1} catalyst)	Pan *et al.* (2014)

2.2.3. Photodegradation coupled with other advanced oxidation processes

AOPs such as H_2O_2, O_3 and Fenton reagent can be combined with photolysis and/or photocatalysis to improve the degradation efficiency of EDCs (Table 2.6). Most of the studies showed an enhancement in ozonation in the presence of UV but a recent pilot scale study by Pešoutová *et al.* (2014) indicated a drop in the degradation rate of E1, E2, E3 and EE2 under O_3/UV and O_3/H_2O_2/UV compared to O_3 on its own. The authors attributed the decline in removal rate to the presence of $^{\bullet}OH$ scavengers such as CO_3^{2-} and HCO_3^-.

The UV/H_2O_2 process has proved to be highly effective compared to utilising photolysis or H_2O_2 alone. For example, degradation of six EDCs under UV/H_2O_2 was 45-197 times that of UV and 11-53 times better than using H_2O_2 alone (Zhang and Li, 2014). The addition of H_2O_2 to TiO_2 photocatalysts increased the rate of degradation of pollutants. Mizuguchi *et al.* (2006) evaluated the influence of H_2O_2 (1.32 mM) on the photodegradation of E1, E2 and EE2 (1 μM) with TiO_2 immobilised on glass beads and found that the estrogens were degraded faster in the presence of H_2O_2 compared to using only TiO_2 (Table 2.4). An increase in the degradation rate of E1 and E2 with increased concentrations of H_2O_2 was observed. H_2O_2 acted as an electron acceptor limiting e^- - h^+ recombination and as a scavenger of VB holes at high concentration (Zhang *et al.*, 2007).

The photo-Fenton process employs Fe^{2+} or Fe^{3+} along with H_2O_2 and a light source and portrays better activity than the dark-Fenton method through the production of additional $^{\bullet}OH$ radicals. For example E1, E2 and EE2 were completely removed within 5 to 10 min when a simulated solar light photo-Fenton process was used (Frontistis *et al.*, 2011b).

Table 2.6. Photodegradation of estrogenic steroidal hormones by UV/O_3, UV/H_2O_2 and photo-Fenton reaction.

Compound	Method	Conditions	Light source	C_o (µg l^{-1})	% Removal	Kinetics	Reference
E2	O_3/UV	pH 6.25, O_3 15.89 µmol min^{-1}	15 W, λ = 254 nm	2.72 x 10^4	~100% E2 in 45 min	-	Irmak *et al.* (2005)
E1, E2, E3 EE2	O_3/H_2O_2/UV	Secondary effluent, O_3: H_2O_2 = 1:1.6, pH 7.4	230 W, λ = 254 nm	E1: 1.95 E2: 2.88 E3: 2.52 EE2: 3.59	99.4% E1, 98.2% E2, 98.7% E3, 99.6% EE2	-	Pešoutová *et al.* (2014)
E2, EE2	UV/H_2O_2	Milli-Q or river water, 10 ppm H_2O_2	4 x 15 W, λ = 253.7 nm,2000 mJ cm^{-2}	E2: 0.2 EE2: 1	-	Pseudo 1st order	Chen *et al.* (2007)
EE2	UV/H_2O_2	5 mg l^{-1} H_2O_2	30 W, λ = 254 nm, 15.093 Wm^{-2}	2000	95% estrogenicity removal in 40 min	Pseudo 1st order, k_{UV} = 0.2753 min^{-1}, $k_{UV/H2O2}$ = 0.4187 min^{-1}	Zhang *et al.* (2010)
E1, E2, EE2	UV/H_2O_2	Wastewater effluent,	700 W	0.4	90% E2, EE2	-	Hansen and Andersen (2012)
EE2	UV/H_2O_2	H_2O_2 = 5 mg l^{-1}	14 W, λ = 254 nm, 154 µW cm^{-2}	650	90% removal (30 min), > 99% (60 min)	Pseudo 1st order, k_{UV} = 0.0075 min^{-1}, $k_{UV/H2O2}$ = 0.0630 min^{-1}	Li *et al.* (2013)
E1, E2, E3 EE2	UV/H_2O_2	H_2O_2 = 0.018 mol l^{-1}, pH 7	75 W, λ = 253.7 nm, 0.069 mW cm^{-2}	0.15	97% E1, 92% E2, 95% EE2, 94% E3 in 2 min	Pseudo 1st order, k_{E1} = 0.282 min^{-1}, k_{E2} = 0.637 min^{-1}, k_{E3} = 0.463 min^{-1}, k_{EE2} = 0.73 min^{-1}	Zhang and Li (2014)
E1, E2, E3, EE2	Nanofiltration/ UV/H_2O_2	100 mg l^{-1} H_2O_2, surface water	λ = 254 nm	1000	>74% removal	Pseudo 1st order	Pereira et al. (2012)

Compound	Method	Conditions	Light source	C_0 (µg l^{-1})	% Removal	Kinetics	Reference
EE2	UV/H_2O_2, Solar/Fe^{2+}	Secondary effluent, Fe^{2+} in $FeSO_4 \cdot 7H_2O$	11 W, 7.15 µeinstein s^{-1}; 150 W solar simulator, 0.174 µeinstein s^{-1}	100	100% in 15 min of UVC/H_2O_2; 86% in 60 min of solar/Fe^{2+}	-	Frontistis *et al.* (2015)
E2	Photo-Fenton	10 mol l^{-1} Fe(III), 1000 mol l^{-1} H_2O_2, pH 3	250 W, $\lambda \geq 313$ nm, 1.7×10^5 lux	5012	75.2% in 160 min	1st order, reaction rate = 0.157 mol l^{-1} min^{-1}	Feng *et al.* (2005)
E2	Photo-Fenton	5 g l^{-1} α-FeOOHR, Fe 0.5 g l^{-1}, 9.7 mM H_2O_2	2 x 15 W, λ = 365 nm, 0.3 mW cm^{-2}	272	86.4% in 8 h	-	Zhao and Hu (2008)
E1, E2, EE2	Photo-Fenton	Secondary effluent, 5 mg l^{-1} Fe^{2+}, 17.2 mg l^{-1} H_2O_2	150 W solar simulator	200	100% in 5-10 min	k_{E1} = 11.1 min^{-1}, k_{E2} = 6.67 min^{-1}, k_{EE2} = 100 min^{-1}	Frontistis *et al.* (2011b)
E2	Photo-Fenton	Wastewater	3 x 30 W, λ = 365 nm	1510	100% in 5-10 min	1st order, k = 0.161 min^{-1} in H_2O_2/Fe(II)	Brienza *et al.* (2014)

2.3 Factors affecting photodegradation

The efficiency of photodegradation of estrogenic steroidal hormones depends on many factors such as the physico-chemical properties and initial concentrations of the pollutants, the light source, photon flux, type and loading of catalysts, and aqueous composition including the presence and type of dissolved organic matter (DOM), pH and temperature.

2.3.1 Photolysis

2.3.1.1. Light source and intensity

Photolysis experiments are conducted under various light sources emitting different wavelengths either monochromatic or polychromatic. Most common sources are UVC, UVB, UVA, simulated solar light and natural sunlight. The degradation efficiency of steroid hormones increased as the wavelength of the source moved from visible to UV as a result of an increase in photon flux and due to the strong absorption of photons by the estrogenic hormones under UVC (Figure 2.1) (Puma *et al.*, 2010). However, the light sources did not have the same effect on all the estrogens. For instance, E1, E2 and EE2 were removed at a similar rate during photocatalysis, while the photolytic degradation efficiency under UVA irradiation followed the order EE2 > E1 > E2 (Coleman *et al.*, 2004). Liu *et al.* (2003a) observed (Table 2.3) that a high pressure (HP) Hg lamp ($\lambda > 365$ nm) did not lead to photodegradation of EE2, while a significant amount of removal occurred in the presence of a UV disinfection lamp ($\lambda = 254$ nm). This was attributed to the fact that EE2 has absorption peaks around 254 nm, whereas its absorption above 350 nm is virtually zero (Figure 2.1). On the other hand, Rosenfeldt and Linden (2004) concluded that a low pressure (LP) UV ($\lambda = 254$

nm) was inefficient in the estrogenic activity removal of E2 and EE2, while medium pressure (MP) UV (λ = 200-300 nm) proved to be effective even under lower fluorescence. The absorption spectrum of E2 and EE2 is 240-330 nm (Mazellier *et al.*, 2008); hence their overlap with natural sunlight is narrow, requiring longer periods of exposure for degradation (Figure 2.1).

An increase in light intensity (*I*) generally results in an increase in the removal efficiency, though the change in rate constant varies depending on the type of pollutants and the range of light intensity (Table 2.7a).

2.3.1.2 Solution matrix

Photodegradation of pollutants depends on the type of water matrices used, with key factors being the source of water (e.g. river water, STP effluent), presence of DOM, initial concentration of the pollutants (C_o) and solution pH. Firstly, if the water composition is considered, the removal efficiency tends to drop as the complexity of the matrix is increased. For instance, Trudeau *et al.* (2011) found that E1 was transformed into lumiestrone under aerobic conditions in acetonitrile, while a slower degradation was observed in sewage water due to the drop in UVB penetration through wastewater. On the other hand, the study by Lin and Reinhard (2005) showed that the photolysis rates were faster in river water compared to that in Milli-Q water due to photosensitisation by DOM in river water. Similar results were reported for EE2 in natural water, with an enhancement factor of 6.1 for the rate constant compared to that in Milli-Q water (Canonica *et al.*, 2008). Matamoros *et al.* (2009) used Milli-Q water, river water and seawater as media for EE2 photolysis and attained similar photodegradation rates. Rosenfeldt *et al.* (2007) observed that the UV fluorescence needed for 90% loss of estrogenicity of EE2 in the presence of H_2O_2 in deionised water

was less than that required in natural water. Therefore it is possible that most of the laboratory studies conducted in deionised water could either underestimate or overestimate the actual rate of removal.

The presence of DOM has shown both positive and negative effects on photodegradation depending on its constituents (Table 2.7b). Photolysis rates generally increased in the presence of DOM such as humic acid (HA) and Suwannee river fulvic acid, because of an increase in free radicals that can oxidise the EDCs. However, the rate of increase is much lower at high DOM concentrations due to the scavenging of oxygen species and a drop in the light transmittance through the solution. Whidbey *et al.* (2012) attributed the drop in E1 photolysis to Suwannee River Fulvic Acid acting as an inner filter. The inhibition of E3 photolysis under elevated light intensity was attributed to the photoactivated HA species being more efficient free radical quenchers than the parent HA (Chen *et al.*, 2013).

The rate of photolytic degradation generally declines with increasing initial concentration (C_o) of the pollutants. It is noteworthy that the EDCs typically exist in the ng l^{-1} range or less in most environmental water matrices, while laboratory studies are conducted mostly at elevated levels ranging from ng l^{-1} to mg l^{-1} (Tables 2.3 – 2.6). Hence, these results have to be extrapolated to real waterways with some degree of uncertainty. Chen *et al.* (2013) observed that the rate constant of E3 photodegradation rose with decreasing C_o, hence predicting that the removal of E3 would be even faster in waterways due to their lower concentration. Similarly an increase in removal rate with decreasing C_o for E1, E2 and EE2 was observed in μg l^{-1} to mg l^{-1} range by Chowdhury *et al.* (2010), Liu and Liu (2004), Liu *et al.* (2003a), Liu *et al.* (2003b) and Zhang *et al.* (2010).

The pH of water affects photolysis rates of E1, E2, E3 and EE2 where the photolysis rate are low under acidic conditions, increasing gradually up to pH 9 and sharply above pH 9. The gradual increase is attributed to the increase in OH^- concentration, which in turn creates more $^{\bullet}OH$ radicals for photolysis. Greater removal efficiency is observed above the pK_a (Table 2.1) values of the estrogens, where more of the pollutants turn from neutral to being negatively charged. Therefore, these compounds undergo electrophilic attack by reactive oxygen species resulting in further degradation. The above trend was observed by Chen *et al.* (2013) for E3 photodegradation, which slightly increased with a rise in pH from 6.0 to 8.0, and rapidly increased for pH between 8.0 and 10.0. A few other studies in the range of pH 2-9 stated pH 7-8 as the optimum (Table 2.7c), since the rate of EDC removal plateaued in that region (Chowdhury *et al.*, 2010; Liu *et al.*, 2003b) although higher photolysis rates might be expected above the pK_a of the hormones.

Table 2.7 (a) Effect of light intensity (I) on photolysis rate constant (k).

Compound	***I* (W m^{-2})**	**Effect of 'I'**	**Reference**
E1	250-1000	$k \propto I$	Chowdhury *et al.* (2010)
E2	250-1000	$k \propto I^{0.5}$	Chowdhury *et al.* (2011)
EE2	2.456-15.09	$\ln k = 2.05 \ln(I) - 6.593$	Zhang *et al.* (2010)

'α': directly proportional

(b) Effect of dissolved organic matter (DOM) on photolysis rates.

Compound	**Type of DOM**	**Effect of DOM**	**Reference**
E2	15 mg l^{-1} HA	+	Leech *et al.* (2009)
E1	10 mg l^{-1} DOM	+	Caupos *et al.* (2011)
E2	0-10 mg l^{-1} HA	+	Chowdhury *et al.* (2011)
E1, E2, EE2	10 g l^{-1} fulvic acid	- (E1) + (E2, EE2)	Whidbey *et al.* (2012)

E3	5 mg l^{-1} HA	+ (Weak sun) - (Intense sun)	Chen *et al.* (2013)

'+': DOM increases photolysis rate; '-': DOM decreases photolysis rate.

(c) Effect of pH on the photolysis rates of estrogenic compounds.

Pollutant	pH range	Optimum pH	Reference
EE2	4- 9	7	Liu *et al.* (2003b)
E1, E2	2- 8	6- 8	Liu and Liu (2004)
E2	3-9	7	Chowdhury *et al.* (2010)
E3	6- 10	8- 10	Chen *et al.* (2013)

2.3.2 Photocatalysis

2.3.2.1 Light source and intensity

Light sources have been shown to have an impact on photocatalysis as well as photolysis. Most of the TiO_2 photocatalytic experiments with estrogenic hormones were conducted using UV sources, with only limited studies being reported with simulated or natural sunlight. The increase in TiO_2 absorptivity and subsequent activity at wavelengths shorter than 400 nm agrees with the results obtained by Coleman *et al.* (2007) where UVA photocatalysis produced better results in comparison to a solar lamp, while UVC/P25 provided the most efficient removal of E2, E3 and EE2. Therefore, though solar photocatalysis is a possible mode of eradicating EDCs, UVC photocatalysis remains most effective.

The photocatalysis rate generally increases in proportion to the light intensity at low intensity, due to the increased production of oxidising species. Increase in the removal rate of EE2 with increasing light intensity has been reported (Dimitroula *et al.*, 2012; Frontistis *et al.*, 2012a). The influence of light intensity on rate becomes less with

increasing intensity, due to recombination reactions or as a result of bimolecular combination of •OH radicals. At high light intensity, the rate is independent of intensity as mass transfer becomes the rate limiting step (Coleman *et al.*, 2005a).

2.3.2.2 Catalyst loading

Optimum catalyst loadings varied between 0.05 and 1 g l^{-1} across different studies (Table 2.8). An increase in the removal rate with increased loading at low to moderate loading is attributed to the rise in availability of active sites. At higher loadings, light penetration can decrease and light scattering can become significant. Agglomeration and sedimentation of catalyst can also become problematic at higher loadings (So *et al.*, 2002; Zhang *et al.*, 2007). Zhang *et al.* (2007) observed that when TiO_2 concentration was increased from 0.5 to 2 g l^{-1}, the degradation of E1 and E2 increased, though a further increase in catalyst concentration to 4 g l^{-1} did not affect the degradation kinetics. The optimum catalyst loading also varies depending on the water matrices (Frontistis *et al.*, 2012b).

Table 2.8. The optimum catalyst loading for the removal of estrogenic hormones during photocatalysis.

Compound	**TiO_2 loading (g l^{-1})**	**Matrix**	**Optimum loading (g l^{-1})**	**Reference**
E1, E2	0.5-4.0	Ultra-pure water	1.0	Zhang *et al.* (2007)
E1	0.01-1.0	Deionized water	0.5	Han *et al.* (2012)
E2	0.1-2.0	Milli-Q water	0.5	Mai *et al.* (2008)
EE2	0.25-0.5	Ultra-pure water	0.5	Frontistis *et al.* (2012a)
	0.5-0.75	Wastewater	0.75	
EE2	0.025-0.25	Ultra-pure water	0.05	Frontistis *et al.* (2012b)
	0.05-1.5	Wastewater	0.15	
EE2	0.125-1.0	Wastewater	1.0	Dimitroula *et al.* (2012)

2.3.2.3 Catalyst doping

Extensive research has been undertaken to improve the activity of photocatalysts through different modes of doping with metals and non-metals. Doping can reduce the incidence of recombination of electrons and holes generated during photocatalysis and also lower the band gap. Though doping has resulted in enhanced removal of many organic pollutants, significant improvements are yet to be observed for estrogenic steroidal hormones compared to P25 alone.

By coating P25 as a thin film to the inner wall of the reactor followed by the deposition of Ag and Pt (Table 2.4), Coleman *et al.* (2005b) tested the impact of doping on E2, E3 and EE2 photodegradation. They observed no notable improvements in the removal efficiency from doping. It was suggested that since the EDCs were in a relatively low concentration (0.8-2.3 mg l^{-1}), the holes and hydroxyl radicals that existed before doping were sufficient and a further increase in these reactive species due to doping was of no importance. Dimitroula *et al.* (2012) prepared TiO_2 catalysts with different dopants (Table 2.4) to examine the removal efficiency of EE2 (along with Bisphenol A and phenol) in secondary treated wastewater. The highest activity for EE2 removal was observed with 0.5% Pt/TiO_2 (B) and 0.5% Pt (0.12%Na)/TiO_2 (J), while P25 (A) also showed relatively similar activity. A 90% conversion of EE2 was attained in 30 min, whereas it took P25 40 to 50 min to achieve the same level of treatment. On the other hand, the addition of Ag and K had a negative impact. Xu *et al.* (2014b) synthesised a TiO_2 hybridised film on magnetic Fe_3O_4 particles via a liquid phase deposition method (Table 2.4) to study the selective removal of E1 under UV light. This new catalyst displayed more selectivity towards E1 at decreasing concentrations, implying that it could be used to remove E1 at low concentrations,

from a mixture consisting of high concentrations of non-target compounds. They observed that their new catalyst had an apparent rate constant 6 times higher compared to TiO_2 when the non-target pollutants in the system were 10 times greater than E1.

Different types of TiO_2 catalysts also result in varied degradation efficiencies. Mboula *et al.* (2015) tested the efficiency of various TiO_2 based catalysts (Table 2.4) for E2 removal under UV and simulated solar irradiation, where P25 exhibited the best activity, though its removal efficiency dropped from 98% in UV to 86% under simulated solar light. A nanocrystalline TiO_2 (ECT-1023t) followed a similar trend as P25; efficiency remained almost the same for N-TiO_2 and a reduced graphene oxide-TiO_2 composite (GO-TiO_2) presented a significant rise in removal efficiency from 48% under UV to 59% under simulated solar light.

2.3.2.4 Solution matrices

The factors that influence photolysis are also applicable to photocatalysis, although there are additional factors that affect photocatalysis. One of the few drawbacks of most of the photocatalysts is their activity towards non-target chemicals. With increasing water complexity, the probability of the hydroxyl radicals being lost due to oxidation of non-target compounds rises. In addition, the active sites of the catalysts become covered by these non-target chemicals, reducing the effective catalyst surface area available for the target pollutants (Katz *et al.*, 2015). Frontistis *et al.* (2012a) reported that the photodegradation rate of EE2 in the presence of P25 decreased for different water matrices in the order: ultrapure water > drinking water > 1:1 mixture of ultrapure water and wastewater > wastewater. The trend was explained as due to the consumption of oxidising agents by the increasing amount of organic matter and the scavenging of $^{\bullet}OH$ radicals by HCO_3^-, Cl^- and SO_4^{2-}.

In a study of the DOM effect, Zhang *et al.* (2007) assessed the impact of HAs (0.01-10 mg l^{-1}) on the photocatalysis of E1 and E2 with P25. The EDC photodegradation rate increased with increasing HA concentration due to its photosensitising effect. In a separate study, polar compounds (PC), midpolar compounds (MPC) and nonpolar compounds (NPC) were all found to inhibit the rate of removal of E1, E2 and E3. Interestingly, inclusion of large molecular weight compounds such as humic or fulvic acids gave a temporary increase in the estrogenic activity of the water before the concentrations of the EDCs fell below detectable levels (Zhang *et al.*, 2012b). This unusual phenomenon can be explained by consideration of the masking effect of the macromolecules. That is, the large molecules absorb the estrogenic compounds and mask their activity. After time, the macromolecules are broken down by the photocatalytic process and release the estrogenic molecules, resulting in a temporary increase in the estrogenic activity. Adsorption of inorganic ions such as HPO_4^{2-}, NH_4^+, and HCO_3^- on the catalyst surface also had an adverse effect on eliminating estrogenicity in SWW, though their influence in secondary effluent was insignificant compared to the inhibition caused by DOM.

The concentrations of estrogenic hormones range from ng l^{-1} or less to μg l^{-1} in surface water and wastewater, and it appears that an increase in initial EDC concentration at low levels does not affect the rate of removal (Frontistis *et al.*, 2012a; Zhang *et al.*, 2007; Zhang and Zhou, 2008). On the other hand, at higher pollutant concentrations, the removal efficiency generally increases with a rise in C_o, due to high probability of the EDC being attacked by the oxidising species, especially during the initial stage of the reaction when the competition with the intermediates is less (Dimitroula *et al.*, 2012; Frontistis *et al.*, 2012a; Frontistis *et al.*, 2012b). A different trend was reported

by Coleman *et al.* (2005a), where the rate of E2 photocatalysis increased with C_o (0.1 to 3 μM) and plateaued at high concentration, due to the catalyst surfaces becoming saturated with E2.

The activity of photocatalysts is also influenced by the pH of water. TiO_2 is amphoteric and has a point of zero charge (PZC) at pH 6.5 (Rincón and Pulgarin, 2004), hence remaining positively charged in acidic conditions while being negative in alkaline conditions. As noted in Section 2.3.1.2, the estrogenic steroidal hormones bear negative charge under alkaline medium due to their pK_a being ~10.4. Therefore, the pollutants and the catalyst may repel each other leading to a drop in photodegradation efficacy. Coleman *et al.* (2000) examined E2 photocatalysis using immobilized TiO_2 in the range pH 1-12. The rate of removal increased up to pH 7, followed by a drop until pH 10, and then increased again up to pH 12. The rise in pH led to more OH^-, hence an increase in $^\bullet OH$. The ionisation of the E2 phenol group to phenoxide at pH 10 led to more competition for OH^-, and at the same time OH^- repulsion resulted through the deprotonation of surface-bound hydroxyl groups. The increase up to pH 12 was attributed to a different mechanism. An unprotonated hydroxy radical O^- can react with the phenoxide ion to produce a neutral phenoxy radical PhO, which can then react directly at the TiO_2 surface without any repulsive effect. Similarly Zhang *et al.* (2007) tested the effect of pH between 2 and 10 on E1 and E2 removal under UV/P25 and observed a rise in rate constant up till pH 7.6 as a result of the formation of more $^\bullet OH$; but above pH 7.6, the rate constant decreased due to the repellence between pollutants and the catalyst.

2.4 Photodegradation kinetics

Based on the available literature, the photodegradation of estrogenic steroidal hormones using photocatalysis follows mostly 1st order or pseudo - 1st order kinetics (Tables 2.3 – 2.6), and the reaction rate (*r*) can be derived using the Langmuir-Hinshelwood (L-H) model:

$$r = k\frac{KC}{1+KC} \quad (5)$$

Where *k* is the reaction rate constant, C is the concentration of substrate and K is the adsorption coefficient. As the concentration of the steroidal hormones in surface water and wastewater is very low (ng l^{-1} or less to μg l^{-1}) and their adsorption onto the surface of the catalyst is considered negligible, KC << 1. Therefore,

$$r = kKC = k_{app}C \quad (6)$$

where k_{app} is the apparent reaction rate constant.

Pseudo-1st order kinetics is described as:

$$ln\left(\frac{C}{C_o}\right) = -kt \quad (7)$$

where *k* is the pseudo - 1st order degradation rate constant.

The half-life ($t_{1/2}$) of the reactants is:

$$t_{1/2} = \frac{ln2}{k} \quad (8)$$

The rate of photodegradation depends on various factors as discussed earlier. In addition, sampling and analytical techniques could also lead to differences in kinetic data. Most studies found the photodegradation rate to decrease in the order of E1 > EE2 > E2 > E3 for both photolysis and TiO_2 photocatalysis (Table 2.9). For example, Coleman *et al.* (2005a) observed the highest photolytic and photocatalytic degradation

rate for EE2 followed by E2 and the slowest rate for E3. The rapid removal of EE2 was attributed to its instability due to the presence of the ethynyl group, which strongly absorbs UV light. On the other hand, the addition of OH groups may make the phenolic rings more stable, resulting in a considerable drop in the removal rate of E2 and a significant decrease for E3. However, EE2 is more resistant to biodegradation than E1 and E2 due to the presence of the ethynyl group at C17 (Clouzot *et al.*, 2008; Zuo *et al.*, 2013). Therefore, the removal rate of steroidal hormones in natural water depends on the synergetic effect of both photodegradation and biodegradation. Different trends have been reported for these processes. For example, slightly higher removal constants were reported for E1 and E2 compared to EE2 in a photocatalytic reactor membrane pilot system (Benotti *et al.*, 2009). The removal of EDCs was considered to be due only to photodegradation, since the pre-chlorinated river water was circulated for two days before measuring the initial EDC concentrations.

Table 2.9. Hormones in decreasing order of degradation rate constant and/ or increasing $t_{1/2}$.

Photolysis		**TiO_2 photocatalysis**	
Hormones	**Reference**	**Hormones**	**Reference**
E1> E2	Liu and Liu (2004)	E1> E2	Zhang *et al.* (2007)
E1> EE2	Atkinson *et al.* (2011)	E1≈ E2	Zhang and Zhou (2008)
EE2> E2	Rosenfeldt and Linden (2004)	E1≈ E2	Nakashima *et al.* (2003)
E1> EE2> E2	Whidbey *et al.* (2012)	E1> EE2> E2	Tanizaki *et al.* (2002)
EE2> E2> E3	Coleman *et al.* (2005a)	E1≈ EE2> E2	Coleman *et al.* (2004)
E1> E2> E3	Zhang *et al.* (2012c)	EE2> E2> E3	Coleman *et al.* (2005a)
E1> EE2≈ E3≈ E2	Lin and Reinhard (2005)	E1> E2> E3	Zhang *et al.* (2012b)
E3> E1> E2> EE2	Fonseca *et al.* (2011)	E1>EE2> E2> E3	Puma *et al.* (2010)
EE2> E1> E2	Coleman *et al.* (2004)	E1> E2> EE2	Benotti *et al.* (2009)
		E2> E1> E3	Zhang *et al.* (2012c)

2.5 Formation of intermediates and degradation pathways

It is evident from the discussion above that the removal of EDCs depends on treatment conditions; hence there is no universal reaction pathway for their photo transformation. Major challenges exist in identifying intermediates and the degradation mechanism/s. The detection and quantification of degradation products is challenging due to their low ambient concentrations and the complexity of the solution matrix (Chen *et al.*, 2009). Therefore, most studies have been conducted at elevated concentrations of these estrogenic compounds. On the other hand, advances in analytical techniques have led to the identification of photoproducts to a certain extent. For example, a photoelectrochemical sensor with a high selectivity towards E2, was developed recently with a limit of detection of 33 fM for E2 (Fan *et al.*, 2014). The most commonly employed techniques for the analysis of EDCs at low concentrations are GC-MS, GC-MS/MS, LC-MS, LC-MS/MS or other similar hyphenated instruments (de Witte *et al.*, 2011; Liu *et al.*, 2011; Ribeiro *et al.*, 2015). A comparison of such techniques was provided by Grover *et al.* (2009). Detailed reviews of the analytical techniques used for the identification of the intermediates formed during AOPs can be found elsewhere (Briciu *et al.*, 2009; de Witte *et al.*, 2011; Kozlowska-Tylingo *et al.*, 2010)

E1 has been shown to convert into the photoproduct lumiestrone (estra-1,3,5(10)-trien-17-one,3-hydroxy-,(13α)-(9CI)), the 13 α-epimer form of E1 (Trudeau *et al.* (2011) within 5 min under illumination (Figure A1). Total degradation of E1 and then of lumiestrone was observed after further illumination. Whidbey *et al.* (2012) tested the direct photolysis of E1 in a solar simulator and observed a notable peak corresponding to lumiestrone under HPLC/UV with a 53% net yield of lumiestrone. Caupos *et al.*

(2011) identified photoproducts of E1 (Figure 2.2) with or without DOM in water, under simulated solar light. A photoproduct formed in the absence of DOM was assigned the structure S2-1 (Figure 2.2), a tautomer of E1. A further four photoproducts were attributed to the presence of DOM, since the products were not detected when the experiments were conducted in pure water. The photoproducts were formed by hydroxylation on C2 (S2-2), C4 (S2-3), C6 (S2-4) and C9 (S2-5) positions of E1 (Figure 2.2). When conducting photodegradation experiments on E1 in a solar simulator, Chowdhury *et al.* (2010) observed a substantial difference between the percentage degradation (98.6±1%) and complete mineralisation efficiency (27±1.1%) and indicated that though E1 was quickly degraded, intermediates were more difficult to degrade further. Phenylacetic acid was the key intermediate. As the light intensities were varied, the maximum concentration of intermediates and the time taken to attain those concentrations differed. Overall, though the aforementioned studies show that E1 forms photoproducts during photolysis, many of the resultant intermediates still retain moderate estrogenic activity, especially in the case of lumiestrone.

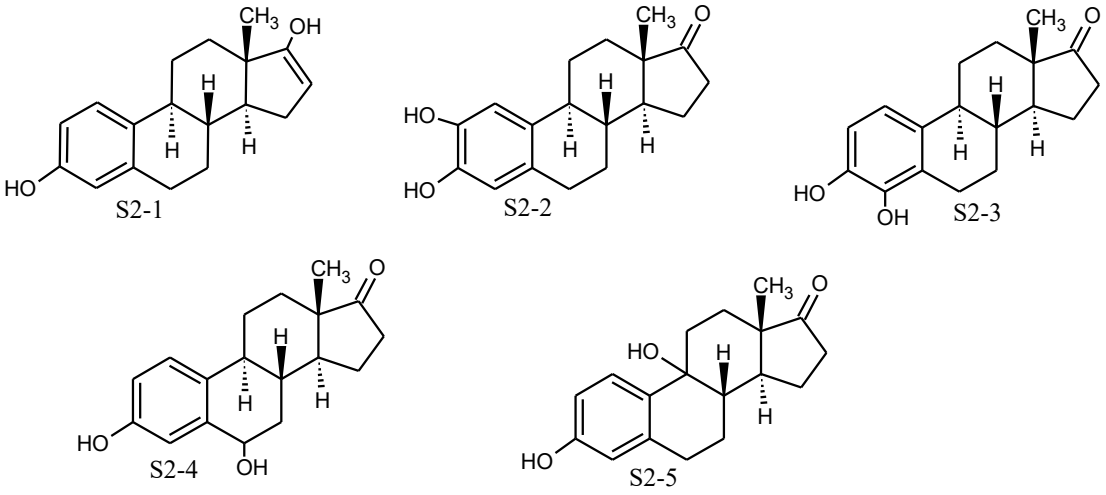

Figure 2.2. Proposed chemical structures of E1 photoproducts. Redrawn from Caupos *et al.* (2011).

Overall, estrogenic activity has been attributed to the interaction of the phenolic moiety with estrogen receptors (Brzozowski *et al.*, 1997; Mboula *et al.*, 2015). Some intermediates possess estrogenicity and are difficult to be degraded further. For example, the photoproduct of E1, lumiestrone, displayed moderate estrogenicity and was quite resistant to further oxidation. Different degradation mechanisms have been reported for E2 but most studies reported the formation of a common intermediate, 10Ɛ-17β-dihydroxy-1,4-estradien-3-one, by the oxidation of the phenol moiety of E2 to a quinone-like moiety (Mai *et al.*, 2008; Mboula *et al.*, 2015; Ohko *et al.*, 2002). E1 was also identified as an intermediate of E2 photodegradation (Mazellier *et al.*, 2008). Similar degradation mechanisms to that of E2 were reported for EE2 (Mai *et al.*, 2008; Sun *et al.*, 2010).

2.6 Au-TiO_2 nanocomposites

Research involving noble metals and TiO_2 composites has attracted much interest recently, especially the use of Ag, Au and Pt. In particular, gold is an attractive option

due to its non-toxicity, stability and biocompatibility (Ayati *et al.*, 2014). Most importantly Au nanoparticles strongly absorb light in the range 520-560 nm wavelength due to localised surface plasmon resonance (LSPR), hence enhancing the visible light activity of photocatalysts (Hidalgo *et al.*, 2009; Primo *et al.*, 2011; Silva *et al.*, 2011; Sonawane and Dongare, 2006; Wu *et al.*, 2009c).

Though bulk Au has low reactivity, studies have shown that it acts as a catalyst in nanoparticulate form. This phenomenon was first reported by Haruta *et al.* (1987) for the oxidation of carbon monoxide. Gold nanocatalysts are useful for the production of H_2 (Priebe *et al.*, 2015), reduction of NO_X (Nguyen *et al.*, 2008), oxidation of CO and in water treatment, for instance azo-dye degradation (Arabatzis *et al.*, 2003) and removal of p-nitrophenol (Ismail *et al.*, 2012).

The addition of gold to TiO_2 enhances its photoactivity in the abatement of water contaminants. Data for model compounds such as methylene blue and methylene orange are shown in Table 2.10. On the other hand, negative effects of Au doping on TiO_2 has also been reported (Carneiro *et al.*, 2009). Therefore, the activity of Au-TiO_2 depends on the preparation techniques employed. In terms of catalyst synthesis, the conditions used such as pH, preparation, drying and calcination temperatures, the type of Au precursor, the type of TiO_2 used (e.g. anatase, rutile or P25) and the percentage of Au doping can all influence the activity. The aforementioned factors can affect the particle size of Au, which has significant impact on photocatalysis. An increase in size generally leads to a decrease in activity and Au particles above 20 nm become very less active (Primo *et al.*, 2011).

Table 2.10. Photocatalysis using Au-TiO_2 catalysts Reproduced from Ayati *et al.* (2014)

Catalyst	Pollutant	Catalyst synthesis method	Light	Removal conditions	Reference
Au/TiO_2	Methyl Orange	Impregnation, DP	UV	Loading: 0.1–8 wt%, calcination: 200–500 ^oC	Tian *et al.* (2008)
Au/TiO_2	Methyl Orange	DP	UV	pH :2, loading: 0.25–1.5 wt%	Oros-Ruiz *et al.* (2012)
Au/TiO_2	Methyl Orange	–	UV, Visible	–	Hou *et al.* (2011)
Au/TiO_2	Methyl Orange	Photodeposition	UV		Khan *et al.* (2012)
Au/TiO_2	Methylene Blue	DP	UV	Calcination: 500–700 ^oC	Haugen *et al.* (2011)
Au/TiO_2	Methylene Blue	Sol–Gel	UV	pH = 5.98, loading: 0.5 wt%	Li and Li (2001)
Au/TiO_2	Methylene Blue	DP	UV	Loading: 0.25–1 wt%	Wang *et al.* (2012)
Au/TiO_2	Methylene Blue	DP	UV	Loading: 0.25–5 wt%	Wang *et al.* (2008b)
Au/TiO_2	Acid Red 1	DP	UV	pH: 3–10, loading: 0–20 wt%	Mrowetz *et al.* (2007)
Au/TiO_2	Acid Red 88	DP	Visible	pH: 7, loading: 8 wt%, calcination: 250 ^oC, C_o: $1x10^{-5}$-$9x10^{-5}$M, Au-TiO_2: 0.6- 2.7 gl^{-1}	Sathishkumar *et al.* (2008)
Au/TiO_2	Orange 16	DP	UV	pH: 3–12, loading: 1–2.5 wt%, Co: 20–120 µM, Catalyst: 0–3.5 gl^{-1}.	Hsiao *et al.* (2011)
Au/TiO_2	Tartazine	Photodeposition	UV, Visible	pH = 7	Rupa *et al.* (2009)
Au/TiO_2	Phenol	Sol–gel	UV	Calcination: 120–400 ^oC	Su *et al.* (2012)
Au/TiO_2	Phenol	DP, photodeposition	UV	Loading: 0.5–1.5 wt%	Hidalgo *et al.* (2009)
Au/TiO_2	Phenol	Photodeposition	UV	Loading: 0.5–2 wt%	Hidalgo *et al.* (2011)
Au/TiO_2	Phenol	DP	UV	Loading: 0.5–5 wt%	Zhao *et al.* (2011)

Catalyst	Pollutant	Catalyst synthesis method	Light	Removal conditions	Reference
Au/TiO_2	4-Chlorophenol	Sol–gel	UV	Loading: 0.05–1.5 wt%	Wongwisate *et al.* (2011)
Au/TiO_2	4-Chlorophenol	DP, photodeposition, colloidal deposition	UV	Loading: 0.25–1.5 wt%, Au particle size: 6–12 nm	Oros-Ruiz *et al.* (2011)
Au/TiO_2	4-Chlorophenol	DP	UV	Loading: 0.42–0.55 wt%	Orlov *et al.* (2006)
Au/TiO_2	4-Chlorophenol	DP	UV	Loading: 0–5.5 wt%	Orlov *et al.* (2004)
Au/TiO_2	2,6-di-tert-butyl phenol	DP	–	–	Cheneviere *et al.* (2010)
Au/TiO_2	2,3,6-trimethyl phenol	DP	–	–	Cheneviere *et al.* (2010)
Au/TiO_2	MTBE	DP	UV	Loading: 0.42–0.55 wt%	Orlov *et al.* (2006)
Au/TiO_2	MTBE	DP	UV	Loading: 0.5–5.5 wt%	Orlov *et al.* (2007)
Au/TiO_2	3,4-dichlorophenylurea	DP	UV	Loading: 0.83 wt%, calcination: 623–973 ^oC	Chusaksri *et al.* (2011)
Au/TiO_2	Sulforhodamine-B	Impregnation	UV		Zhu *et al.* (2009)
Au/TiO_2	1,4-dioxane		UV	Loading: 1 wt%	Min *et al.* (2009)
Au/TiO_2	L-asparagine, L-glutamic acid		UV	Loading: 2.7 wt%	Dolamic and Büergi (2011)
Au/TiO_2 nanotube	Acid Orange 7	–	UV	–	Paramasivam *et al.* (2008)
Au/TiO_2 nanotube	Acid Red G, Methylene Blue	–	UV	–	(Zhang *et al.*, 2012a)
Au/TiO_2 nanotube	Methyl Orange	Photodeposition	UV		Zhao *et al.* (2009b)
Au/TiO_2 nanofibers	Methylene Blue		Solar		Thomas and Yoon (2012)
Au nanotube/ TiO_2 nanotube	Acid Orange 7	Eletrodeposition	Visible	Loading: 2.5–10 wt%	Luo *et al.* (2011)
Au nanotube/ TiO_2 nanotube	Cr (VI)	Eletrodeposition	Visible	Loading: 2.5–10 wt%	Luo *et al.* (2011)
Au/TiO_2 thin film	Phenol	Sol–gel	Sun	Loading: 1–2 wt%, calcination: 275–500 ^oC	Sonawane and Dongare (2006)

2.6.1. Preparation methods of Au-TiO_2

The activity of Au based catalysts strongly depends on the preparation methods used. Several techniques such as anion adsorption, cation adsorption, incipient wetness impregnation (Bowker *et al.*, 2007), photodeposition, deposition-precipitation, co-precipitation and chemical vapour deposition have been developed to enhance the performance of Au-TiO_2. Among these methods DP remains by far the best, since smaller Au nanoparticles (2-3 nm) could be synthesised.

2.6.1.1 Anion adsorption

The catalysts were prepared at pH 2, lower than the isoelectric point of TiO_2, which was around pH 7 (Fernández-Ibáñez *et al.*, 2003). The detailed synthesis of Au-TiO_2 by anion adsorption is outlined in Zanella *et al.* (2002). In summary, 1g of TiO_2 was added to 100 ml of 4.2 x 10^{-3} M $HAuCl_4$ aqueous solution (to obtain 8 wt.% Au theoretical loading) thermostated at 80 ºC, stirred for 15 h, centrifuged, washed with water, dried and calcined at 300 ºC.

2.6.1.2 Cation adsorption

The precursor complex $[Au(ethanediamine)_2]^{3+}$ (100 ml, 4.2 x 10^{-3} M) was added to 1g TiO_2 and the pH is adjusted to pH 10.3 (above the isoelectric point of TiO_2) through the addition of ethanediamine drops. Stirring and the steps that follow were similar to those of anion adsorption (Block and Bailar, 1951; Zanella *et al.*, 2002).

2.6.1.3 Incipient wetness impregnation

The gold precursor solution $HAuCl_4$ was added to the TiO_2 support, where the volume of $HAuCl_4$ was equal to the pore volume of TiO_2, so as to fill the pores with the

solution via capillary action. The volatile components were removed by drying followed by calcination. For instance, Bowker *et al.* (2007) prepared Au/TiO_2 by adding 1.25 ml (0.08g/ml) $HAuCl_4.3H_2O$, followed by the addition of 1.43ml (1M) Na_2CO_3 while stirring. Then the mixture was washed on vacuum filter 5 times (with 14ml Na_2CO_3 + 100ml H_2O) and was washed 5 times with 100ml water. The catalysts were dried overnight at room temperature and at 120 ºC for 2 h and finally the samples were calcined at 400 ºC for 2 h.

The catalysts synthesised through this method displayed poor activity as a result of poisoning and sintering of Au particles due to the presence of chloride ions. Also, this method did not result in high dispersion of Au particles, thus reducing the catalyst efficiency (Wolf and Schüth, 2002). Modified impregnation techniques have also been reported with improved catalyst activity. For example, Li *et al.* (2006) utilised a procedure in which $Au(OH)_3$ was deposited within TiO_2 pores, hence eliminating the problematic Cl^- ions.

2.6.1.4 Coprecipitation

The method developed by Haruta *et al.* (1989) is as follows: $HAuCl_4$ aqueous solution and a metal nitrate solution were added to Na_2CO_3 while stirring. The precipitate obtained was washed and dried under vacuum and calcined at 400 ºC for 4 h in air.

2.6.1.5 Chemical Vapour Deposition

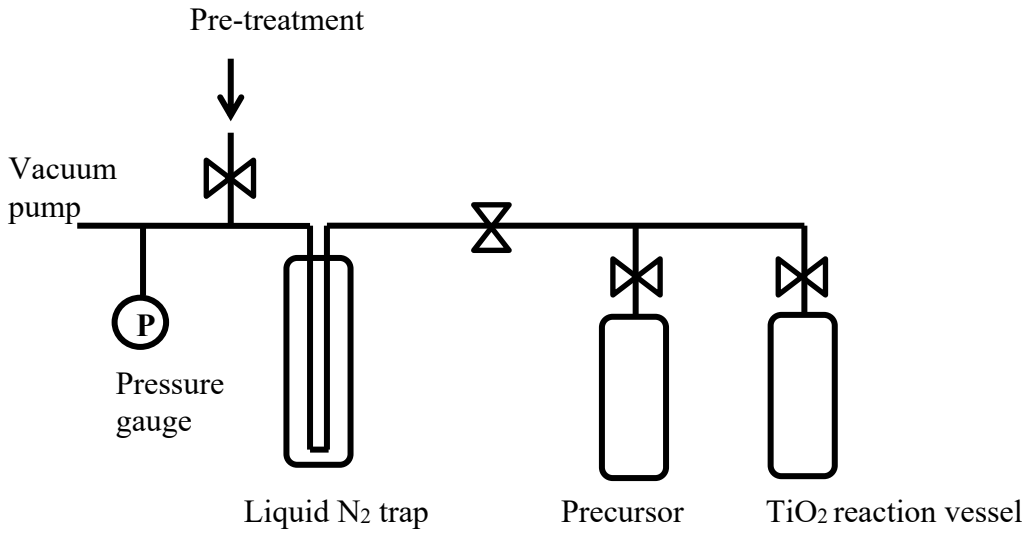

Figure 2.3. Schematic diagram of chemical vapour deposition. Redrawn from Okumura *et al.* (1997).

Okumura *et al.* (1997) developed Au/TiO_2 catalysts by using the chemical vapour deposition method as shown in Figure 2.3. In summary, the volatile precursor $(CH_3)_2Au(CH_3COCH_2COCH_3)$ is heated from 28 to 45 ^oC fixed temperature, which in turns evaporates the Au precursor gradually, that gets absorbed onto TiO_2 surface in the reaction vessel kept at 33 ^oC. The as prepared catalysts are calcined at 200 ^oC to remove the organic ligands.

2.6.1.6 Photodeposition

A suitable light source (e.g. 300W Xe lamp) was used to irradiate the TiO_2 solution, hence generating electrons and holes. The Au precursor ($HAuCl_4$) added to the solution will be reduced by the electrons formed, resulting in Au metal deposition on TiO_2 surface, while the holes are scavenged by an alcohol (e.g. methanol, isopropanol). The Au-TiO_2 catalyst was obtained by stirring the system for a fixed

time (e.g. 2 h) followed by filtration and drying (Hidalgo *et al.*, 2009; Priebe *et al.*, 2015). However the Au particles produced by this method was relatively larger in size (10- 30nm) (Primo *et al.*, 2011).

2.6.1.7 Deposition- Precipitation (DP)

DP is the most commonly utilised method for the preparation of Au-TiO_2 due to its benefits such as the formation of smaller Au nanoparticles (2-3 nm), higher yield, higher Au loading, formation of active catalysts and reproducibility (Hammer *et al.*, 2007; Primo *et al.*, 2011). The DP procedure is discussed in detail in Section 4.2.2. Briefly, NaOH was added drop wise to bring the pH of $HAuCl_4$ solution thermostated at 80 ^oC to pH 8, then TiO_2 is added, stirred for 4 h, washed 4 times, dried and calcined at 300 ^oC for 4h (Haruta, 1997). The above synthesis could also be carried out with urea in place of NaOH (Zanella *et al.*, 2002).

2.6.2 Factors affecting Au-TiO_2 catalyst activity

2.6.2.1 Catalyst preparation method

The preparation methods as discussed above affect the efficiency of the Au/TiO_2 catalyst mainly through factors such as the gold particle size and the interaction between the TiO_2 support and gold. Zanella *et al.* (2002) studied different methods of preparation such as DP with NaOH, DP with urea, incipient wetness impregnation, anion adsorption and cation adsorption. The results DP urea method was the most efficient method with smaller Au particle size (~2 nm), higher yield (~100%) and higher Au loading. Meanwhile, Au-TiO_2 synthesised by anion adsorption resulted in low Au loading (~1.5 *wt.*%) with the average Au particle size of 4 nm. On the other hand, though cation adsorption led to smaller Au particle size (2 nm), Au loading did

not surpass 2 *wt.*%. In terms of incipient wetness impregnation, a significant amount of Au was lost while washing, with only about 0.9 *wt.*% of Au remaining regardless of initial concentration of Au. Therefore, though this result suggests a strong interaction between TiO_2 and Au, higher loading could not be achieved.

2.6.2.2 Preparation conditions

Using DP with NaOH, Zanella *et al.* (2002) found that the pH of DP solution, the initial concentration of Au precursor, DP time, the addition of magnesium citrate and calcination temperature all had an influence on Au nanoparticle size and loading. For a theoretical addition of 8 *wt.*% Au, higher loading of 3.3 *wt.*% with smaller Au particle size of 1.4 nm was formed at pH 7, while pH 8 resulted in 1.8 *wt.*% with 1.8 nm Au NPs. A marginal rise of 1.8 to 2.4 *wt.*% in Au loading was observed with an increase of DP time from 1 to 16h, with a drop in particle size from 1.8 to 1.5 nm. The addition of magnesium citrate enhanced Au loading, with lower particle size, due to the avoidance of sintering in calcination. Also studies have found that calcination temperatures between 200 ºC (Ide *et al.*, 2013) and 400 ºC (Wu *et al.*, 2009c) as ideal, while further increase in temperature led to both sintering of gold and in the transition of anatase to rutile. For instance, Tian *et al.* (2008) reported an increase in photodegradation rate of methylene orange with an increase in Au-TiO_2 calcination temperature from 100 to 300 ºC, though the removal efficiency dropped with further increase in temperature.

2.6.2.3 Level of gold loading

Various studies have reported different optimum Au loadings (Table 2.10). The values differ depending on the target compounds, catalyst preparation methods and

experimental conditions used. For instance, Orlov *et al.* (2007) found out that for an Au loading 0 - 5.5 *at*.%, the optimum photodegradation of methyl tert-butyl ether was achieved at 0.55 *at*.% Au loading, with a three times enhancement compared to that of the unmodified TiO_2. The authors attributed this increase in activity to the smaller particle size of Au ≤ 3 nm, below which Au may not be metallic and to the electron transfer from semiconducting Au to the CB of titania. In another study, Oros-Ruiz *et al.* (2011) observed that 0.5 *wt.*% Au loading provided the best results for 4-Chlorophenol with an 80% rise in photodegradation compared to commercial TiO_2, in the range 0 - 1.5 *wt.*% Au content prepared by DP method. However, 1.5 *wt.*% Au loading had a negative impact on photocatalysis.

It can be concluded that the activity of Au/TiO_2 increases up to a certain Au loading beyond which it decreases. Also the amount of Au loading has an impact on its particle size, where the loading which gives the smallest particle size is generally desired. An increase in Au loading also reduces the effective surface area available for photocatalysis, leads to aggregation of Au particles, blocks the TiO_2 pores, reduces the penetration of light and acts as e-h recombination centres, thus reducing the overall activity (Wu *et al.*, 2009c; Zhu *et al.*, 2012).

2.6.2.4 Gold nanoparticle size

Small Au nanoparticles (<20 nm) on TiO_2 surfaces yield photoactive catalysts, with the optimum Au size being <5 nm (Haruta, 1997). The Au particle size can be controlled as described in Section 2.6.1. An increase in Au nanoparticle size has similar disadvantages to that of elevated Au loadings, especially through the blocking the active sites of TiO_2 support (Tian *et al.*, 2008). However, Kowalska *et al.* (2009) reported effective visible light photocatalysis of 2-propanol under Au/TiO_2 with Au

nanoparticle size of 30 - 60 nm, while observing negligible visible activity for Au-P25 fine particulates. The authors attributed this trend to the higher photoabsorption ability of larger Au nanoparticles in a wider wavelength range.

2.7 Immobilisation of catalysts

2.7.1 Suspended vs. immobilised catalysts

Most photocatalytic systems for estrogenic steroidal hormones have utilised suspended photocatalysts while a few have used immobilised catalysts (Tables 2.4 and 2.5). Both approaches have strengths and weaknesses. Suspended systems are more efficient compared to immobilised systems based on the same quantity of catalyst. This is mainly due to the dispersed catalyst particles having considerably higher available surface area, which in turn allows for better mass transfer processes. The main drawback of suspended systems is the economically unfeasible recovery of the suspended catalysts from the slurry after the completion of the photodegradation process.

In the immobilised mode the catalyst is generally supported on a surface, for example, by coating on materials such as glass (Mizuguchi *et al.*, 2006), ceramic, metal (Coleman *et al.*, 2000), quartz (Tanizaki *et al.*, 2002) or polytetrafluoro ethylene (PTFE) (Nakashima *et al.*, 2003). The advantage of this mode is the elimination of a catalyst recovery stage, making it a commercially viable application, although its catalytic efficiency is less than that of the suspended mode. In addition, immobilisation also has some other limitations, such as the loss of catalytic activity during their addition onto the support, fouling and/or deactivation due to the blockage of the

catalyst surface with pollutants or their transformation products, and leaching of the catalysts into the aqueous medium with time.

2.7.2 Photocatalyst supports

Different types of anchors are used to immobilise TiO_2 photocatalysts as discussed in Section 2.7.1. Here, the most commonly used substrates are briefly discussed. A detailed review of the types of supports used for immobilisation of TiO_2 along with the various techniques used for immobilising the catalysts could be found elsewhere (Shan *et al.*, 2010).

2.7.2.1 Glass

Borosilicate glass is the most commonly used anchor for TiO_2 based photocatalysts due to a number of reasons: Glass can handle high calcination temperatures, which is required for successful TiO_2 catalyst synthesis. Glass is inert, hence avoids any reaction with the catalysts or the pollutants. They are also transparent thus allows efficient light transfer. The shape/structure of the glass is determined based on the type of the photoreactor and/or the light sources used. Few such common shapes include glass beads (Denny *et al.*, 2009), glass tubes, reactor walls (Coleman *et al.*, 2007), glass plates/slides (Zainal *et al.*, 2005) and rings (Lizama *et al.*, 2001).

Coleman *et al.* (2007) prepared two types of immobilised TiO_2 catalysts, one using a sol-gel method and the other by coating the inner wall of the reactor with P25. The efficiency of the above systems was compared for the removal of E2, E3 and EE2. For example, the P25 coated reactor was 2.5 times more efficient compared to the one prepared by the sol-gel technique in removing E3 due to the higher activity of P25. However, the authors noted immobilisation using the sol-gel method as the most

suitable type for commercial applications since TiO_2 could not be easily removed from the reactor. Similarly, immobilisation of P25 on a hollow glass cylinder by a dip coating method proved to be an efficient method in removing 95% of E1, E2 and E3 in 100 min under UVA (Zhang *et al.*, 2012c).

A few recent studies using ZnO immobilised systems have also demonstrated considerable activities (Table 2.5). For example, ZnO nanorod arrays grown on glass substrate removed 87% of E1 in 6 h (Liu *et al.*, 2012a). Koutantou *et al.* (2013) reported 80% degradation of EE2 in 90 min with ZnO immobilized onto glass plates by heat attachment, but Zn leaching was also detected.

2.7.2.2 Other TiO_2 supports

Activated carbon is another commonly used anchor to immobilise TiO_2 catalysts (El-Sheikh *et al.*, 2007). The main advantages of activated carbon is the availability of high surface area, which enhances photocatalytic activity, by providing good interaction between the catalyst and the pollutants. However, the high adsorption ability of activated carbon may hinder the diffusion of the pollutants to the catalyst, thus slowing down the photocatalysis process (El-Sheikh *et al.*, 2007).

Polymer based supports have also been studied (Damodar and Swaminathan, 2008; Lei *et al.*, 2012). Such polymers include polyethylene films, polystyrene beads, PVC among others. They are an attractive choice due to their inertness, stability and affordability (Fabiyi and Skelton, 2000).

2.8 Optical Fibres for photocatalysis

Optical fibres are thin (μm diameter) glass/polymer fibres that are used to transmit light over long distances (up to thousands of km). The propagation of light through

optical fibres is based on total internal reflection that takes place at the boundary/interface of two mediums when the light passes from a medium with high refractive index towards a medium with low refractive index, if the angle of incidence is greater than the critical angle. Total internal reflection is achieved in optical fibres as the core is made of high index material covered by a material (known as cladding) that has low index. Generally, the optical fibre is coated with an optically inactive protective material. Acceptance angle of a fibre is the maximum angle at which the light can enter the fibre for transmittance along the fibre instead of passing through the sidewalls.

The use of optical fibres in TiO_2 photocatalysis started in the 1970s (Marinangeli and Ollis, 1977). Optical fibres allow the light to be transmitted to longer distances with minimum loss, potentially making bench studies practical in real environments. The catalysts could either be immobilised onto the fibres (Lin *et al.*, 2015a; Lin *et al.*, 2017; Sun *et al.*, 2000) or the light emitted by the fibres could be cast to the catalysts coated on another surface (Denny *et al.*, 2009; Lin and Valsaraj, 2005). However, end emission from the fibres is insufficient to activate large surface areas of the catalysts. A few studies have used side emitting optical fibres to address the aforementioned issues. On the other hand, most of the light in these fibres propagates in the forward direction, hence resulting in only a small portion of side emission, which may be insufficient for excellent photocatalytic activity. In addition, the light cannot be transmitted for longer distance as a result of the loss due to side emission. Therefore, new techniques to attain sufficient side emission from optical fibres is required. Novel engineered air-clad optical fibres that provide efficient side emission of light is used in this work.

2.9 Summary

Estrogenic steroidal hormones are a group of EDCs known to induce adverse effects on living organisms even at trace levels. TiO_2 remains the best choice of catalyst for the removal of the EDCs under UV light, mainly due to its superior activity, chemical and photo stability, cheap commercial availability, capacity to function at ambient conditions and low toxicity. However, sunlight contains only a small percentage of UV (~ 4%), thus visible light active photocatalysts are attractive candidates to facilitate efficient processes. This study utilises gold modified TiO_2 catalysts to attain visible light activity. The research also investigates the changes in photodegradation rates of the pollutants under different light sources and water matrices and identifies degradation by-products.

Suspended catalysts prove to be more efficient in the photocatalytic removal of EDCs compared to immobilised catalysts but the latter are considered more suitable for commercial scale applications. Therefore, TiO_2 catalysts immobilised onto borosilicate glass beads are examined in this work. Another challenge faced by the existing photocatalysis technologies is the limitation of light sources that may be used underwater efficiently. Therefore, this research uses a novel technique to modify air-clad optical fibres to transmit light efficiently underwater. The use of waterproof LED strips have also been investigated.

Chapter 3: Materials and methods

Chapter 3: Materials and methods

3.1 Introduction

This chapter presents the chemicals and materials used for conducting experiments, the equipment used in evaluating the experimental results and the experimental setups.

3.2 Experimental materials

3.2.1 Chemicals

The chemicals used along with their purity (if specified) and their suppliers are listed in Table 3.1.

Table 3.1. List of chemicals and materials.

Compound	Supplier	Purity (%)
Acetonitrile	Sigma-Aldrich	UHPLC- MS
Estriol	Sigma-Aldrich	≥97%
Estrone	Sigma-Aldrich	≥99%
Gold granules	AGS Metals	99.99%
Hydrochloric acid (36%)	RCI Labscan	
Hydrofluoric acid (48%)	Sigma-Aldrich	
Methanol	Fisher Scientific	Optima LC/MS grade
Nitric acid (70%)	RCI Labscan	
Paint stripper	Bunnings warehouse	
Potassium permanganate	BDH	
Rhodamine B	Ajax Chemicals	
Sodium hydroxide	Chem-Supply	
Sodium thiosulfate pentahydrate	Ajax chemicals	
TiO_2 (Aeroxide P25)	Sigma-Aldrich	≥99.5%
Ultrapure water (Milli-Q)	Merck Millipore	18.2 MΩ, 3 ppb TOC
17β-Estradiol	Sigma-Aldrich	≥98%
17α-Ethynylestradiol	Sigma-Aldrich	≥98%

Aeroxide P25 TiO_2

Aeroxide P25 TiO_2 nanopowder (≥ 99.5%, 21 nm primary particle size (TEM) was used to synthesise the gold modified photocatalysts. P25 TiO_2 is a mixture of 80% anatase and 20% rutile with a specific surface area of 35 - 65 $m^2 g^{-1}$ (BET).

3.2.2 Synthetic wastewater

Details of the chemicals used in the preparation of SWW are listed in Table 3.2 below:

Table 3.2. Constituents of synthetic wastewater.

Compound	Concentration (mg l^{-1})	Fraction of organics	Supplier	Purity (%)
Beef extract	1.8	0.065	Chem-Supply	-
Peptone	2.7	0.138	Chem-Supply	-
Humic acid	4.2	0.082	Fluka	80
Tannic acid	4.2	0.237	Sigma-Aldrich	99
Sodium lignin sulfonate	2.4	0.067	Aldrich	-
Sodium lauryl sulphate	0.94	0.042	APS	-
Arabic gum powder	4.7	0.213	Sigma-Aldrich	-
Arabic acid (polysaccharide)	5.0	0.156	Sigma	-
$(NH_4)_2SO_4$	7.1	0	Unilab	98.5
K_2HPO_4	7.0	0	Unilab	99
NH_4HCO_3	19.8	0	Unilab	98
$MgSO_4.7H_2O$	0.71	0	Sigma	≥99.5

3.3 Characterisation techniques

3.3.1 X-ray Diffractometer

Powder XRD patterns were collected using a Bruker D8 Discover diffractometer using Cu Kα radiation, in the scattering angle 2θ range 15 - 90°. Approximately 0.5 g powder samples were placed on the sample holders for XRD analysis.

3.3.2 Raman Spectrometer

Raman spectra were collected using a Renishaw inVia spectrometer (Gloucestershire, UK) with a 17 mW Renishaw He - Ne 633 nm laser and CCD array detector.

3.3.3 UV-Vis Spectrometer

UV-visible absorbance spectra of the pollutants and the catalyst solutions were collected using a Shimadzu 1700 UV-Vis spectrophotometer operating in the wavelength range 190 - 800 nm.

3.3.4 Scanning Electron Microscope and Energy Dispersive X-ray Spectroscopy

The morphology and elemental composition of the catalysts were examined using a Zeiss Supra 55VP SEM (10 kV) and an Oxford energy dispersive X-ray spectroscopy (EDS) system, respectively. SEM/EDS samples were prepared by adding a droplet of sonicated catalyst (in ethanol) onto a silicon wafer which was placed on a carbon tape, followed by drying in air.

3.3.5 Inductively coupled plasma mass spectrometry

An Agilent 7900 ICP-MS was used to measure the gold loadings in the catalysts. Gold in the catalysts was digested using *aqua regia* (5 ml, 1:3 HNO_3: HCl) at reflux (120

°C) for 3 h. The resultant mixture was centrifuged; the supernatant was diluted, filtered with 0.2 PTFE syringe filter and gold concentration was measured by the ICP-MS.

3.3.6 Zetasizer

A Malvern Nano ZS zetasizer (Malvern Instruments Limited, UK) was used in the determination of zeta potential and hydrodynamic particle size of the nanocatalysts. The catalyst solutions of 100 mg l^{-1} concentration were prepared by sonicating the catalyst powders in Milli-Q water. The pH values were adjusted using 0.1 to 1 M HNO_3 or NaOH as required. Measurements were repeated three times and the average values are reported. The standard deviations were less than 5%.

3.3.7 Thermogravimetric Analyser

Thermogravimetric analysis (TGA) was carried out using SDT Q600 (TA Instruments), in which the catalysts (~5 mg) in alumina crucibles were heated in nitrogen gas (25 ml min^{-1}) from 60 °C to 600 °C at 10 °C min^{-1}.

3.3.8 Light Microscope

The cross section of the air-clad fibres before and after collapsing the holes were imaged using Zeiss optical microscope.

3.3.9 Fusion splicer

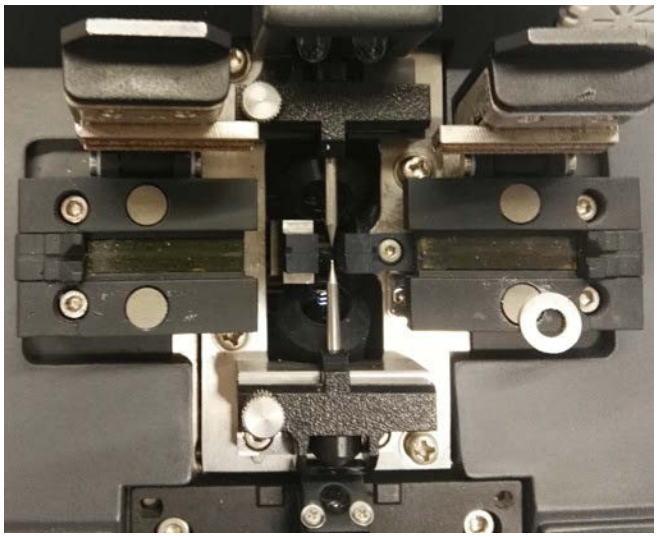

Figure 3.1. A fusion splicer that provides the electric arc required for collapsing the air-cladding.

A FiTel S175 single-fibre fusion splicer (Figure 3.1), which uses a controllable electric arc to melt the glass, was utilised to collapse the air holes. The optimum arc power and arc duration were found through trial and error method.

3.4 Experimental setup for photodegradation studies

3.4.1 Photoreactor for slurry system

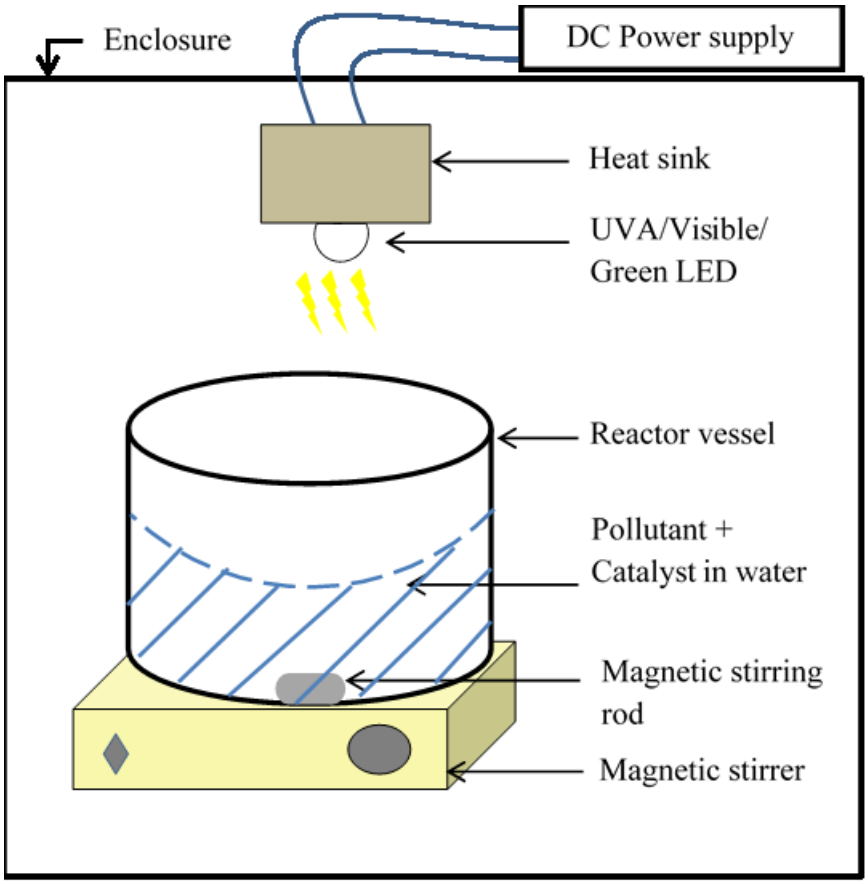

Figure 3.2. Photoreactor for suspended photocatalysis system.

A cylindrical reactor vessel (capacity 900 ml) was used to contain E1 solutions (500 ml, 1000 μg l^{-1}) loaded with 50 mg l^{-1} of catalyst. The slurry was stirred using a magnetic stirrer. An 11W UV LED (λ = 365 nm), cool white (λ > 410 nm) or green (λ = 523 nm) LED (LED Engin) that consisted of a heat sink and connected to a direct current (DC) power supply was placed 5 cm above the liquid surface of the reactor and homogenous mixing was ensured by magnetic stirring. The slurry reactor system is shown in Figure 3.2.

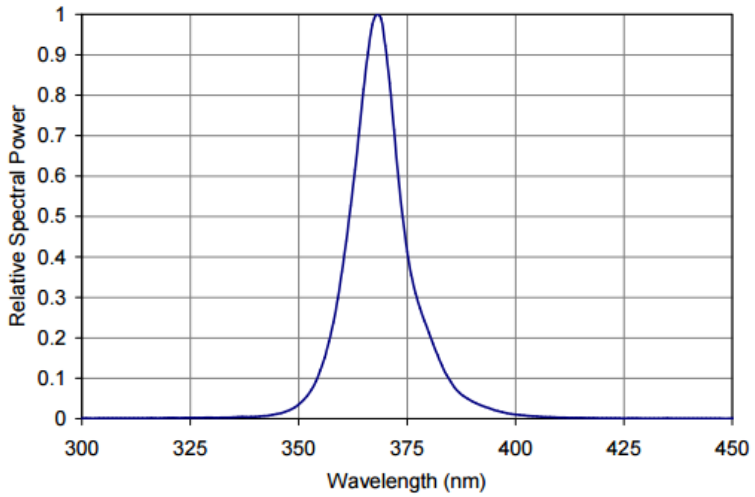

Figure 3.3. Wavelength distribution of UVA LED (from LED Engin).

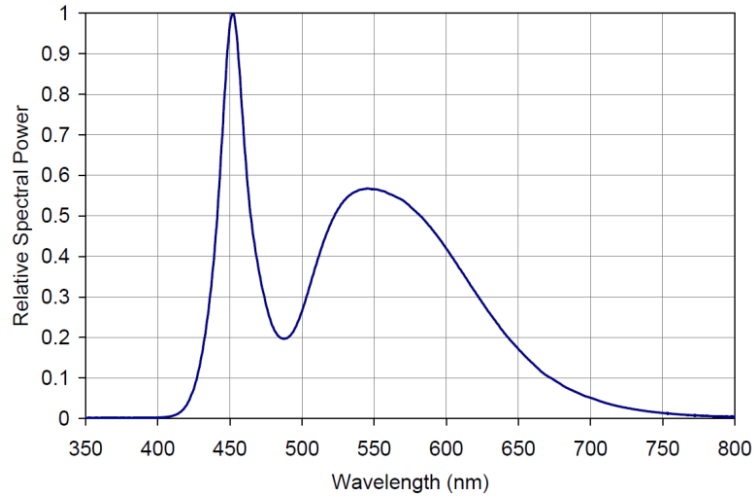

Figure 3.4. Wavelength distribution of cool White LED (from LED Engin).

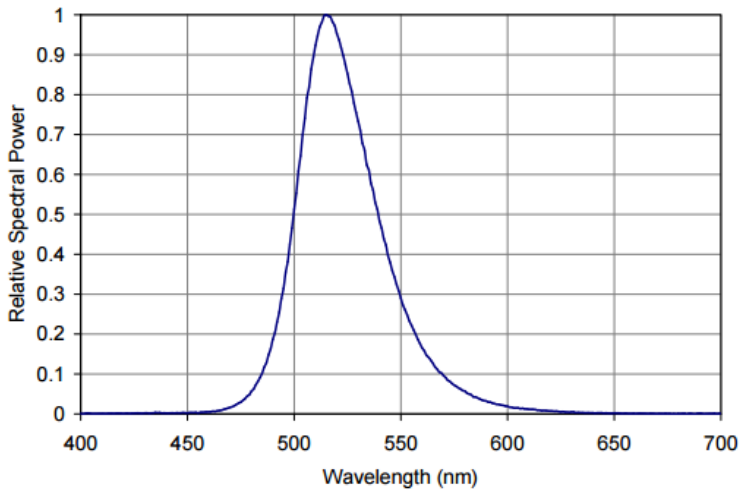

Figure 3.5. Wavelength distribution of green LED (from LED Engin).

3.4.2 Modified air-clad optical fibre photocatalytic reactor setup

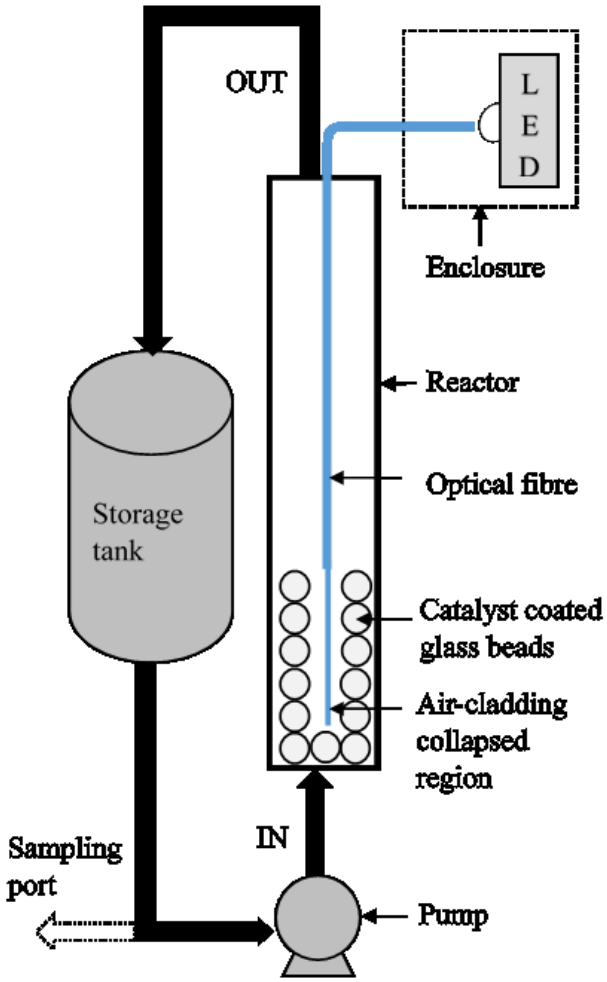

Figure 3.6. Modified air-clad optical fibre photocatalytic reactor setup.

The optical fibre reactor setup is shown in Figure 3.6. An acrylic column with a 12 mm inner diameter and 55 mm in height was used as the reactor. Catalyst-coated glass beads were placed in the reactor, and the modified optical fibres were immersed into the reactor surrounded by the catalyst coated beads. Both the ends of the fibre were hand-cleaved with ceramic tiles to ensure a flat end face so that the fibre could be coupled with the LED for efficient transmission of light and provide a good end emission. Photodegradation studies were conducted using one of the two light sources: 11 W UVA ($\lambda = 365$ nm) or cool white ($\lambda > 410$ nm) LEDs (LED Engin). The emission

spectra of the lamps are provided in Figures 3.3 - 3.4. The light source was isolated from the reactor to ensure that the light received by the catalysts was transmitted solely through the fibre. The reactor was flushed with ultrapure water prior to starting the experiment. A total volume of V = 200 ml EE2 solution was circulated (using Watson-Marlow peristaltic pump) through the reactor for 30 min in the dark to attain adsorption-desorption equilibrium. Measurements under darkness were conducted for 2 h to find the equilibrium time and 30 min was chosen, since the concentrations of the pollutants did not change after the first 20 minutes. Samples were withdrawn at specified intervals, filtered through 0.20 PTFE syringe filter and then analysed in LC/MS-QQQ.

3.4.3 Waterproof LED strip reactor setup.

Figure 3.7. Flexible, waterproof, 12 V cool white LED strip (50 mA per section and there are three LEDs in each section, 1000 mA m^{-1}, 850 lm m^{-1}).

Flexible, waterproof, cool white LED strips (Figure 3.7) with the dimensions 1000 mm (L) x 10 mm (W), consisting of 60 (5050-SMD type) LEDs were obtained from Jaycar Electronics, Australia with the following specifications: 12 V DC, 50 mA per $section^{-1}$ (3 LEDs per section, each section is 5 cm long), 1000 mA m^{-1}, 850 lm m^{-1}. The LED strips were IP67 rated, where IP stands for ingress protection. The first IP number refers to the protection against solid objects, normally dust. Number ‘0’ indicates no protection while number ‘6’ means full protection against dust. The second IP number stands for the protection level against liquids, where ‘0’ means no

protection while ‘7’ indicates protection for immersion between 15 cm to 1 m underwater for 30 min. Although the aforementioned waterproof LED strips can be used underwater it is recommended they be immersed under water for a limited time. Under the experimental conditions used here, the LED strip was found to remain waterproof for periods of 6 h.

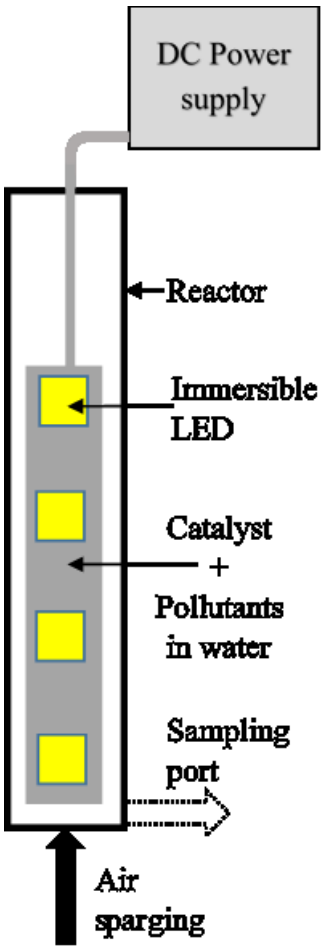

Figure 3.8. Waterproof LED strip photocatalytic reactor setup.

The waterproof LED strip reactor setup is shown in Figure 3.8. An acrylic column with ϕ = 16 mm inner diameter and height h = 300 mm was used as a batch reactor. The aqueous E3 solution (C_o = 100 μg l^{-1}, V = 45 ml) was filled in the reactor, along with the photocatalyst (m = 5 mg). Continuous mixing of the reactor contents was

ensured through air-sparging. A total of 15 LEDs (3 sections of the strip) were used for photocatalysis, while the unused LEDs in the strip were covered by aluminium foil. Progress in the photodegradation of E3 was analysed using an LC/MS-QQQ method similar to that used for EE2.

3.5 Analytical techniques for water matrices

3.5.1 Organic Carbon Analyser

Dissolved organic carbon (DOC) and inorganic carbon (IC) were measured by a Multi N/C 3100 Analytikjena total organic carbon (TOC) analyser.

3.5.2 Ion Chromatography

Anions Cl^-, Br^-, NO_2^-, NO_3^- and SO_4^{2-} concentrations were measured by ion chromatography (Metrohm 790 Personal IC) consisting of a Metrosep A sup 5-150 (150 mm × 4 mm, 5 µm) column. Na_2CO_3 (3.2 mmol l^{-1}) and $NaHCO_3$ (1.0 mmol l^{-1}) in MilliQ water was used as the mobile phase with a flow rate of 0.7 ml min^{-1}.

3.5.3 Ultra-high performance liquid Chromatography-Quadrupole Time-Of-Flight-Mass Spectrometer

Quadrupole time-of-flight liquid chromatography-mass spectrometry (QTOF-LC-MS, Agilent 6510), equipped with an Agilent 1290 ultra-high performance liquid chromatography (UHPLC) system, binary pump and Agilent Poroshell 120 EC-C_{18} column (2.7 µm, 4.6 mm x 50 mm) was used for the quantitative analysis of E1. The mobile phase A was Milli-Q water with 0.1% v/v formic acid and mobile phase B was methanol with 0.1% v/v formic acid. The flow rate was 0.35 ml min^{-1} and the injection volume was 20 µl. The elution gradient was initiated with 95% A and 5% B for 3 min,

then 10% A and 90% B for the next 4 min followed by 1% A and 99% B for another 2 min, before returning to the initial conditions for the final 4 min. The analytes were filtered using 0.20 μm PTFE syringe filters before injection.

3.5.4 Triple Quadrupole Liquid Chromatograph Mass Spectrometer

A Shimadzu 8060 triple quadrupole liquid chromatography-mass spectrometer (LC-MS-QQQ) consisting of a Shimadzu UHPLC system with binary pump and an Agilent Poroshell 120 EC-C18 column (2.7 μm, 4.6 mm x 50 mm) was used to detect EE2 and E3. Electrospray ionisation (ESI) technique was used to produce ions. The MS was operated in negative ion mode. The mobile phases were, A: Milli-Q water and B: methanol. The flow rate was 0.35 ml min^{-1} and the injection volume was 1 μl. The elution gradient was: 95% A and 5% B for 3 min, 10% A and 90% B for the next 4 min followed by 1% A and 99% B for another 2 min and 95% A and 5% B for the final 4 min. 0.20 μm PTFE syringe filters were used to filter the analytes before injection.

3.6 Auxiliary laboratory equipment

PO_4^{3-} (as P) and chemical oxygen demand (COD) were analysed using a DR 3900 Hach (Germany) spectrophotometer. Hach COD Reactor (100 – 150 ºC) was used to heat the COD sample vials. Stuart (UK) vortex mixer was used to mix the reagents. An Agilent 4100 microwave plasma - atomic emission spectroscopy (MP-AES) was used to measure Na, K, Mg, Ca, Fe and Al. Turbidity was measured using a 2100P portable Hach turbidimeter. Alkalinity was determined by titration with 0.01M H_2SO_4 solution. pH readings were obtained using Hach pH meter. The pH meter was calibrated using three buffer solutions with pH 4.01, 7.01 and 10.01.

A heating magnetic stirrer (Velp Scientifica) was used to stir the Au-TiO_2 catalyst mixture thermostated at 80 ºC during catalyst synthesis. Centrifugation of the mixtures was carried out using a Sigma 2-16KL (Germany) centrifuge at 10,000 rpm. Catalysts were dried in a Labec (Australia) oven and calcined using a Labec (Australia) muffle furnace. Powersonic UB-405 digital ultrasonic bath was used to disperse the catalyst in solution by sonication, prior to the photocatalysis experiments. ABJ 120-4NM - Kern & Sohn analytical balance was used to weigh the chemicals. The LEDs used as light source for photocatalysis experiments were powered by Skytronic adjustable DC power supply (0 - 10 A, 0 - 30 V). A magnetic stirrer (Industrial Equipment & Control PTY LTD, Australia) was used to continuously mix the photocatalytic reactor contents.

Chapter 4: Synthesis and characterisation of gold modified TiO_2 photocatalysts

Chapter 4: Synthesis and characterisation of gold modified TiO_2 photocatalysts

4.1 Introduction

Advanced oxidation processes (AOPs) use free radicals and are effective in the abatement of EDCs. Photodegradation by photolysis and photocatalysis are considered to be efficient AOPs for the removal of trace level EDCs. TiO_2 is an attractive photocatalyst due to its high activity, chemical and photo stability and commercial availability (Schneider *et al.*, 2014). The band gap energy of TiO_2 (3.2 eV for anatase) requires UV light for activation, which is only about 4% of the incident solar radiation (Dette *et al.*, 2014). The modification of TiO_2 to lower the band gap hence enabling visible light absorption is therefore attracting significant research interest.

A few studies have shown the effect of modified TiO_2 materials on the degradation of steroidal hormones (Sornalingam *et al.*, 2016). TiO_2 composites with noble metals (e.g., silver, gold and platinum) have been examined with gold emerging as an attractive option due to its non-toxicity, stability and biocompatibility (Ayati *et al.*, 2014). Bulk gold has low reactivity but this can be significantly increased when used in nanoparticulate form (Haruta, 1997). Gold nanoparticles may also absorb visible light to enhance the activity of photocatalysts (Hidalgo *et al.*, 2009). Au-TiO_2 has been found to show photocatalytic activity for the production of H_2 (Priebe *et al.*, 2015), reduction of NO_X (Nguyen *et al.*, 2008), oxidation of CO (Li *et al.*, 2006) and for the removal of pollutants from water, for example, azo-dye degradation (Arabatzis *et al.*, 2003) and removal of *p*-nitrophenol (Ismail *et al.*, 2012). A detailed review of the use of Au-TiO_2 for the removal of pollutants from water may be found elsewhere (Ayati

et al., 2014). On the other hand, the de-activating effects of Au upon addition to TiO_2 have also been reported, indicating that the activity of Au-TiO_2 depends on the preparation techniques and conditions employed (Carneiro *et al.*, 2009).

This chapter describes the synthesis and characterisation of gold modified TiO_2 photocatalysts. A gold precursor solution was prepared in the laboratory and deposition-precipitation (DP) method was used for Au-TiO_2 synthesis. Photocatalyst nanoparticles with different levels of gold loadings on the commercial P25 TiO_2 were prepared. The catalysts were characterised using TGA, XRD, Raman spectroscopy, UV-Vis spectroscopy, SEM, ICP-MS, zeta potential and particle size analysis.

4.2 Catalyst preparation

4.2.1 Tetrachloroauric acid preparation

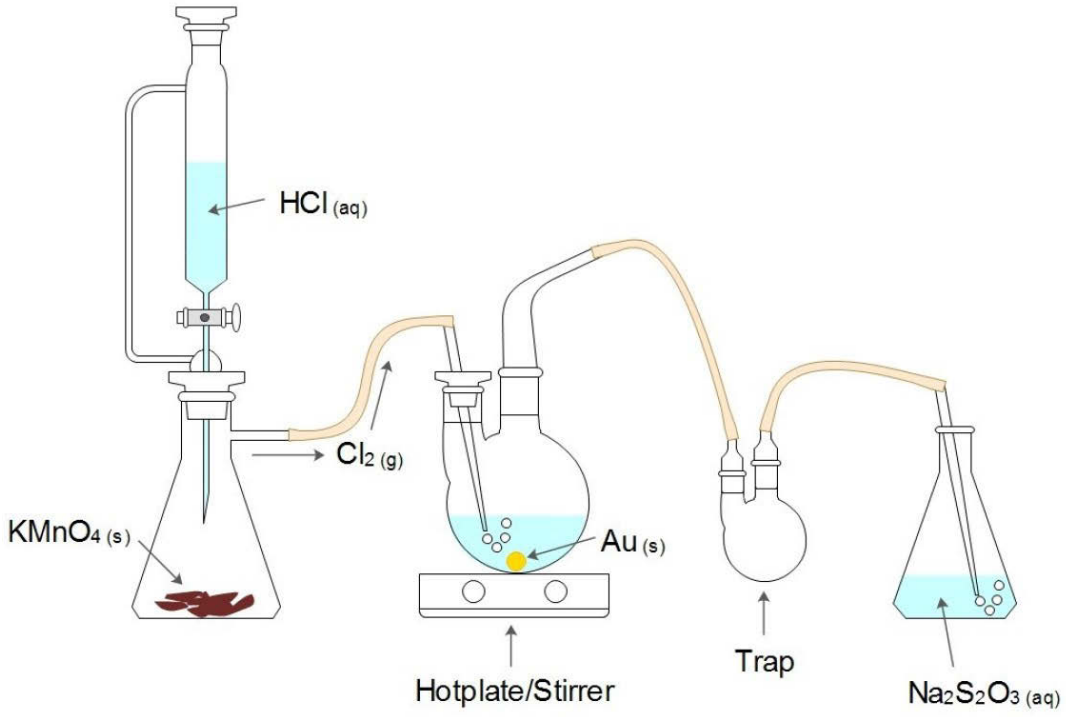

Figure 4.1. Preparation method for $HAuCl_4$ solution. Reproduced with permission from King *et al.* (2015).

An aqueous solution of tetrachloroauric acid ($HAuCl_4$) was prepared using the method of King *et al.* (2015) as depicted in Figure 4.1. Briefly, chlorine gas produced by mixing aqueous hydrochloric acid (14 ml, 36%) with potassium permanganate (3.0 g) was bubbled through water containing gold pellets (~300 g) at 50 ºC.

4.2.2 Au-TiO_2 synthesis

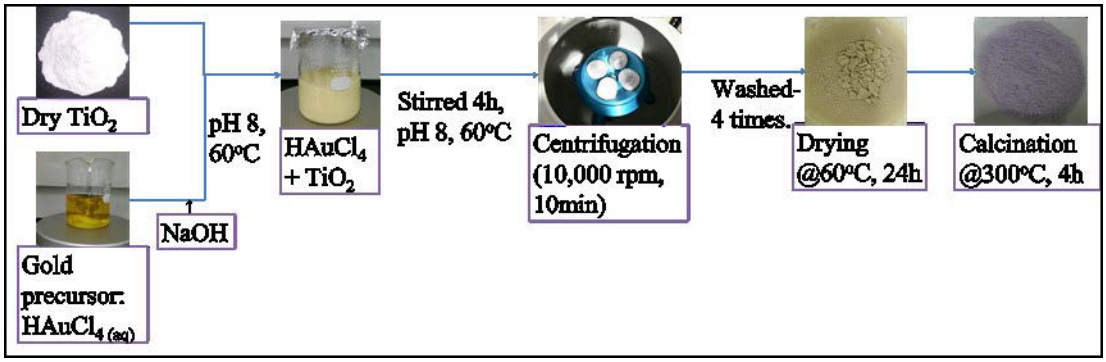

Figure 4.2. Synthesis of Au-TiO_2 photocatalysts by deposition-precipitation method.

Au-TiO_2 was prepared by a DP method described by Haruta (1997) (Figure 4.2). Briefly, 100 ml of aqueous $HAuCl_4$ solution (26.25 µM to 4.2 mM) at 80 ºC was readjusted to pH 7 by the dropwise addition of aqueous sodium hydroxide (1 M). P25 TiO_2 (1.0 g) was added and the pH was adjusted to pH 7. The mixture was stirred for 4 h at 80 ºC and then centrifuged at 10,000 rpm for 10 min. The resultant solid was washed with ultrapure water several times, dried in an oven at 60 ºC for 24 h and then calcined at 300 ºC for 4 h.

4.3 Results and discussion

4.3.1 Calcination temperature - Thermogravimetric analysis

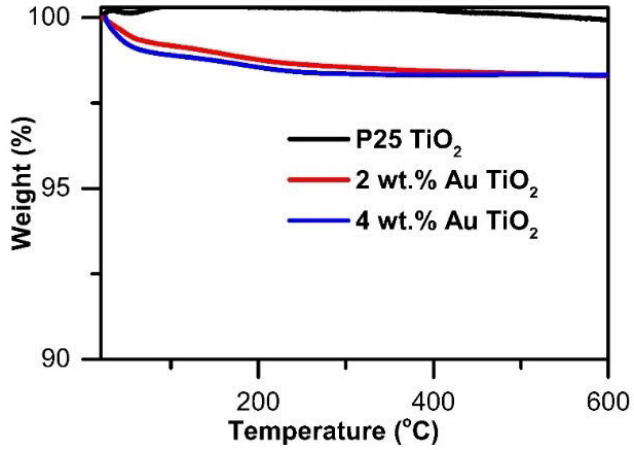

Figure 4.3. TGA of catalyst powders.

TGA experiments using uncalcined catalysts showed mass losses of ~2% across a temperature range of 60 to 600 °C (Figure 4.3). These losses are assigned to the removal of small amounts of adsorbed or interstitial water (Nafria *et al.*, 2013) and/or chloride (from $AuCl_4^-$) (Bond and Thompson, 1999). No significant weight loss was observed above 300 ºC at which the catalysts were calcined.

4.3.2 Powder X-ray Diffraction

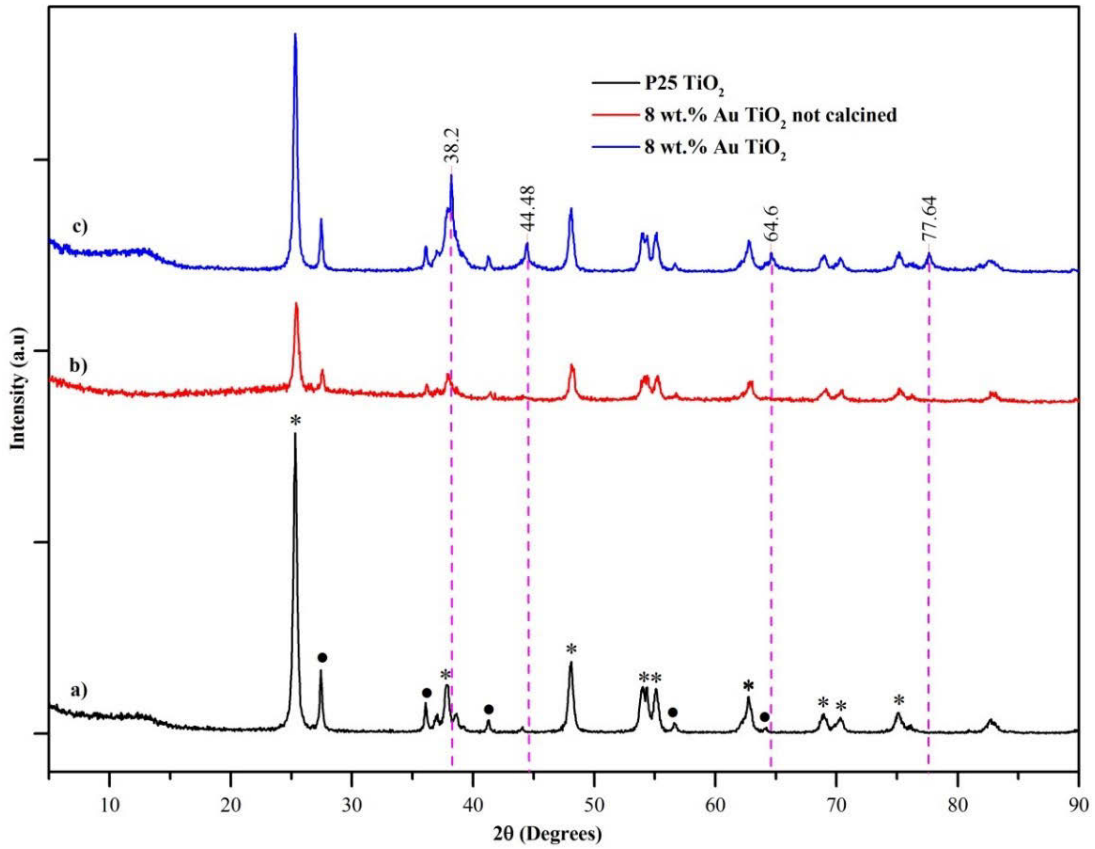

Figure 4.4. Powder XRD patterns of a) P25 TiO_2, b) uncalcined 8 *wt.%* Au-TiO_2 and c) calcined 8 *wt.%* Au-TiO_2. * indicates anatase peaks, • indicates rutile peaks and dashed vertical lines indicate the 2θ angles corresponding to Au.

P25 TiO_2 showed peaks for only anatase (~80%) and rutile (~20%) (Figure 4.4) (Tellez *et al.*, 2012). Peaks matching metallic gold at 38.2º, 44.4º, 64.6º and 77.6º (Pany *et al.*, 2014; Tian *et al.*, 2009) were detected for 8 *wt.%* Au-TiO_2 powders calcined at 300 ºC for 4 h, while no peaks related to gold were observed in samples prior to calcination. We attribute this to gold remaining as Au^{3+} ions in the uncalcined materials, which subsequently form Au^0 on TiO_2 surfaces upon calcination. The similar diffraction peaks for Au-TiO_2 and P25 TiO_2 indicates that the addition of the gold does not significantly change the TiO_2 crystal structure. Peaks corresponding to

gold were not unambiguously detected by XRD at the lower levels of gold loading (0.05% to 4%).

4.3.3 Raman Spectroscopy

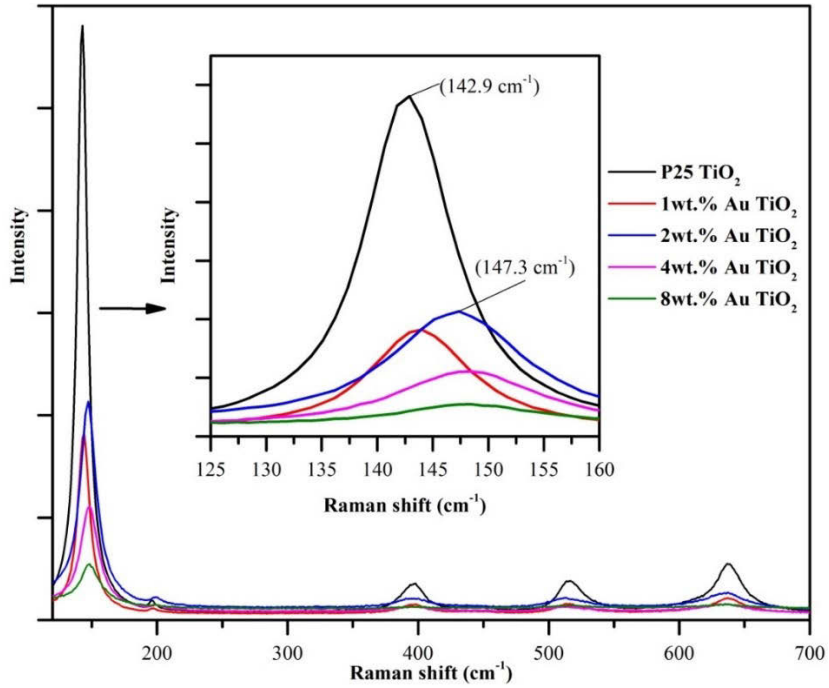

Figure 4.5. Raman spectra of catalysts with different Au loading.

Raman spectra of the catalysts are shown in Figure 4.5. The peaks at 143, 196, 397, 514 and 637 cm^{-1} were assigned to the anatase component (Ohsaka *et al.*, 1978; Su *et al.*, 2008). Peaks at 517 and 638 cm^{-1}, which are reported for rutile (Arabatzis *et al.*, 2003), were not apparent although XRD data confirms its presence. An increase in Au loading gave broader anatase peaks (Figure 4.5 inset) that shifted marginally to higher wavenumber indicating that the addition of gold introduced defects in the structure, which may enhance photocatalytic activity by entrapping photoelectrons and limiting electron-hole recombination (Li *et al.*, 2007).

4.3.4 UV-Vis Spectroscopy

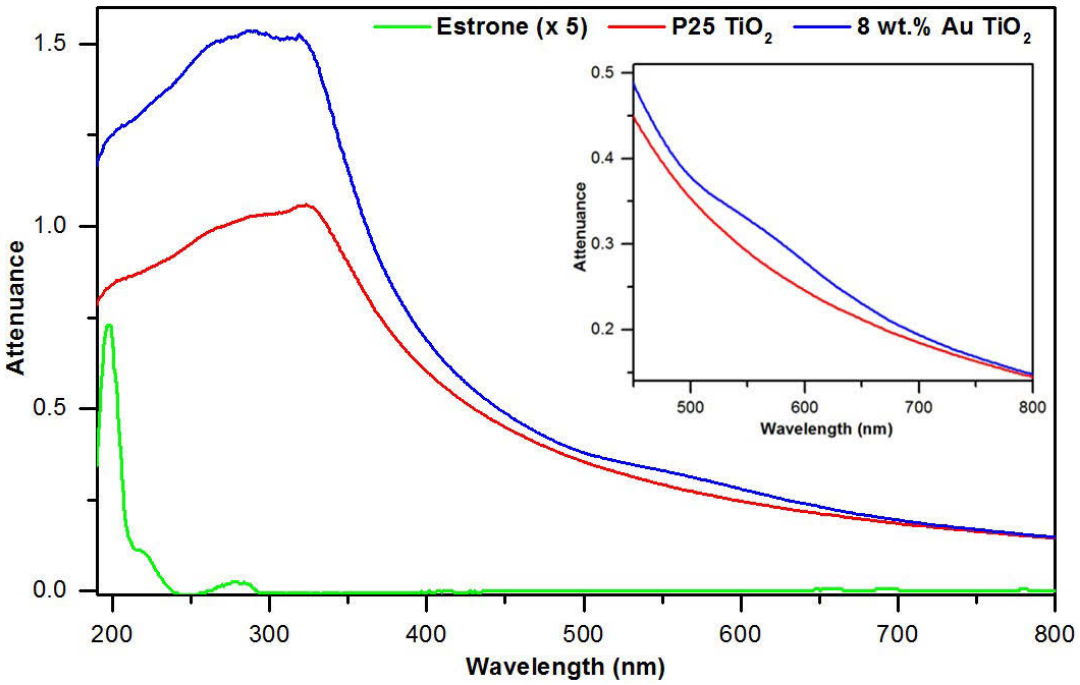

Figure 4.6. UV-Visible absorption spectra of P25 TiO_2, 8 *wt*.% Au-TiO_2 and estrone. The insert shows the broad absorption peak between 500 and 650 nm for 8 *wt*.% Au-TiO_2.

The activity of a photocatalyst depends on its ability to absorb photons to produce free radicals. The absorbance wavelength of P25 TiO_2 is below 400 nm (Figure 4.6), hence portraying good activity under UV, while being inactive under visible irradiation. The addition of gold to TiO_2 resulted in an absorption band between 500 and 600 nm (Figure 4.6 insert) due to surface plasmon resonance of gold nanoparticles on the TiO_2 surface (Lin *et al.*, 2015b). Detailed discussions can be found in Section 5.3.

4.3.5 Scanning Electron Microscopy and Energy Dispersive X-ray Spectroscopy

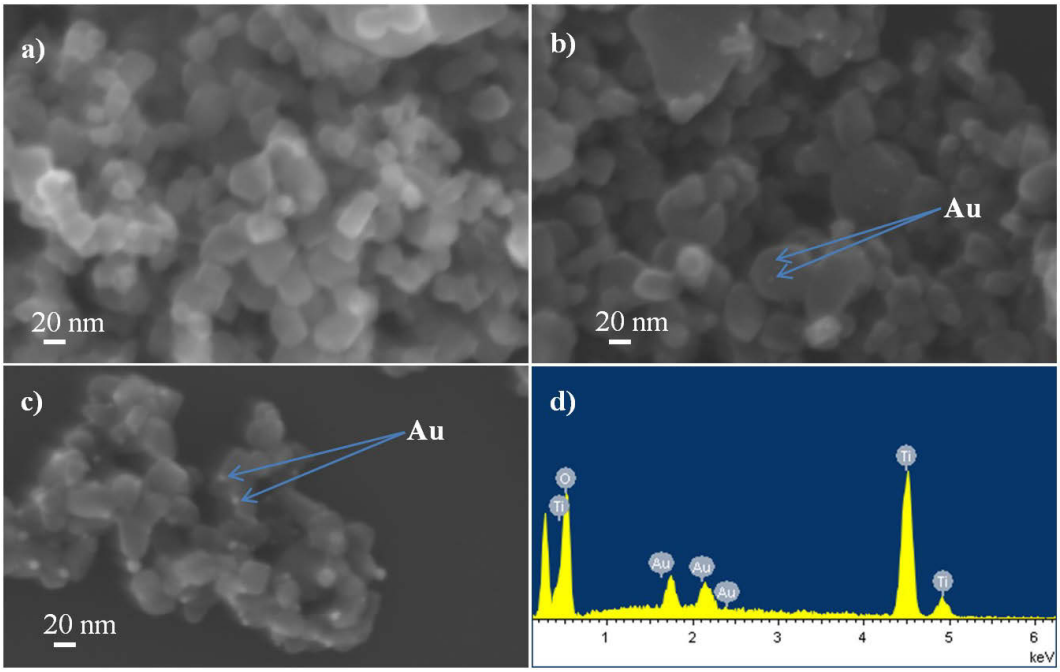

Figure 4.7. SEM images of a) P25 TiO_2, b) 2 *wt.%* Au-TiO_2 and c) 8 *wt.%* Au-TiO_2 and d) EDS of 8 *wt.%* Au-TiO_2.

SEM images reveal spherical gold nanoparticles on the surface of the spheroidal shaped TiO_2 nanoparticles (Figure 4.7a-c). The EDS of 8 *wt.%* Au-TiO_2 indicates the presence of Ti, O and Au (Figure 4.7d) and the absence of chloride ions (present in the gold precursor solution), which can inhibit photodegradation by surface blockage or through scavenging of hydroxyl radicals (Katz *et al.*, 2015).

4.3.6 Inductively coupled plasma mass spectrometry

The gold loadings obtained by the DP method were measured using EDS as well as ICP-MS. The results show that the measured amount of gold on TiO_2 is similar to the theoretical loadings (Table 4.1).

Table 4.1. Average gold loadings on TiO_2 measured by EDS and ICP-MS. The measurements were repeated twice and the average is reported. The standard deviation was less than 5%.

Catalyst	Theoretical Au loading (*wt.%*)	Actual Au loading (*wt.%*)	
		EDS	ICP-MS
P25 TiO_2	0	0	0
1 *wt.%* Au-TiO_2	1	0.8	0.9
2 *wt.%* Au-TiO_2	2	2.46	2.04
4 *wt.%* Au-TiO_2	4	3.58	3.86
8 *wt.%* Au-TiO_2	8	8.08	8.38

4.3.7 Zeta potential and hydrodynamic particle size

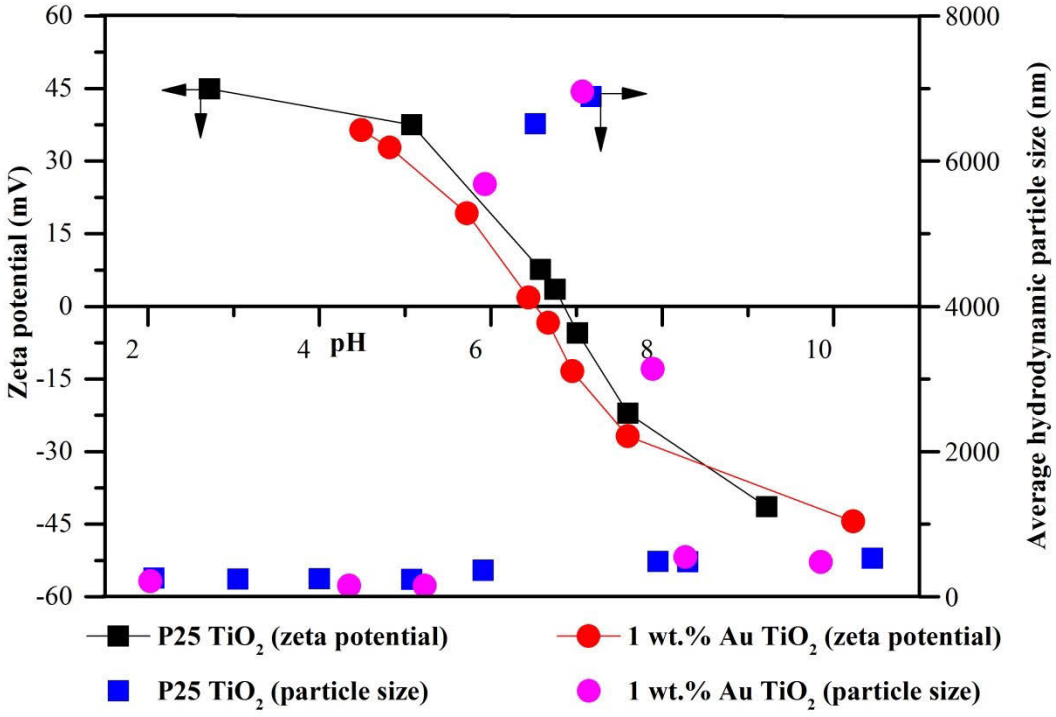

Figure 4.8. Average hydrodynamic particle size and zeta potential values of catalyst solutions for different pH values. The readings were repeated three times and the standard deviation was less than 5%.

The deposition of Au nanoparticles onto P25 TiO_2 did not considerably change the PZC nor the hydrodynamic particle size (Figure 4.8). The zeta potential values were greater than +30mV for pH < 5 and less than -30 mV for pH > 8. The suspension becomes stable due to electrostatic repulsion between particles if the zeta potential is above 30 mV or below -30 mV (Chalasani and Vasudevan, 2013). A PZC of ~6.8 for P25 TiO_2 was recorded which is similar to the value of 6.5 reported by Rincón and Pulgarin (2004). The zeta potential of 1 *wt.%* Au-TiO_2 was slightly lower than that of P25 TiO_2. At pH values away from the PZC, the hydrodynamic particle size was small (100-400 nm). The largest hydrodynamic particle size (~7 μm) was obtained for pH values close to the PZC. At PZC, the particles have no charge, therefore the repulsion between particles is negligible. Thus, the particles form aggregates which results in large hydrodynamic particle sizes. The results obtained agree with the results reported in the literature (Jiang *et al.*, 2009; Suttiponparnit *et al.*, 2011). The photodegradation experiments in this study were performed at pH 6-8 and some aggregation of the catalysts was expected.

4.4. Conclusions

Gold modified TiO_2 photocatalysts were synthesised using a DP method. Different amounts of aqueous $HAuCl_4$ solutions were added to P25 TiO_2 to attain 0 to 8 wt.% gold loadings. The catalysts were characterised using XRD, Raman spectroscopy, UV-Vis spectroscopy, SEM, ICP-MS, zeta potential and particle size analysis and TGA.

Similar XRD peaks corresponding to anatase and rutile for Au-TiO_2 and P25 TiO_2 indicate that the addition of the gold does not significantly change the TiO_2 crystal structure. The absence of peaks corresponding to gold for uncalcined Au-TiO_2 and the detection of peaks matching metallic gold after calcination reveals that the Au^{3+} in the

uncalcined materials subsequently forms Au^0 on TiO_2 surface upon calcination. In the Raman spectra, anatase peaks became broader with increased gold loadings indicating that the addition of gold introduced defects in the structure, which may enhance photocatalytic activity by entrapping photoelectrons and limiting electron-hole recombination.

The UV-vis spectrum of P25 TiO_2 shows absorption below 400 nm, while the Au-TiO_2 catalysts showed a wide absorption band between 500 – 600 nm due to surface plasmon resonance of gold nanoparticles on the TiO_2 surface, which is a key contributor to the Au-TiO_2's visible light photocatalytic activity. SEM images revealed spherical gold nanoparticles on the surface of the spheroidal shaped TiO_2 nanoparticles, though agglomeration of gold nanoparticles were observed at high gold loading (8 wt.%). Both EDS and ICP-MS results showed that the actual gold loadings were close to the theoretical loadings. The PZC of both P25 TiO_2 and Au-TiO_2 were found to be ~6.8. The largest hydrodynamic particle size was obtained for pH values close to the PZC. A small weight loss (~2 %) in TGA was recorded for the uncalcined catalysts in the temperature 60 – 600 ^oC. The loss in weight could be attributed to the removal of interstitial water and/or chloride.

Chapter 5: Enhanced photocatalysis of estrone and 17β-estradiol in water using Au-TiO_2 catalysts under UVA and visible LEDs

Chapter 5: Enhanced photocatalysis of estrone and 17β-estradiol in water using Au-TiO_2 catalysts under UVA and visible LEDs

5.1 Introduction

EDCs that can cause damage to living organisms are of increasing concern. EDCs interfere with the normal functions of natural hormones (García-Reyero *et al.*, 2001) and may cause adverse effects even at trace level concentrations (< 1 μg l^{-1}) (Snyder *et al.*, 2003). It is well known that natural and synthetic hormones enter the environment from STP effluents (Grover *et al.*, 2011). In particular, steroidal estrogens have been identified as the main contributor to estrogenicity in STP effluents (Desbrow *et al.*, 1998).

E1 (Figure 1.1) is a natural mammalian estrogenic steroidal hormone that reaches STPs primarily through human and animal waste. Conventional water treatment facilities generally do not completely remove E1, mainly due to its resistance to biodegradation (Johnson and Sumpter, 2001). In some cases, an increase in the concentration of E1 after treatment has been reported due to the formation of E1 as a degradation by-product of the even more potent E2 and/or the deconjugation of E1 sulfonide (Carballa *et al.*, 2004; Johnson and Sumpter, 2001).

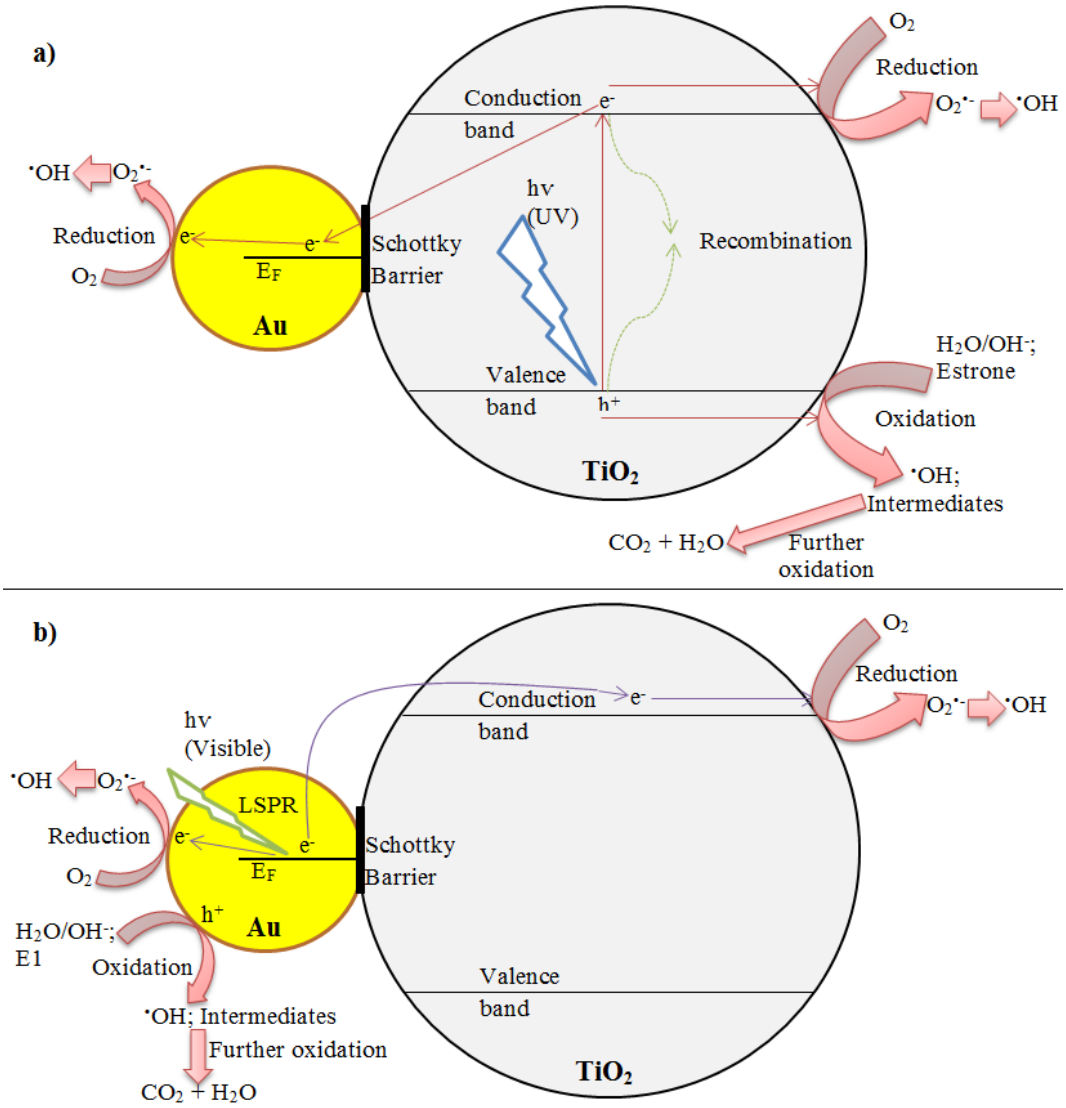

Figure 5.1. Proposed photocatalytic degradation mechanisms of E1 by Au-TiO_2 under a) UV light, and b) visible light (Lin *et al.*, 2015b; Sornalingam *et al.*, 2018).

AOPs that use free radicals are useful for the effective removal of EDCs. Au-TiO_2 photocatalysts are excellent for the abatement of EDCs due to Au-TiO_2's activity under both UV and visible light. The photocatalytic mechanism of Au-TiO_2 varies depending on the light source. Upon UV irradiation, electrons in TiO_2 are transferred from the VB to the CB generating holes in the VB (Figure 5.1a). Electrons may migrate to the gold nanoparticles on TiO_2 surface to produce electron-hole separation (i.e., the gold nanoparticles act as electron sinks) (Chen *et al.*, 2012; Silva *et al.*, 2011;

Tan *et al.*, 2016). Surface-adsorbed water molecules may combine with holes to produce hydroxyl radicals, while CB electrons may react with molecular oxygen to form superoxide radical anions. These radical species can then degrade E1 via intermediates to form CO_2 and H_2O.

Visible light irradiation is insufficient to overcome the band gap of TiO_2. However, electrons in gold nanoparticles can be excited, typically at wavelengths ~500-600 nm (Wu *et al.*, 2009b). Electrons with sufficient energy to overcome the Schottky barrier may cross to the CB of TiO_2 to reduce molecular oxygen adsorbed on the TiO_2 surface. Gold nanoparticles that lose electrons may oxidise surface adsorbed organic species (Figure 5.1b) (Kowalska *et al.*, 2010). The Schottky barrier also prevents the low energy electrons from readily passing between Au and TiO_2, hence reducing electron-hole recombination. Some electrons in gold nanoparticles that gain high kinetic energy (hot electrons) move to the gold surface to form $O_2^{-\bullet}$ radicals by reducing molecular oxygen which in turn degrade the pollutants adsorbed on the gold nanoparticles' surface (Lin *et al.*, 2015b).

The occurrence of E1 in wastewater, surface water and even in drinking water has been reported (Belhaj *et al.*, 2015; Conley *et al.*, 2017; D'Ascenzo *et al.*, 2003; Fine *et al.*, 2003; Wang *et al.*, 2008a). The efficiency of E1 removal by photodegradation varies depending on the water matrix (Silva *et al.*, 2016). Positive and negative effects are imparted by the components within the water matrix to the abatement of EDCs. Higher E1 photolysis rates have been observed with river water compared to purified water (Lin and Reinhard, 2005), where the faster degradation was attributed to the photosensitisation effect of the DOM present in river water. Similarly, HA in water has been shown to increase E1 photocatalytic removal rates (Zhang *et al.*, 2007). Most

photocatalysts are not target specific; therefore as the complexity of the water matrix increases more free radicals are lost in degrading non-target chemicals along with a loss in the effective catalyst surface area due to surface blockage (Katz *et al.*, 2015). For example, EE2 photocatalytic rates decreased for water matrices in the order: ultrapure water > drinking water > wastewater (Frontistis *et al.*, 2012a).

Here gold modified TiO_2 nanoparticles were utilised to degrade the estrogenic hormone E1. In this context, Coleman *et al.* (2005b) reported that the addition of silver or platinum to TiO_2 had an insignificant effect on the photodegradation rates of natural and synthetic hormones. Similarly, Dimitroula *et al.* (2012) reported that P25 TiO_2 was more active compared to Pt-TiO_2 in degrading phenol, Bisphenol A and EE2. In the current work, significant enhancement in the photodegradation rate of E1 was achieved using gold-modified TiO_2 photocatalysts compared to P25 TiO_2. The improvements were observed under UV, white and green light irradiation. Degradation by-products of E1 for TiO_2 photocatalysis were examined for the first time (by QTOF-LC-MS). The influences of different water matrices in E1 photodegradation were studied using UPW, SWW and WW.

5.2 Experimental setup

Three different water matrices, UPW, SWW and WW were used in the photodegradation studies. UPW was acquired from Milli-Q water system. SWW was prepared using the chemicals as presented in earlier Table 3.2 (Johir *et al.*, 2016). The as-prepared SWW was filtered using 1.2 μm glass fibre filter to remove any undissolved or particulate constituents. WW effluent from membrane bioreactor was obtained from Central Park, Sydney and was used as received. Both SWW and WW

were refrigerated at 4 ºC and used within 5 days. The characteristics of the water matrices are provided in Table 5.1.

Table 5.1. A comparison of physicochemical characteristics of different water.

Parameter	**Ultrapure water**	**Synthetic wastewater**	**Wastewater**
pH	6.30	7.41	7.55
Conductivity (μS cm^{-1})	0.055	56.3	621.0
DOC (mg l^{-1})	0.003	5.40	8.04
IC (mg l^{-1})	-	3.71	39.23
Turbidity (NTU)	0.15	1.79	0.40
UV_{254} (cm^{-1})	-	0.325	0.191
Alkalinity (mg $CaCO_3$ l^{-1})	-	6.0	27.5
COD (mg l^{-1})	0.5	23.6	26.2
Dissolved oxygen, DO (mg l^{-1})	7.9	8.5	5.2
Cl^- (mg l^{-1})	-	1.47	32.68
Br^- (mg l^{-1})	-	0.65	0.54
NO_3^- (mg l^{-1})	-	0.34	35.30
NO_2^- (mg l^{-1})	-	0.04	-
PO_4^{3-} (as P) (mg l^{-1})	-	3.82	0.21
SO_4^{2-} (mg l^{-1})	-	6.95	33.03
Na (mg l^{-1})	-	3.04	103.88
K (mg l^{-1})	-	2.25	21.82
Ca (mg l^{-1})	-	0.18	19.99
Mg (mg l^{-1})	-	0.15	4.95
Fe (mg l^{-1})	-	0.08	0.10
Al (mg l^{-1})	-	-	0.05

- Not detected

A 1 g l^{-1} stock solution of E1 was prepared in methanol and shielded from light using amber glass bottle and aluminium foil and refrigerated at 4 ºC. The desired concentration of E1 aqueous solutions (1000 μg l^{-1}) were made through dilution of the stock. Higher initial concentrations of E1 compared to its presence in environmental

matrices (ng l^{-1} to µg l^{-1}) were selected to ensure accuracy in using the QTOF-LC-MS and to allow sufficient timeframes for degradation, especially under UV light.

The reactor setup used in this study is depicted in Figure 3.2. A cylindrical reactor vessel was filled with 500 ml of 1000 µg l^{-1} E1 solution consisting of 50 mg l^{-1} of catalyst and stirred for 30 min under darkness to achieve adsorption-desorption equilibrium. Preliminary studies were conducted (up to 2 h) to determine the time required to reach adsorption-desorption equilibrium under darkness. The E1 concentration did not change after 30 min for all the catalysts used, therefore 30 min was chosen for equilibrium experiments. An 11 W UV LED (λ = 365 nm) (LED Engin) connected to a heat sink was placed 5 cm above the liquid surface of the reactor and homogenous mixing was ensured by magnetic stirring. Similar experiments were conducted under cool white (λ > 410 nm) and green (λ = 523 nm) LEDs (LED Engin). Spectral powers vs. wavelength distributions of the lamps are shown in Figures 3.3 - 3.5. The light intensities of the lamps were measured at 5 cm to be 27 mW cm^{-2} for UVA LED (measured by UV-Optometer, SUSS MicroTec at λ = 365 nm) and 260 µW cm^{-2} and 170 µW cm^{-2} for cool white (at λ = 450 nm) and green (at λ = 525 nm) LEDs respectively (measured by Newport 2832C power meter).

The concentrations of E1 at different times obtained through experiments were fitted to pseudo - 1st order kinetics as follows: $C_t/C_o = e^{-kt}$, where C_o (µg l^{-1}) and C_t (µg l^{-1}) are the concentrations of E1 before irradiation and at a given time t (min or h) since turning the light source on, respectively; k is the pseudo - 1st order rate constant (min^{-1} or h^{-1}). The half-life $t_{1/2}$ (min or h) of E1 was calculated using the equation $t_{1/2} = (\ln 2)/k$.

5.3 Photodegradation of estrone

Figure 5.2 shows data obtained for the photodegradation of E1 in UPW under different conditions. Direct photolytic degradation of E1 under any of the light sources was negligible due to the lack of absorption of photons by E1 (Figure 4.6) in agreement with previous work (Han *et al.*, 2012) although Puma *et al.* (2010) reported significant removal of E1 using a UVA light source (300- 420 nm), which might be due to some absorbance by E1 near 300 nm.

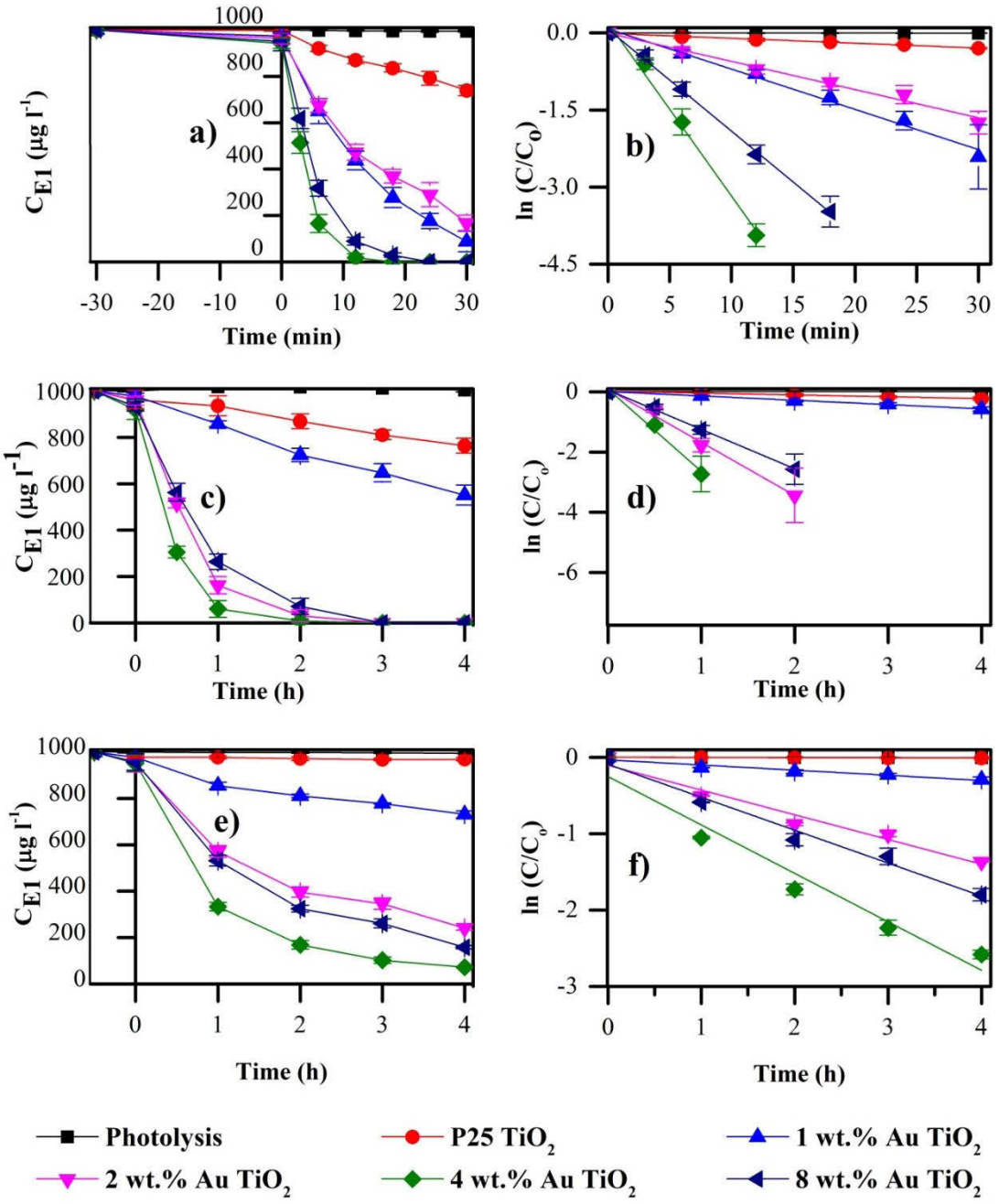

Figure 5.2. Plots for the photodegradation of E1 (1000 µg l^{-1}, 500 ml) using different catalysts (50 mg l^{-1}) and different light sources*. (a) E1 concentration vs. time using UVA LED, (b) 1st order kinetic data under UVA LED. (c) E1 concentration vs. time using "cool white" LED, (d) 1st order kinetic data under "cool white" LED. (e) E1 concentration vs. time using green LED, (f) 1st order kinetic data under green LED.

Negative x-axis indicates the period of dark adsorption. *Spectra for the LEDs are available in Figures 3.3 to 3.5. Each experiment was repeated three times.

Initial adsorption of E1 onto the catalyst surface in the absence of light was up to 9% (Figure 5.2). It was found that the photocatalytic degradation of E1 followed pseudo - 1st order kinetics model. The rate constants, and $t_{1/2}$ for E1 photodegradation under different light sources in the presence of different catalysts are presented in Table 5.2.

Table 5.2. Pseudo 1st order kinetic data for E1 photodegradation in the presence of different catalysts and light sources.

Catalyst	UVA			Cool white			Green		
	k (min^{-1})	R^2	$t_{1/2}$ (min)	k (h^{-1})	R^2	$t_{1/2}$ (h)	k (h^{-1})	R^2	$t_{1/2}$ (h)
P25 TiO_2	0.01±0.00	0.96±0.04	69±2	0.06±0.01	0.95±0.04	13.1±3.4	-	-	-
1 wt.% Au-TiO_2	0.08±0.01	0.97±0.04	9±2	0.14±0.01	0.99±0.00	4.9±0.4	0.08±0.01	0.90±0.04	8.9±0.9
2 wt.% Au-TiO_2	0.06±0.01	0.97±0.00	13±1	1.81±0.36	0.98±0.01	0.4±0.1	0.36±0.00	0.95±0.00	1.9±0.0
4 wt.% Au-TiO_2	0.28±0.01	0.98±0.00	2±0	2.44±0.36	0.97±0.03	0.3±0.0	0.72±0.01	0.93±0.02	1.0±0.0
8 wt.% Au-TiO_2	0.19±0.02	0.10±0.00	4±0	1.30±0.18	0.98±0.02	0.5±0.1	0.46±0.03	0.97±0.01	1.5±0.1

The activity of a photocatalyst depends on its ability to absorb photons to produce free radicals. The absorbance wavelength of P25 TiO_2 is shorter than 400 nm (Figure 4.6), hence displaying good activity under UV, while being inactive under visible irradiation. This is reflected in the degradation of E1, where 26% loss was observed under UVA in 30 min, while it took 4 h to attain similar results under cool white light and no loss in E1 was found in 4 h under green LED. The slower yet noticeable degradation rate under white light source could have resulted from the small percentage of UVA emitted by the light source (Serra *et al.*, 2015).

All of the gold modified TiO_2 catalysts (1 - 8 *wt.%* Au) showed activity superior to that of P25 TiO_2, under all the three different light sources utilised. The improvement in activity under UVA is due to gold nanoparticles acting as electron sinks to minimise electron-hole recombination. For example, the best performing catalyst (4 *wt.%* Au-TiO_2) resulted in k_{E1} 0.28 min^{-1}, while for P25 it was only 0.01 min^{-1} under UVA irradiation. With regard to visible light activity, the addition of gold to TiO_2 resulted in an absorption band between 500 and 600 nm (Figure 4.6) due to surface plasmon resonance of gold nanoparticles on the TiO_2 surface (Lin *et al.*, 2015b). This is reflected in the results obtained using cool white and green light sources. Under cool white light *k* values were 0.06 ± 0.01 h^{-1} and 2.44 ± 0.36 h^{-1} in the presence of P25 TiO_2 and 4 *wt.%* Au-TiO_2 respectively. Slower E1 degradation rates were obtained under green light, where *k* was 0.72 ± 0.01 h^{-1} in the presence of 4 *wt.%* Au-TiO_2, with virtually no change in E1 level for P25 TiO_2. The relatively slower rates for gold modified TiO_2 under green light can be ascribed to the low light intensities of the green LED (170 µW cm^{-2} at 5 cm) compared to the white light LED (260 µW cm^{-2} at 5 cm). In addition, the removal rate increases with decreasing wavelengths of the light

sources as the energy of the photons emitted by them increases. Therefore, E1 degradation rate decreased in the order: UVA > cool white > green LED.

The gold loading on the TiO_2 played a vital role in the photocatalytic activity. The addition of gold (1 to 8 *wt.%* loading) substantially increased the performance of the catalysts. Photocatalytic activity increased up to 4 *wt.%* gold loading followed by a slight drop for 8 *wt.%* loading (Figure 5.2). Under UVA irradiation, gold nanoparticles deposited on TiO_2 surface trap increasing number of electrons (from TiO_2) generated by light, thus minimising the recombination of electrons and holes. Therefore, with increasing gold loading (up to ~4%), electron-hole recombination is reduced. The optimum gold loading was found to be 4 *wt.%* in this study. At 8 *wt.%* loading, gold can provide sufficient recombination centres (Wu *et al.*, 2009c) to reduce the photocatalytic activity. Gold nanoparticles at elevated levels may impose a screening effect on the P25 TiO_2, i.e., the contribution of gold as an electron sink may be less than that of the adverse effect it poses on the loss of P25 TiO_2 surface area available for the photocatalysis of the pollutants.

Uncalcined catalysts showed low activity compared to the ones calcined at 300 ^oC (Figure 5.3). During calcination, ionic gold is reduced to metallic gold and deposits on TiO_2 surface, thus enhancing the photocatalytic activity (Oros-Ruiz *et al.*, 2013). This is evident from the XRD results, in which the peaks corresponding to gold appears only after calcination (Figure 4.4).

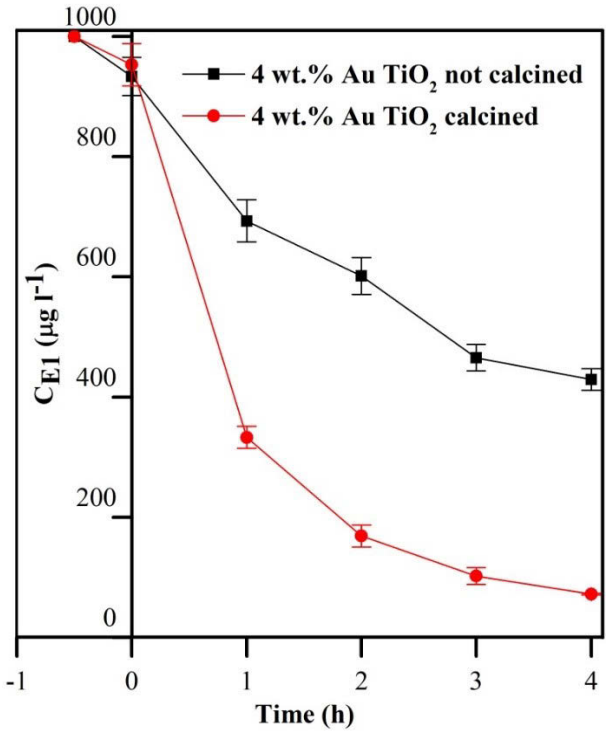

Figure 5.3. Effect of calcination on the photocatalytic performance of 4 *wt.%* Au-TiO_2 catalysts under green light LED. Each experiment was repeated three times.

5.4 Effect of catalyst loading

Previous studies on the removal of estrogenic hormones using TiO_2 utilised catalyst loadings of 10 - 4000 mg l^{-1} (Sornalingam *et al.*, 2016). In the current study, four catalyst loadings (25 mg l^{-1}, 50 mg l^{-1}, 75 mg l^{-1} and 100 mg l^{-1}) were examined to select a suitable loading for further experiments. The rate of photocatalysis of E1 increased linearly as the catalyst concentration was increased (Figure 5.4), due to the availability of more catalyst active sites for the pollutants. It is expected that high catalyst loading will have a negative impact on removal efficiency due to the aggregation of catalyst particles and a decrease in light penetration (Lea and Adesina, 1998). A loading of 50 mg l^{-1} was chosen as an appropriate catalyst concentration to allow monitoring of E1 degradation under UV light over a reasonable period.

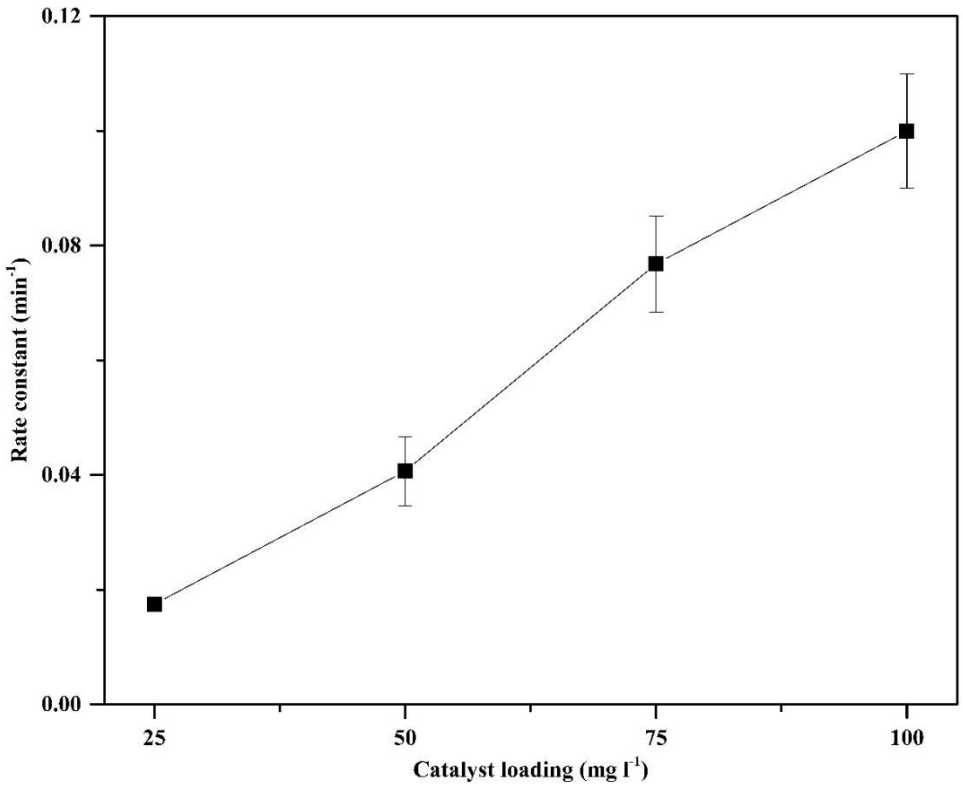

Figure 5.4. Effect of catalyst loading (25-100 mg l^{-1}) on photocatalytic performance of 4 *wt.%* Au-TiO_2 catalysts under UVA LED for the photodegradation of E1 (1 mg l^{-1}, 500 ml). Each experiment was repeated three times.

5.5 Stability of the catalysts

Two experiments were performed to examine the stability of the catalyst after several cycles. First, the catalyst was recovered by centrifugation after each cycle, followed by drying and weighing. Between 15-25% loss of catalyst (~25%) occurred as a result of the recovery process, which was compensated for by reducing solution volume to maintain the original catalyst loading (i.e. 50 mg l^{-1}). After three cycles of photocatalysis, the activity did not diminish by any significant amount (< 3% loss). In the second set of experiments, all recovered catalyst (by centrifugation) from a

previous cycle was immediately returned to a fresh solution of E1 (500 ml of 1 mg l^{-1}). After 18 min under UVA irradiation, 98%, 89% and 78% of E1 was degraded during cycle 1, 2 and 3, respectively (Figure 5.5). While these data indicate a reduction of the activity, they demonstrate the efficiency of photocatalysis for E1 degradation over 3 cycles.

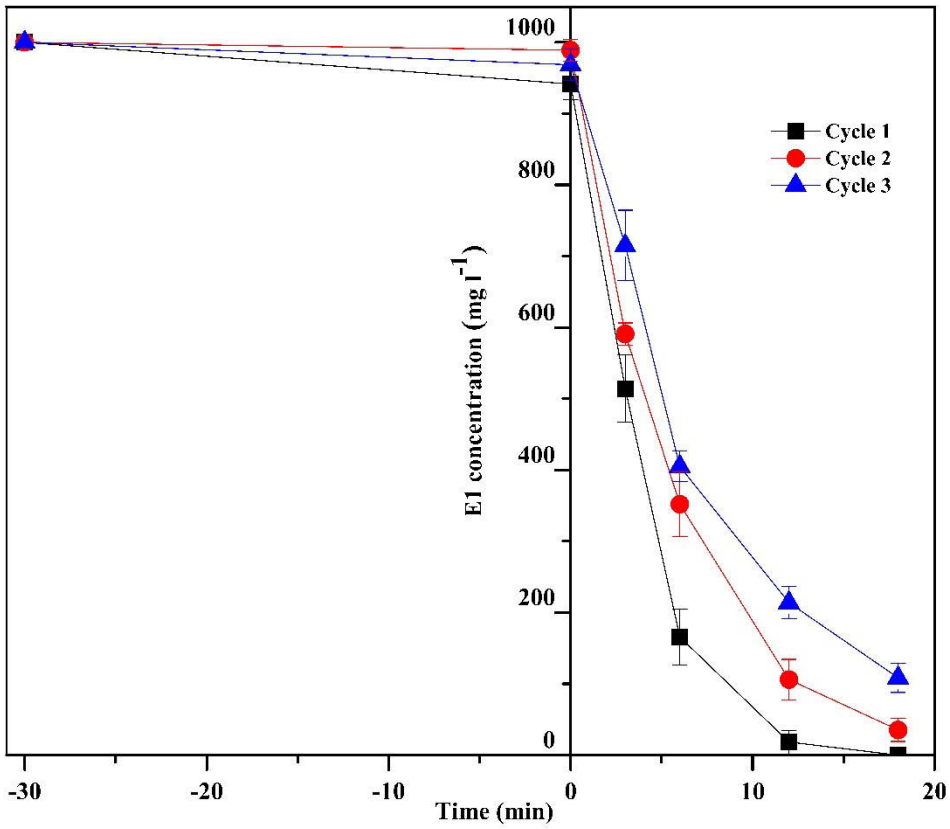

Figure 5.5. Photocatalytic performance of 4 *wt.%* Au-TiO_2 catalysts under UVA LED for the photodegradation of E1 (1 mg l^{-1}, 500 ml) for three consecutive cycles.

The stability of the Au-TiO_2 catalysts in terms of Au release to the solution was monitored by analysing the solution (after centrifugation to remove the catalysts), using ICP-MS. The gold content in the solution was found to be 0.13 ± 0.06 % of the total Au present in the catalyst, at the end of each cycle, showing good stability of the photocatalysts. Each experiment was repeated three times.

5.6 Effect of water matrices on estrone degradation

The influence of different water matrices (UPW, SWW and WW) on E1 photodegradation was studied (a) in the absence of a TiO_2 catalyst, (b) using P25 TiO_2, and (c) with 4 *wt.%* Au-TiO_2 photocatalyst. Photolysis (no TiO_2 catalyst) did not degrade E1 during the experimental time tested under UVA (0.5h), cool white (2h) and green (2h) LED light sources (Figure 5.6). Compared to P25 TiO_2, the gold modified catalyst showed enhanced photocatalytic activity for E1 removal in each of the water matrices under all light sources. However, E1 degradation rate decreased in the order: UPW > SWW ≈ WW. For example, the complete removal of E1 using 4 *wt.%* Au-TiO_2 under UVA lamp took 18 min in UPW, while 1.5 h was required in SWW and WW (Figure 5.6 a-c). Similarly, under white light in 1 h, 93%, 34% and 29% of E1 degradation was achieved using 4 *wt.%* Au-TiO_2 in UPW, SWW and WW respectively, which was substantially higher than using P25 TiO_2 achieving only 3%, 6% and 5%, respectively in 1 h (Figure 5.6 d-f).

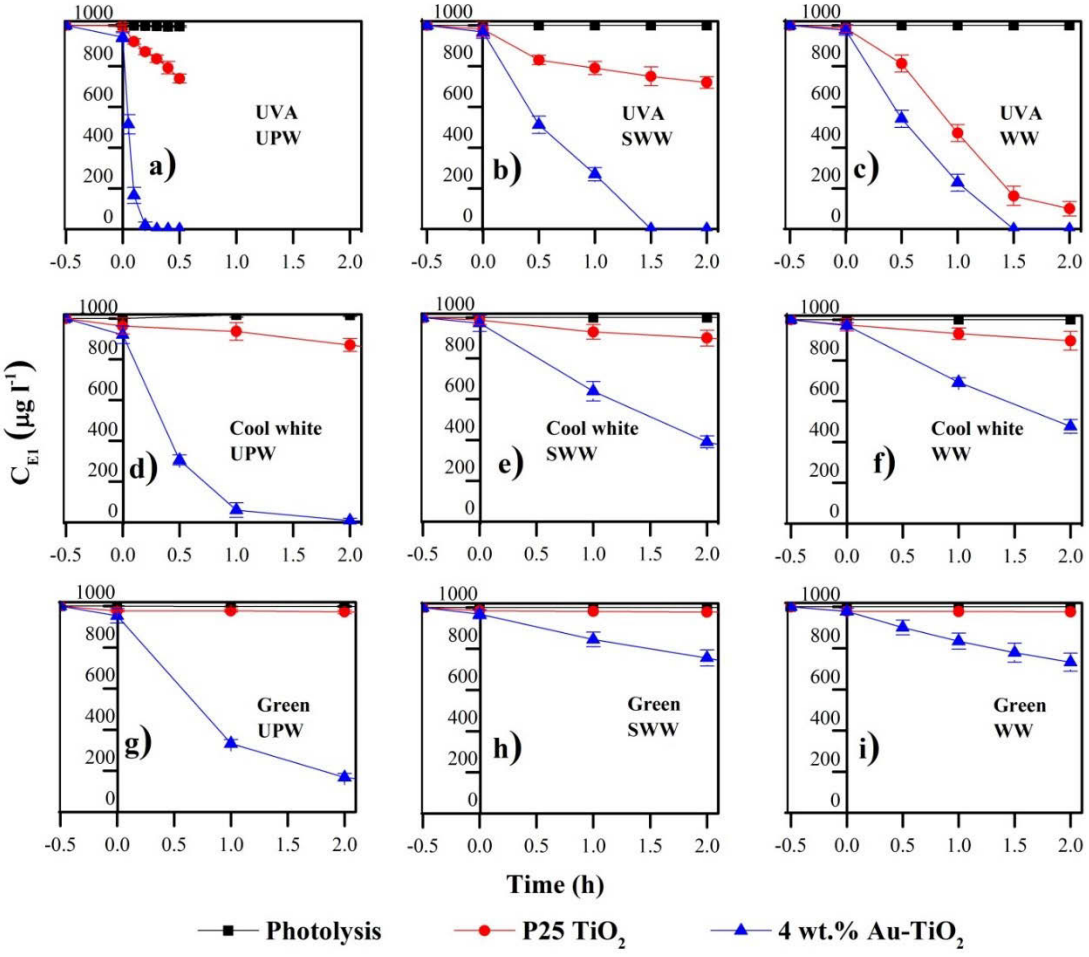

Figure 5.6. Change in E1 concentration vs. time for photodegradation in different water matrices under different light sources. (a) E1 in UPW under UVA LED, (b) E1 in SWW under UVA LED, (c) E1 in WW under UVA LED, (d) E1 in UPW under "cool white" LED, (e) E1 in SWW under "cool white" LED, (f) E1 in WW under "cool white" LED, (g) E1 in UPW under green LED, (h) E1 in SWW under green LED, (i) E1 in WW under green LED. (Negative x-axis indicates the period of dark adsorption). Each experiment was repeated three times.

As the complexity of the water matrix (Table 5.1) increased, the removal efficiency of the target compounds decreased. TiO_2 catalysts are not target specific (Xu *et al.*, 2014b), therefore due to the absence of competitive chemicals in UPW, E1 degradation rate was high. However, DOM present in SWW and WW competed with

E1 for the catalyst surface and for hydroxyl radicals, thus reducing the E1 removal efficiency (Katz *et al.*, 2015; Nasuhoglu *et al.*, 2012). The WW used was an effluent from the membrane bioreactor that had not gone through UV treatment and chlorination. Therefore, the slightly slower E1 degradation rate in WW compared to SWW could be attributed to the non-biodegradable compounds present in WW. In addition, anions such as HCO_3^-, SO_4^{2-} and Cl^- among others may act as hydroxyl radical scavengers (Frontistis *et al.*, 2012a; Katz *et al.*, 2015). Even though studies have shown enhanced photodegradation due to the photosensitisation effect of the substances such as humic and fulvic acids (Zhang *et al.*, 2007), the overall influence of the components present in SWW and WW was found to reduce E1 photocatalysis in this study.

The mineralisation of organic material during photodegradation was measured by the TOC analyser. Methanol, which was used as the solvent for the E1 stock solution, was the major contributor of TOC in the solution (0.5 ml methanol with initial TOC = 297 mg l^{-1} in 500 ml solution). The initial TOC of E1 in the reactor was 0.8 mg l^{-1}. The decline in TOC (4.6 ± 1.2%) under dark conditions was due to the adsorption of organics to the catalyst. The photocatalysts reduced the TOC further under UVA and visible light (Figure 5.7). TOC removal by the catalysts (10-12 % TOC removal by catalysts) under UVA irradiation decreased in the order: 4 *wt.%* Au-TiO_2 ≥ P25 TiO_2 > photolysis (no catalyst). Under visible light, 4 *wt.%* Au-TiO_2 resulted in a small amount of TOC removal (6.2%), while P25 TiO_2 was inactive. The mineralisation rate (Figure 5.7) was low compared to the photodegradation rate of E1 (Figure 5.2). The low mineralisation was mainly due to the presence of methanol along with the

formation of further intermediates of the parent compounds (both methanol and E1) during photodegradation.

The effect of catalysts on the WW matrix during photodegradation was studied by monitoring the change in TOC of the WW in the absence of E1. The initial TOC of WW was 8.04 mg l^{-1}. The change in TOC for the duration of the study by both UVA (1h) and visible (2h) photolysis (no catalyst) was negligible. The adsorption of organic molecules onto catalysts under darkness was 4.9 ± 1.2%. In terms of UVA photocatalysis, P25 TiO_2 and 4 *wt.%* Au-TiO_2 performed similarly with 6.5 % TOC reduction in 1h. However, under visible irradiation, both 4 *wt.%* Au-TiO_2 and P25 TiO_2 had virtually no effect on mineralising WW in 1h.

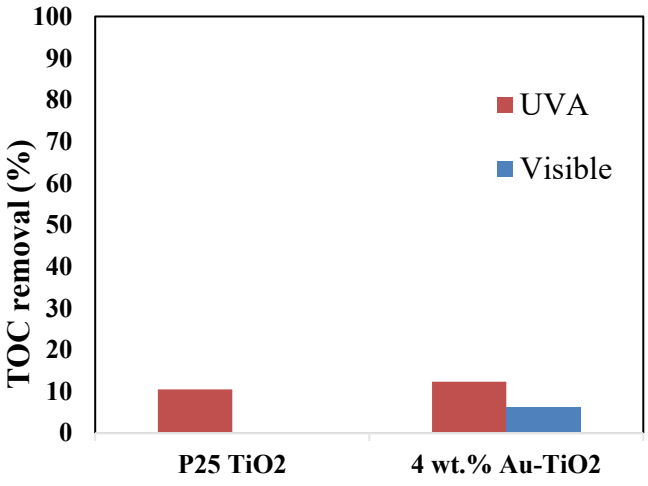

Figure 5.7. TOC removal percentage of E1 (1 mg l^{-1}) in water (500 ml) in the presence of 0.5 ml methanol.

5.7 By-products of estrone photodegradation

Experiments were conducted to identify by-products, to aid in understanding the photocatalytic mechanism. Previous studies have identified some of the photolytic by-

products of E1 (Caupos *et al.*, 2011; Trudeau *et al.*, 2011; Whidbey *et al.*, 2012), and here we show the intermediates formed by photocatalysis of E1 by Au-TiO_2. To elucidate the E1 photoproducts, aliquots of the E1 aqueous solutions collected during photocatalytic experiments were analysed using QTOF-LC-MS in negative and positive ion modes. Total ion chromatograms (TICs) of the initial and photocatalysed E1 solution in negative mode are shown in Figure 5.8a. The by-products were further analysed in MS/MS mode to determine possible structures. The *m/z* of the parent compound and the by-products, their retention time (RT), elemental composition and their respective fragmentation ions are shown in Table 5.3.

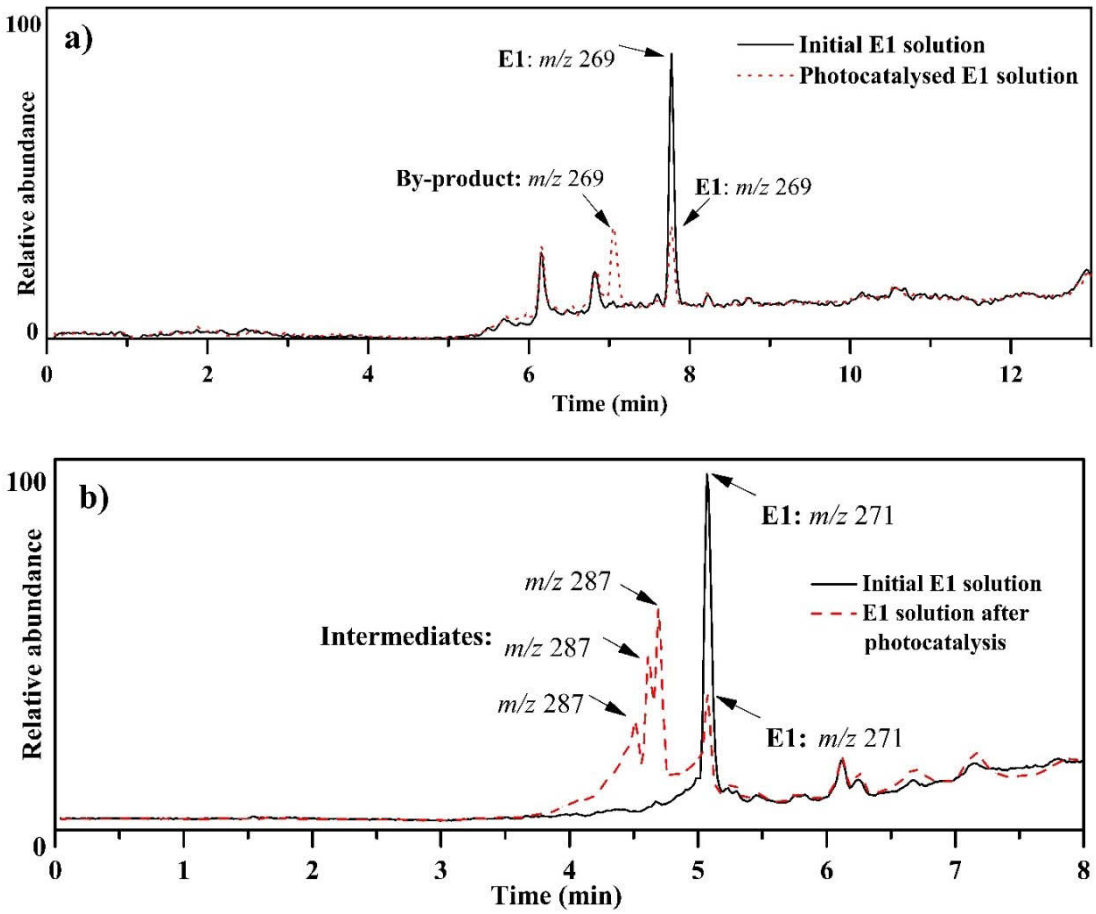

Figure 5.8. Total ion chromatograms of E1 and its photodegradation (4 *wt.%* Au-TiO_2) by-products under UVA LED using QTOF-LC-MS in a) negative ionization mode and b) positive ionization mode.

Table 5.3. Details of QTOF-LC-MS analysis of E1 and its photodegradation by-products.

Ionization mode	**Compound**	**RT (min)**	***m/z***	**MW (Da)**	**Fragmentation ions (*m/z*)**
Negative	E1	7.777	269 $[M-H]^-$	270	145
	Lumiestrone	7.046	269 $[M-H]^-$	270	145
Positive	E1	5.068	271 (MH^+)	270	253, 197, 172, 157, 133
	1- E1-OH	4.692	287 (MH^+)	286	269, 133
	2- E1-OH	4.609	287 (MH^+)	286	269, 133
	3- E1-OH	4.510	287 (MH^+)	286	269, 133

The mass spectra showed that the concentration of E1 (*m/z* 269, RT 7.777 min) decreased with increasing time of irradiation, though the rate of degradation varied depending on the light source and catalyst used. As E1 was degraded, a by-product (*m/z* 269, RT 7.046 min) was formed (Figure 5.8a). To further investigate this intermediate, samples were analysed using selective ion monitoring (SIM) at *m/z* 269, which showed only two peaks corresponding to E1 and its intermediate. The MS/MS at negative mode for both E1 and its by-product resulted in the same main product ion *m/z* 145, indicating that the photo-product could be an isomer of E1. This by-product was identified as lumiestrone (the 13 α-epimer of E1) by comparison with literature data (Caupos *et al.*, 2011; Trudeau *et al.*, 2011). Lumiestrone also possesses estrogenic potency (Trudeau *et al.*, 2011; Whidbey *et al.*, 2012). The lumiestrone intermediate was also degraded with further Au-TiO_2 photocatalysis, demonstrating the ability of

the photocatalysts to effectively remove E1 as well as its photoproduct, although the lumiestrone by-product was also resistant to photodegradation (Figure 5.9).

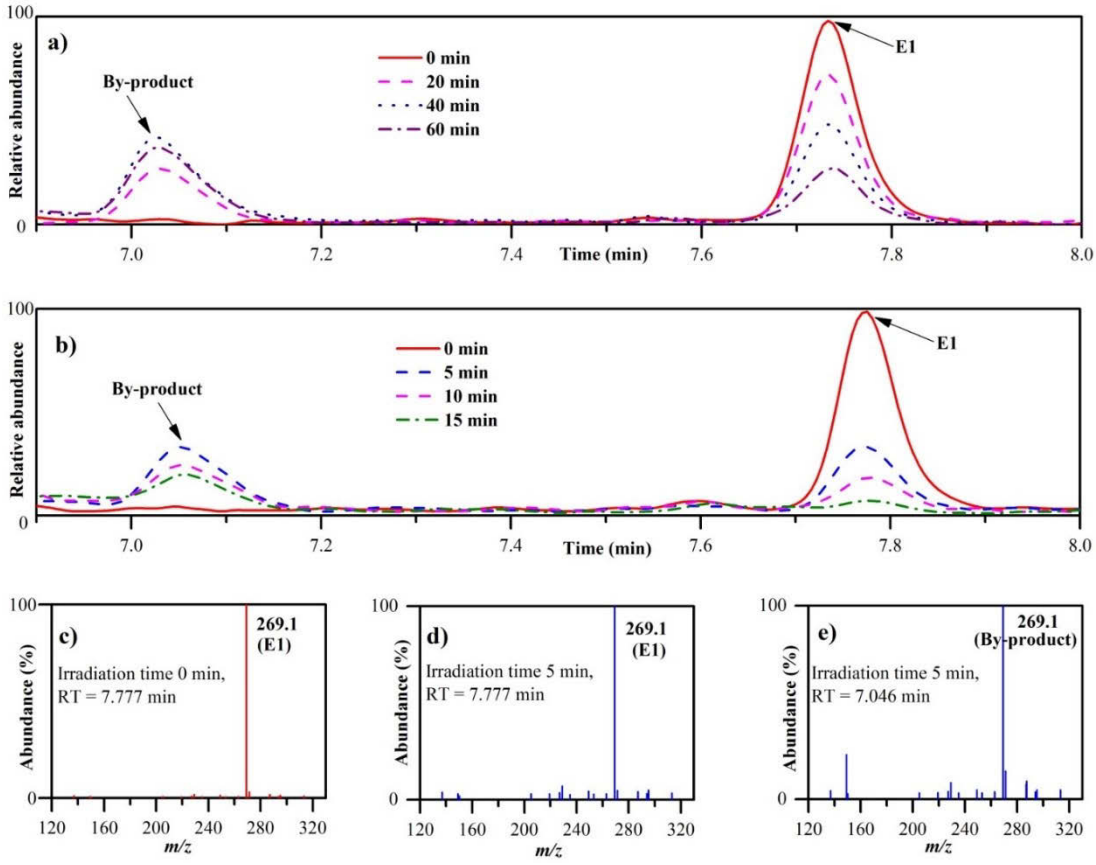

Figure 5.9. Chromatograms of E1 (1000 µg l^{-1}) and its photodegradation by-product under UVA LED using a) P25 TiO_2 b) 4 *wt.%* Au-TiO_2 catalysts. Mass spectra of E1 solution photocatalysed using 4 *wt.%* Au-TiO_2 under UVA c) at 0 min irradiation and retention time (RT) 7.777 min, d) at 5 min irradiation and RT 7.777 min and e) at 5 min irradiation and RT 7.046 min.

To detect other intermediates, a photocatalytic study was conducted with elevated E1 concentration (2.5 mg l^{-1}) and the irradiated samples were analysed in QTOF-LC-MS in positive ion mode (Figure 5.8b). Three other intermediates were detected with signals corresponding to *m/z* 287. These could be assigned to the addition of one hydroxyl group to E1 at different positions. The by-products formed were further

analysed using MS/MS, with their fragment ions shown in Table 5.3. Based on the mass spectrometry results, a possible degradation mechanism of E1 is proposed (Figure 5.10).

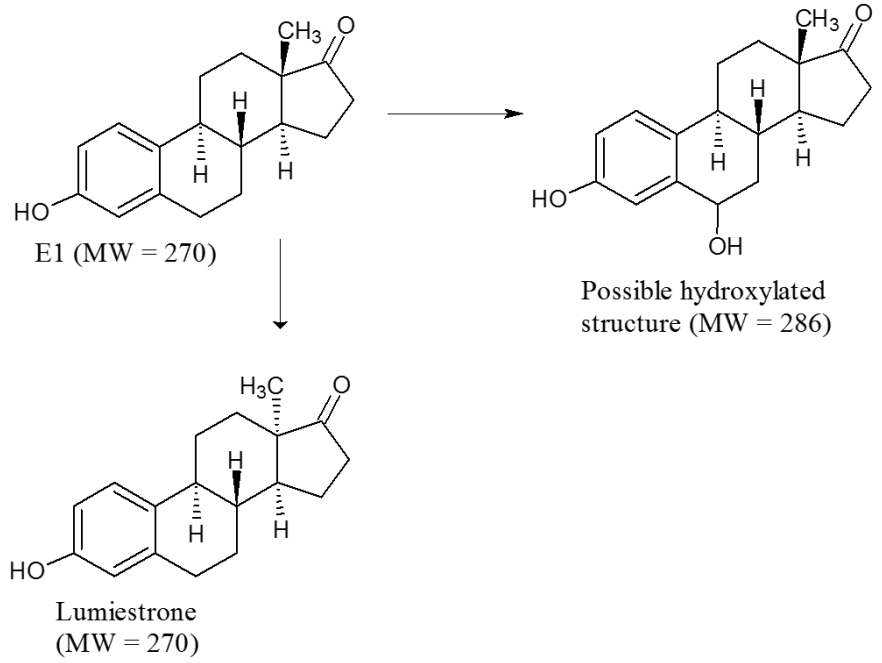

Figure 5.10. Proposed mechanism for photodegradation of E1 by Au-TiO_2 catalysts.

5.8 Photodegradation of 17β-estradiol

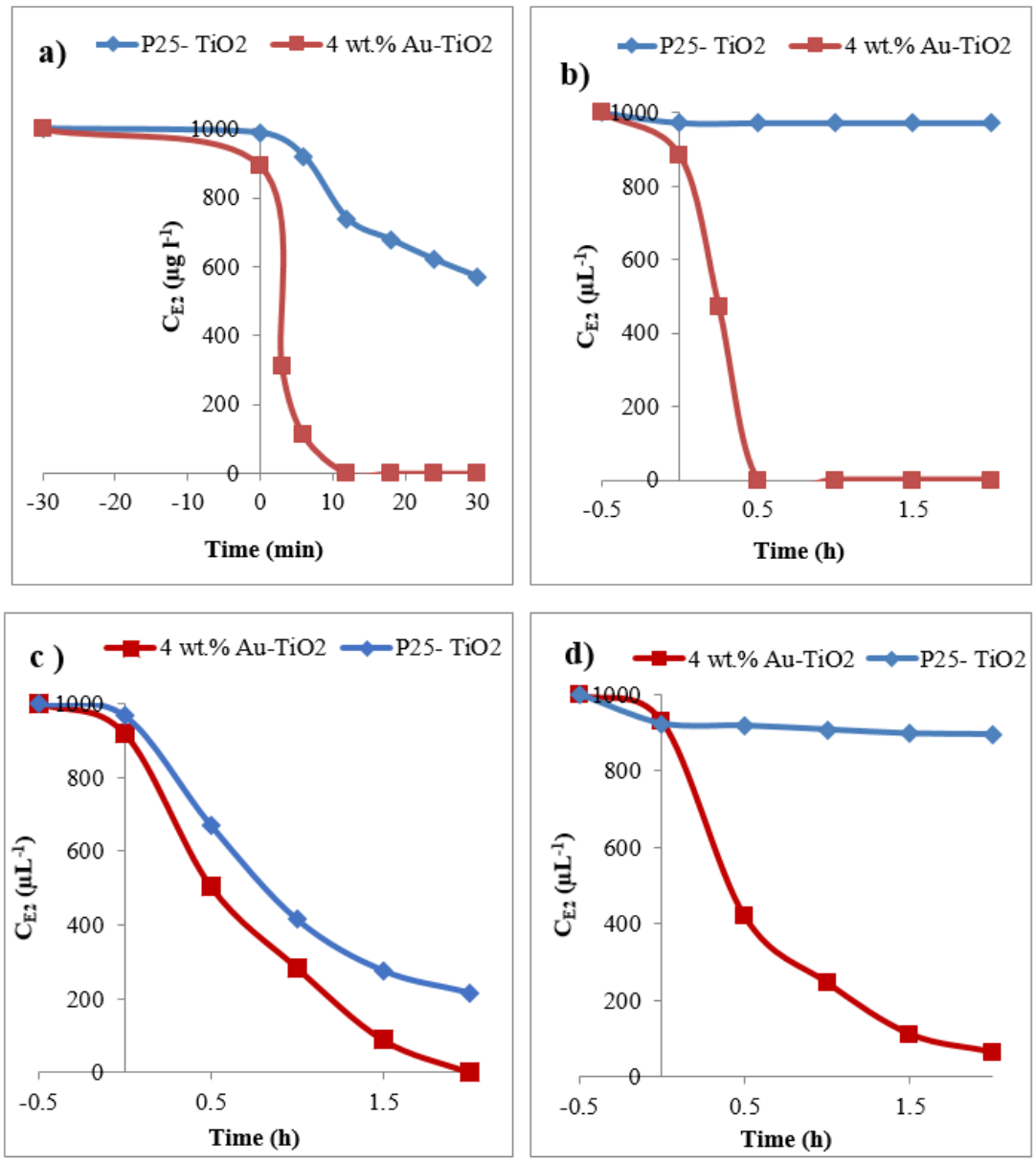

Figure 5.11. Plots for the photodegradation of E2 (1000 µg l^{-1}, 500 ml) using different catalysts (50 mg l^{-1}) and different water matrices under different light sources. (a) E2 concentration vs. time in UPW using UVA LED, (b) E2 concentration vs. time in UPW using "cool white" LED, (c) E2 concentration vs. time in WW using UVA LED, (d) E2 concentration vs. time in WW using "cool white" LED.

Similar to the photodegradation studies for E1 (1 mg l^{-1}), the photocatalysis of E2 in UPW and WW under UVA and cool white LEDs were conducted. The change in E2 concentration with time was analysed using QTOF-LC-MS. The photodegradation rate of E2 (Figure 5.11) was similar to that of E1 under the same experimental conditions. The photocatalysis of E2 was found to follow pseudo 1st order kinetics (Table 5.4).

Table 5.4. Pseudo 1st order kinetic data for E2 photodegradation in the presence of different catalysts, light sources and water matrices. a) in UPW, b) in WW.

a) UPW

Catalyst	UVA			Visible light		
	k (h^{-1})	R^2	$t_{1/2}$ (h)	k (h^{-1})	R^2	$t_{1/2}$ (h)
P25 TiO_2	1.16	0.97	0.6	_	_	_
4 wt.% Au-TiO_2	20.95	0.99	0.03	2.52	0.99	0.28

b) WW

Catalyst	UVA			Visible light		
	k (h^{-1})	R^2	$t_{1/2}$ (h)	k (h^{-1})	R^2	$t_{1/2}$ (h)
P25 TiO_2	0.79	0.99	0.88	_	_	_
4 wt.% Au-TiO_2	1.42	0.96	0.49	1.38	0.99	0.5

5.9 Photodegradation by-products of 17β-estradiol

The formation of photo by-products of E2 by 4 *wt*.% Au-TiO_2 catalysts were analysed using QTOF-LC-MS in positive ion mode, with E2 *m/z* = 273.2 (the molecular weight of E2 = 272.2 g mol^{-1}). Two reaction intermediates were detected with *m/z* 271.2 and *m/z* 289.2 (Figure 5.12). The intermediates formed were further degraded by the photocatalysts with increasing reaction time. The by-product with *m/z* 271.2 was verified as E1 by comparing with a known E1 standard. This agrees with the previous

literature where E1 concentration was found to increase due to the partial oxidation of E2 (Carballa *et al.*, 2004). The by-product with *m/z* 289.2 has a *m/z* 16 units greater than the parent compound E2 (*m/z* 273.2). This indicates the addition of a hydroxyl group, i.e., hydroxylated by-product of E2.

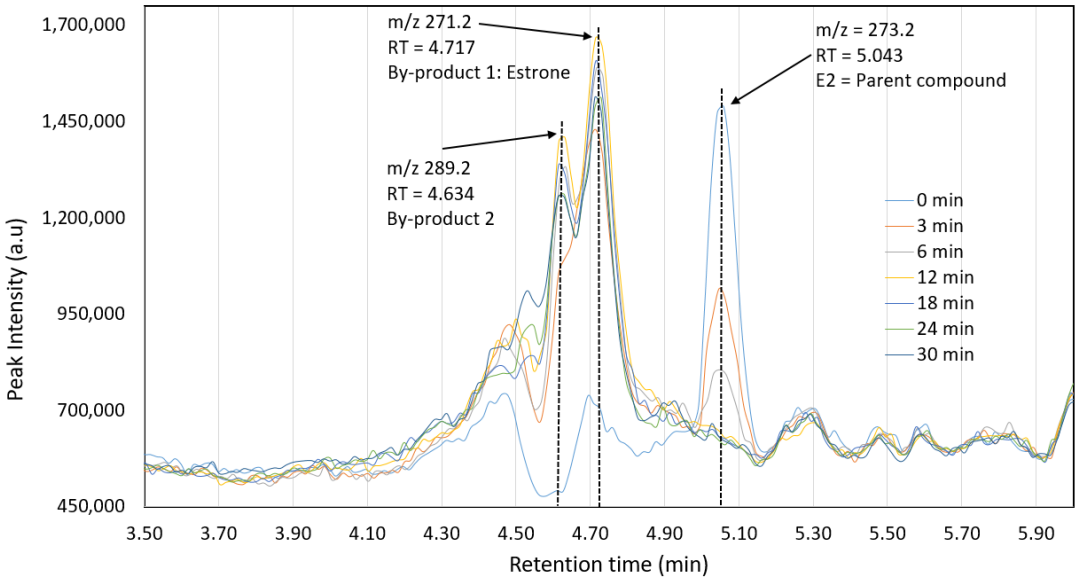

Figure 5.12. Total ion chromatograms of E2 and its photodegradation by-products (under UVA LED in the presence of 4 *wt.*% Au-TiO_2) obtained using QTOF-LC-MS in positive ionization mode.

5.10 Conclusions

The Au-TiO_2 catalysts were more efficient than P25 TiO_2 in removing E1 under UVA and visible LEDs. This is attributed to gold nanoparticles acting as electron sinks to minimise electron-hole recombination under UVA and due to increased absorption of light in the 500-600 nm wavelength. The catalysts' performance decreased for the light sources in the order: UVA > cool white > green light. Photocatalysis of E1 followed pseudo 1st order kinetics. E1 degradation was significantly more efficient by using 4 *wt.%* Au-TiO_2 than P25 TiO_2 under UVA (k = 0.28 ± 0.01 min^{-1} vs. 0.01 min^{-1}) and

under cool white light (k = 2.44 ± 0.36 h^{-1} vs. 0.06 ± 0.01 h^{-1}). Under UVA illumination, 93% E1 degradation was observed in 30 min with 4 *wt.%* Au-TiO_2, while P25 resulted in 26% of E1 removal. Under visible light P25 was inactive while 4 *wt.%* Au-TiO_2 degraded all the E1 in 2h. The photocatalytic activity under visible light decreased in the order 4 *wt.%* Au-TiO_2 > 8 *wt.%* Au-TiO_2 > 2 *wt.%* Au-TiO_2 > 1 *wt.%* Au-TiO_2 > P25 TiO_2.

Four by-products were identified during the photocatalysis of E1, of which one was identified as lumiestrone and the other three as hydroxylated forms of E1. For E2 photocatalysis, two intermediates - a hydroxylated from of E2 and E1 were detected. In addition, the photoproducts of E1 and E2 were also degraded with further irradiation. The photodegradation rate of E1 decreased for the water matrices in the order, UPW > SWW ≈ WW. This could be due to the negative effects of the constituents present in wastewater. It can be concluded that 4 *wt.%* Au-TiO_2 performed significantly better than P25 TiO_2 under UVA and visible light in all of the water matrices.

Chapter 6: Photocatalysis of 17α-ethynylestradiol and estriol using engineered immersible optical fibres and light emitting diodes

Chapter 6: Photocatalysis of 17α-ethynylestradiol and estriol using engineered immersible optical fibres and light emitting diodes

6.1 Introduction

Of current global concern are the endocrine disrupting chemicals (EDCs) - exogenous chemicals that alter the functions of the endogenous hormones, to cause adverse effects especially in reproductive health (Frontistis *et al.*, 2015; Roig *et al.*, 2013) to the animals and potential human (McLachlan, 2001). EDCs can be natural substances such as estrone (E1) and estriol (E3) or synthetic chemicals such as alkylphenols and 17α-ethynylestradiol (EE2), although their biological potency can vary by several orders of magnitude (Rutishauser *et al.*, 2004). It is widely reported that the effluents from the sewage treatment plants (STPs) are one of the key sources of EDCs discharges to the natural aquatic environment (Laganà *et al.*, 2004). Steroidal hormones are resistant to biodegradation, hence their complete removal by conventional water treatment facilities is difficult (Khanal *et al.*, 2006). As a result, advanced sewage treatment technology is widely researched, including those based on adsorption and photocatalysis.

Photocatalysis under UV light irradiation has been widely researched. TiO_2 is considered an attractive advanced oxidation process due to its high photocatalytic activity under UV irradiation, commercial availability and photo-stability (Fox and Dulay, 1993; Primo *et al.*, 2011). However, only UV light, which is 3-5% in the sunlight, can activate pure TiO_2 (Frontistis *et al.*, 2011a). Hence the use of visible light for photocatalysis is of great interest, by using solar energy as the driving force hence

making the process a green technology. Noble metals (Ag, Au, Pt, Pd and Ru) are proved to be efficient in enhancing the UV light activity of TiO_2 while introducing a notable visible light response (Sornalingam *et al.*, 2018; Yan *et al.*, 2013). Gold is favoured due to its non-toxicity, stability and biocompatibility (Ayati *et al.*, 2014).

Under UVA irradiation, the electrons from the valence band of the TiO_2 catalyst particles get excited and move to the conduction band leaving a hole in the valence band. If H_2O or adsorbed OH^- ions reduce the hole, then $HO^\bullet$ free radicals are formed, which in turn oxidise the organic pollutants. The electron in the conduction band is accepted by molecular oxygen to form $O_2^{\bullet-}$ free radicals, which then forms $^\bullet OH$. The enhanced photocatalytic performance of Au-TiO_2 compared to P25 TiO_2 under UVA could be attributed to the following: Some electrons from TiO_2 conduction band crosses to gold nanoparticles on the TiO_2 surface; therefore, electron-hole recombination is reduced (Chen *et al.*, 2012). On the other hand, for Au-TiO_2 under visible light, the electrons in Au nanoparticles that gain sufficient energy to overcome the schottky barrier will cross to the conduction band of TiO_2, thus leading to the visible light activity of the catalyst (Lin *et al.*, 2015b). At nanoparticulate form localised surface plasmons can be excited in gold by visible light ~ λ = 520 nm (Jain *et al.*, 2008). The electrons that gain sufficient energy - excited by LSPR, will flow to TiO_2, enabling photocatalysis.

Photocatalysis studies in water treatment normally use a light source located outside of the reactors. This results in significant loss of transmitted light before reaching the photocatalysts thus limiting activity to the surface layer of the slurry (Peill and Hoffmann, 1996). Here we examine the use of flexible, waterproof LED strips or modified air-clad fibres to overcome the significant limitation of light penetration.

Optical fibres are thin (μm diameter) glass/polymer fibres that are used to transmit light over long distances. The propagation of light through optical fibres is based on total internal reflection that takes place at the boundary/interface of two mediums when the light passes from a medium with high refractive index towards a medium with low refractive index, if the angle of incidence is greater than the critical angle. Total internal reflection is achieved in optical fibres as the core is made of high index material covered by a material (known as cladding) that has low index. Generally, the optical fibre is coated with an optically inactive protective material.

Multimode air-clad fibres (Canning, 2011; Windeler *et al.*, 1999) have a large surface area, high numerical apertures (*approaching 1*) together with high spectral transmission, which makes them attractive for low light collection (Åslund and Canning, 2009) and suitable for carrying light underwater. Pure silica cores can resist photo-darkening at shorter wavelengths (required for photocatalysis) compared to conventional doped cores which photodarken with UV exposure. Emission from the end of fibres alone is insufficient to activate large surface areas of the catalysts but side-emitting fibres have been reported (Denny *et al.*, 2009; Xu *et al.*, 2008). However, light cannot be transmitted for long distances due to the loss of light through sides of the side-emitting fibres. Du *et al.* (2008) reported that the relative light intensity emitted from the side was quickly attenuated in the first 10 cm of the fibre. Uniform side emission from fibres over longer distances (10 m) has been reported (Xu *et al.*, 2008) but most of the light in these fibres propagates in the forward direction, hence resulting in only a small portion of side emission. Catalysts can be immobilised onto fibres (Lin *et al.*, 2015a; Lin *et al.*, 2017; Sun *et al.*, 2000) or the light emitted by the

fibres can be projected onto catalysts coated on other surfaces (Denny *et al.*, 2009; Lin and Valsaraj, 2005).

In addition to optical fibres, LEDs present a cost-effective method to introduce light into a reactor system. Immersible LED strips are now commercially available and have not yet been reported as light sources in this context.

We examined the effectiveness of two new light delivery methods by measuring the degradation of the estrogenic steroidal hormones EE2 and E3 (Figure 1.1) in reactors equipped with optical fibres or LEDs.

6.2 Methodology

6.2.1 Preparation of Au-TiO_2 catalyst and immobilisation onto glass beads

An aqueous solution of tetrachloroauric acid ($HAuCl_4$) was prepared using the method of King *et al.* (2015). Au-TiO_2 nanoparticles were synthesised by a deposition-precipitation method (DP) described by Haruta (1997). The detailed preparation procedures and the material characterisations of the catalysts can be found in previous work (Sornalingam *et al.*, 2018). To immobilise the catalysts onto glass beads, the surface of the beads was first etched in 5 v/v% HF solutions for 30 min and washed thoroughly with ultrapure water. Then 50 ml of the catalyst slurry (10 mg l^{-1}) was prepared by sonicating the catalyst powder in ultrapure water for 30 min. Next, the glass beads were dipped into the catalyst suspension for 10 min to attain a catalyst coating. The coated beads were dried at 110 °C for 4 h in an oven and then transferred to a furnace for 1 h at 300 °C. The coating and drying cycles were repeated twice more to achieve sufficient catalyst coating. Finally, the catalyst coated glass beads were

thoroughly washed with ultrapure water to remove any loosely bonded catalyst particles.

6.2.2 Modification of the optical fibres

The side-emission of light from a selected length (L = 5 cm) of the air-clad fibre was achieved by collapsing the air holes at set intervals. Prior to collapsing the air-holes, the outer polymer protective coating of the fibre was removed by wiping off with paint stripper followed by cleaning with isopropyl alcohol. A FiTel S175 single-fibre fusion splicer (Figure 3.1), which uses a controllable electric arc to melt the glass, was used for collapsing the air cladding, after optimising arc power and duration. This approach was chosen due to its simplicity, low cost, rapidity and high reliability. (Other approaches could be used, e.g. a CO_2 laser that offers a route to inscribe longer collapsed regions).

6.2.3 Photodegradation experiments

A 1 g l^{-1} EE2 and E3 stock solutions in methanol were prepared separately and refrigerated at 4 °C (the bottle was covered in aluminium foil to avoid photodegradation). The 200 µg l^{-1} EE2 aqueous solutions were made from a dilution of the stock for optical fibre related studies, while 100 µg l^{-1} E3 solutions were made for LED strip reactor. The optical fibre reactor setup is shown in Figure 3.6 and the waterproof LED strip reactor setup is shown in Figure 3.8.

The initial concentration of the EDC was chosen based on the reactor setup, the conditions, and the analytical techniques used. A loading of 1000 µg l^{-1} was selected for E1 and E2 in reactor 1 that utilised suspended catalysts that have high rates of degradation due to the large surface area, thus resulting in notable degradation within a reasonable timeframe (up to 4h). Reactor 2 (optical fibre) used immobilised catalysts

with lower active surface area and less UV light reaching the catalyst, therefore a lower concentration of 200 µg l^{-1} was chosen for EE2 to achieve a reasonable degradation within 4h. In reactor 3 (LED strip), the system used visible light (unlike the other reactors that used UVA), resulting in slow degradation rates. Therefore a low concentration of 100 µg l^{-1} was chosen for E3 in reactor 3.

6.3 Results and discussion

6.3.1 Material characterisation

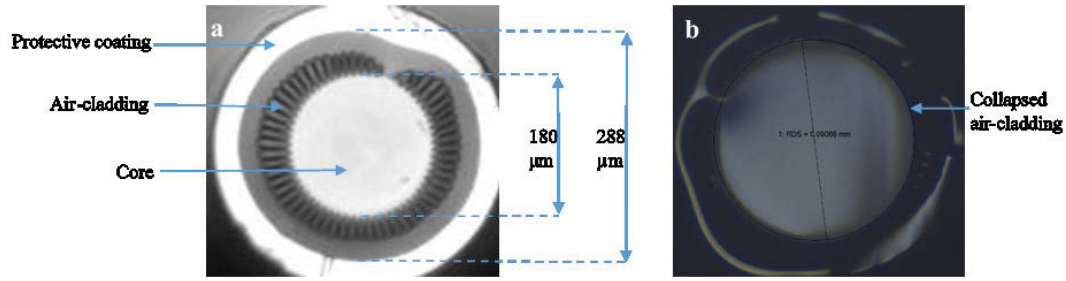

Figure 6.1. Air-clad optical fibre cross-section: a) Before collapsing the air-cladding, and b) after collapsing the air-cladding.

Figure 6.1 shows the cross-section of the air-clad optical fibre before and after applying the electric arc (arc power = 245 arbitrary unit, arc duration = 50 ms). Without air cladding, the immersed silica core comes into contact with water in the reactor, permitting light to escape through the sides of the fibre and illuminating the photocatalysts. Fluorescence arising from aqueous Rhodamine B was used to detect the light emission from the air-clad fibre before and after collapsing the air-rings (Figure 6.2) (Rhodamine B absorbs UV irradiation and emits visible red light).

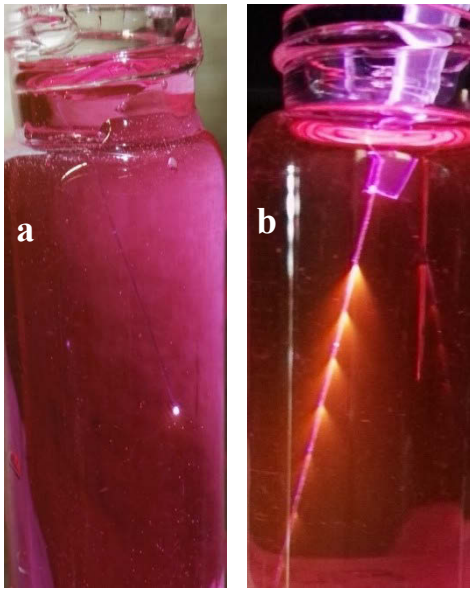

Figure 6.2. a) End emission of light through air-clad optical fibre before modification, b) side emission of light through the air-ring collapsed portions of the optical fibre in Rhodamine B solution.

The light intensity at the far end of the fibre was measured (Newport 2832C power meter) before and after collapsing the air-ring. The side emission intensity decreased as more air-rings were collapsed, with no significant side emission observed after four arcs under the conditions used in this work. Therefore, four arcs were chosen to get the optimum amount of side emission. A 75±5% drop in the end emission intensity of the fibre was obtained when four arcs were applied.

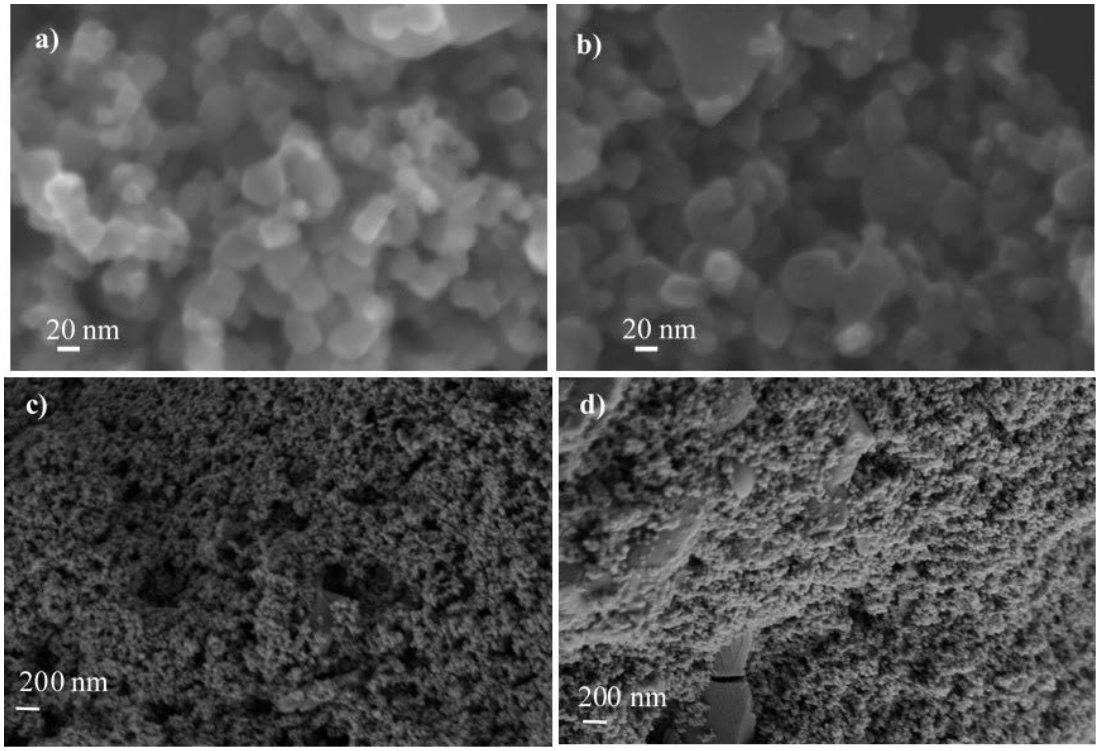

Figure 6.3. SEM images of catalyst powders: a) P25 TiO_2 and b) 4 *wt*.% Au-TiO_2 and catalysts immobilised onto glass beads: c) P25 TiO_2 and d) 4 *wt*.% Au-TiO_2.

The photocatalysts were observed using an SEM, Figure 6.3, which shows the surface morphology of spheroidal shaped TiO_2 catalyst particles. Detailed SEM images of catalysts could be found in our previous work (Sornalingam *et al.*, 2018). The successful immobilisation of the photocatalyst onto glass beads by dip-coating method are shown in figure 6.3c-d.

6.3.2 Photodegradation of 17α-ethynylestradiol and estriol

6.3.2.1 Optical fibre reactor experiments

The air-clad optical fibres efficiently transmitted light from the light source to the catalysts coated onto the glass beads, enabling the photodegradation of the pollutant EE2 under UVA irradiation for both P25 TiO_2 and 4 *wt*.% Au-TiO_2 photocatalysts (Figure 6.4). The EE2 removal rate in the presence of 4 *wt*.% Au-TiO_2 was higher

compared to using P25 TiO_2 (Figure 6.4a). The rate of photodegradation for both the catalysts were found to follow pseudo first order kinetics (Figure 6.4b). EE2 $t_{1/2}$ were 1.26 h and 0.78 h, in the presence of P25 TiO_2 and 4 *wt*.% Au-TiO_2 catalysts respectively (Table 6.1). No apparent loss in EE2 was noted under white light irradiation for the duration of the experiment (2 h). P25 TiO_2 was virtually inactive under white light LED, since the photonic energy from white light irradiation was insufficient to overcome the bandgap of TiO_2. The visible light active Au-TiO_2 (as shown in our previous photocatalysis work on the removal of estrone (Sornalingam *et al.*, 2018)) failed to remove any EE2 in 2 h. This was attributed to the small amount of the light transmitted and dispersed by the fibre.

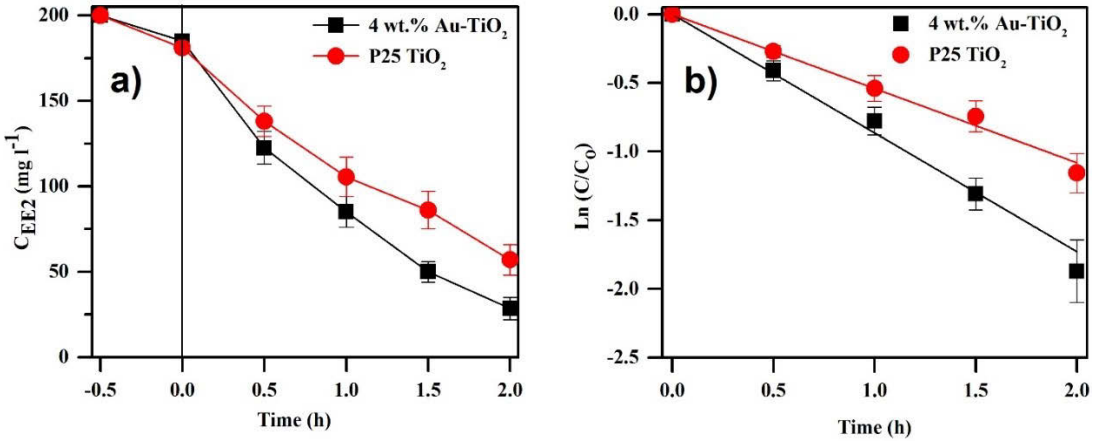

Figure 6.4. Plots for the photodegradation of EE2 (200 µg l^{-1}) under UVA LED in optical fibre reactor system, using P25 TiO_2 and 4 *wt*.% Au-TiO_2 photocatalysts immobilised onto glass beads: (a) EE2 concentration *vs.* time, (b) Pseudo-first order kinetic data. Each experiment was repeated three times.

Table 6.1. Pseudo-first order kinetic data for EE2 photodegradation in the presence of immobilised P25 TiO_2 and 4 *wt*.% Au-TiO_2 photocatalysts under UVA LED in optical fibre reactor.

Photocatalyst	k (h^{-1})	R^2	$t_{1/2}$ (h)
P25 TiO_2	0.55 ± 0.07	0.98	1.26 ± 0.16
4 *wt*.% Au-TiO_2	0.89 ± 0.11	0.99	0.78 ± 0.09

6.3.2.2 Waterproof LED strip experiments

Photocatalysis experiments with E3 were conducted using cool white light waterproof LED strip as the light source (Figure 3.7). No degradation of the pollutants were observed under the white light LED irradiation in the absence of the catalysts (photolysis). Under darkness 8.9 ± 3.9% and 45.5 ± 2.5% decrease in E3 concentration was observed in the presence of P25 TiO2 and 4 *wt*.% Au-TiO_2 due to adsorption. There was no change in the E3 concentration after the adsorption under darkness, in the presence of P25 TiO_2, since it is inactive under visible light (Figure 6.5a). Au-TiO_2 degraded E3 following pseudo-first order kinetics, with k = 0.13 h^{-1} and $t_{1/2}$ = 4.62 h (Figure 6.5).

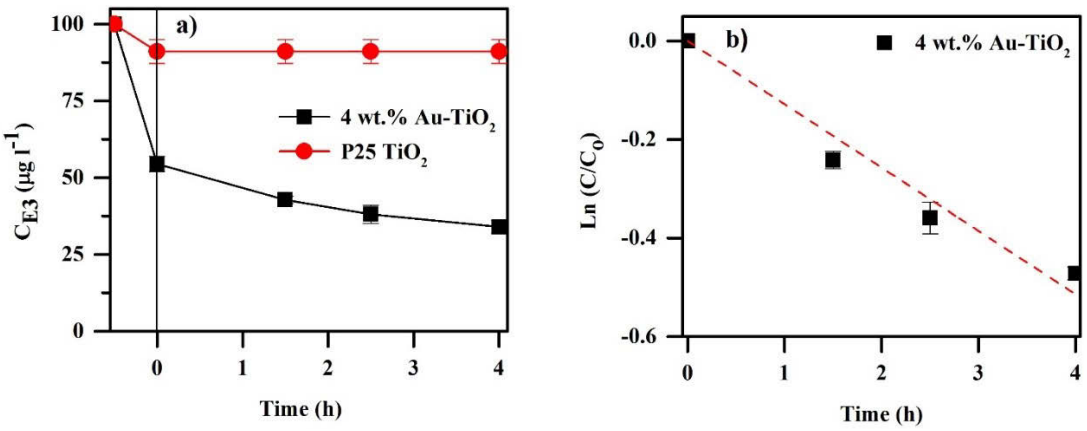

Figure 6.5. Plots for the photodegradation of E3 (100 µg l^{-1}) in immersible LED strip reactor system, using P25 TiO_2 and 4 *wt*.% Au-TiO_2 photocatalysts: (a) E3 concentration *vs.* time, (b) Pseudo-first order kinetic data. Each experiment was repeated three times.

6.3.3 Reusability of the optical fibres, catalyst coated glass beads and the LED strip

The reusability of the optical fibres and the catalysts coated onto glass beads were examined by reusing the catalysts and the fibres for up to three treatment cycles. The catalyst coated beads were removed from the reactor after each run, washed with ultrapure water and were calcined at 300 °C prior to reusing them. The optical fibre coupled to the LED light source was kept intact for all the three cycles to avoid the change in the intensity of the light that exited the fibre. However, the fibre was washed by circulating ultrapure water through the reactor. The ability of the catalysts to remove the pollutants decreased by ~ 6% after three cycles. Similar trend was observed elsewhere (Tasbihi *et al.*, 2007; Verma *et al.*, 2014). This shows the stability of the fibres and the catalysts. Similarly, the reusability of the waterproof LED reactor system was tested for three treatment cycles. Here, the LED strip was removed from the reactor, washed with ultrapure water and air dried before reuse. The removal rate of E3 in the LED strip reactor did not change after three cycles (error ~ 3%).

For all the EDCs (E1, E2, E3 and EE2) the degradation efficiency did not change much after three cycles when the recovered catalysts were calcined at 300 ^{o}C. For E1 and E2, an approximately 3% drop in removal efficiency was observed while EE2 and E3 resulted in similar (up to 6%) drops after three cycles. When the catalysts were directly reused without calcination, significant losses in catalyst performance were observed. This was due to the degradation by-products remaining on the catalyst and competing with the fresh EDC solution, thus decreasing the overall removal efficiency.

The dip coating method used in this study to immobilise the catalysts onto the glass beads resulted in the formation of rings where the beads contacted each other and the

container surface. Some, cracks in the catalyst coating was also observed. Therefore, when the glass beads were refilled into the reactor after each cycle, the amount of catalyst exposed to the light emitted by the fibre varies, which may result in a change in photodegradation rates too. Nevertheless, the results obtained after three cycles show that the overall change in EE2 removal rates were not significantly affected by this change.

6.4. Conclusions

P25 TiO_2 and gold-modified TiO_2 photocatalysts were successfully illuminated with air-clad optical fibres coupled to high efficacy LEDs or with flexible waterproof LED strips. These setups were effective at degrading EE2 and E3. The reactor setups addressed a major challenge faced by suspended photocatalysis systems: the introduction of light into reactor systems. Efficient side emission of light from the optical fibres was obtained by collapsing the air-holes of an air-clad optical fibre using a fusion splicer.

The optical fibre photocatalytic reactor system efficiently removed the pollutants under UVA, where 4 *wt*.% Au-TiO_2 showed enhanced activity compared to P25 TiO_2. The rate of photodegradation for both the catalysts followed pseudo first order kinetics. EE2 $t_{1/2}$ under UVA were 1.26 h and 0.78 h, in the presence of P25 TiO_2 and gold modified catalysts respectively. The catalysts, as well as the fibres were found to be stable for three reaction cycles with a small loss of activity at the end of each cycle (6% decrease in degradation efficiency was noted after three cycles).

A reactor using waterproof LED strips removed the pollutant E3 in the presence of 4 *wt*.% Au-TiO_2 photocatalysts, following pseudo first order kinetics with $k = 0.13\ h^{-1}$

and $t_{1/2}$ = 4.62 h. No degradation of the pollutants were observed in the absence of the catalysts (photolysis).

Overall, engineered air-clad optical fibres that enable selective side emission of light and flexible waterproof LED strips are promising modes of light delivery for underwater photocatalysis.

Chapter 7: Conclusions and recommendations

Chapter 7: Conclusions and recommendations

7.1. Conclusions

The main objectives of this study were to synthesise and characterise gold modified TiO_2 photocatalysts designed to degrade the estrogenic steroidal endocrine disrupting hormones E1, E2, E3 and EE2. The influence of different water matrices on the photodegradation rate of these pollutants was studied. The degradation by-products were examined using QTOF-LC-MS and a removal mechanism of E1 was proposed. In addition, the photocatalysts were immobilised onto glass beads to address the shortcomings of suspended reactor systems. The difficulty in transmitting light to the site of contamination, a challenge in photocatalysis, was addressed by two techniques: (i) a modified air-clad optical fibre and (ii) a flexible waterproof LED strip, reactor systems.

7.1.1. Synthesis and characterisation of gold modified TiO_2 photocatalysts

Gold modified TiO_2 photocatalysts were synthesised by a DP method. Different amounts of aqueous $HAuCl_4$ solutions were added to P25 TiO_2 to attain 0 to 8 *wt.*% gold loadings. The catalysts were characterised using different techniques such as TGA, XRD, Raman spectroscopy, UV-Vis spectroscopy, SEM, ICP-MS, zeta potential and particle size analysis.

A small weight loss (~2 %) in TGA was recorded upon heating the uncalcined catalysts in the temperature range 60 – 600 ^oC. The loss in weight could be attributed to the removal of interstitial water and/or chloride. XRD peaks corresponding to anatase and rutile for Au-TiO_2 and P25 TiO_2 indicate that the addition of the gold does not significantly change TiO_2 crystal structure. The absence of peaks corresponding to

gold for uncalcined Au-TiO_2 and detection of peaks matching metallic gold after calcination reveals that the Au^{3+} ions in the uncalcined materials subsequently form Au^0 on TiO_2 surface upon calcination. In Raman spectra, anatase peaks became broader with increased gold loadings indicating that the addition of gold introduced defects in the structure, which may enhance photocatalytic activity by entrapping photoelectrons and limiting electron-hole recombination.

The UV-vis spectrum of P25 TiO_2 showed absorbance of light with wavelength less than 400 nm, while the Au-TiO_2 catalysts showed a wide absorption band between 500 – 600 nm due to surface plasmon resonance of gold nanoparticles on TiO_2 surface, which is a key contributor to the Au-TiO_2's visible light photocatalytic activity. SEM images revealed spherical gold nanoparticles on the surface of the spheroidal shaped TiO_2 nanoparticles, though agglomeration of gold nanoparticles were observed at high gold loading (8 *wt.*%). Both EDS and ICP-MS results showed that the actual gold loadings were closer to the theoretical loadings. The PZC of both P25 TiO_2 and Au-TiO_2 were found to be ~6.8. The largest hydrodynamic particle size was obtained for pH values close to the PZC.

7.1.2. Enhanced photocatalysis of estrone and 17β-estradiol in water using Au-TiO_2 catalysts under UVA and visible LEDs

The photodegradation of E1 in the presence of P25 TiO_2 and Au-TiO_2 was studied under three different water matrices: UPW, SWW and WW, and using three types of LEDs: UVA, cool white and green. Four catalyst loadings (25 mg l^{-1}, 50 mg l^{-1}, 75 mg $l^{-1}$and 100 mg l^{-1}) were examined to select a suitable loading for the photocatalytic experiments. The rate of photocatalysis of E1 increased linearly as the catalyst concentration was increased due to the availability of more catalyst active sites for the

pollutants. A loading of 50 mg l^{-1} was chosen as an appropriate catalyst concentration to allow monitoring of E1 degradation under UV light over a reasonable period. After three cycles of photocatalysis, the activity did not diminish by any significant amount (97-100%), showing the reusability of the photocatalysts.

Au-TiO_2 catalysts were more efficient than P25 TiO_2 in removing E1, under UVA and visible LEDs, attributed to gold nanoparticles acting as electron sinks to minimise electron-hole recombination under UVA and due to increased absorption of light in the 500 - 600 nm wavelength. The catalysts' performance decreased for the light sources in the order: UVA > cool white > green light. Photocatalysis of E1 was found to follow pseudo 1st order kinetics. E1 degradation was significantly more efficient by using 4 *wt.%* Au-TiO_2 than P25 TiO_2 under UVA ($k = 0.28 \pm 0.01$ min^{-1} vs. 0.01 min^{-1}) and under cool white light ($k = 2.44 \pm 0.36$ h^{-1} vs. 0.06 ± 0.01 h^{-1}). The photocatalytic activity under visible light decreased in the order 4 *wt.%* Au-TiO_2 > 8 *wt.%* Au-TiO_2 > 2 *wt.%* Au-TiO_2 > 1 *wt.%* Au-TiO_2 > P25 TiO_2.

Four by-products were identified during the photocatalysis of E1, of which one was identified as lumiestrone and the other three as hydroxylated forms of E1. The photoproducts were also degraded with further irradiation. The photodegradation rate of E1 decreased for the water matrices in the order: UPW > SWW ≈ WW. This could be due to the negative effects of the constituents present in wastewater. It can be concluded that 4 *wt.%* Au-TiO_2 performed significantly better than P25 TiO_2 under UVA and visible light in all the water matrices.

7.1.3. Photocatalysis of 17α-ethynylestradiol and estriol using engineered immersible optical fibres and light emitting diodes

P25 TiO_2 and gold-modified TiO_2 photocatalysts were successfully illuminated with air-clad optical fibres coupled to high efficacy LEDs or with flexible waterproof LED strips. These setups were effective at degrading EE2 and E3. The reactor setups addressed a major challenge faced by suspended photocatalysis systems: the introduction of light into reactor systems. Efficient side emission of light from the optical fibres was obtained by collapsing the air-holes of an air-clad optical fibre using a fusion splicer.

The optical fibre photocatalytic reactor system efficiently removed the pollutants under UVA, where 4 *wt*.% Au-TiO_2 showed enhanced activity compared to P25 TiO_2. The rate of photodegradation for both the catalysts followed pseudo first order kinetics. EE2 $t_{1/2}$ under UVA were 1.26 h and 0.78 h, in the presence of P25 TiO_2 and gold modified catalysts respectively. The catalysts, as well as the fibres were found to be stable for three reaction cycles with a small loss of activity at the end of each cycle (6% decrease in degradation efficiency was noted after three cycles).

A reactor using waterproof LED strips removed the pollutant E3 in the presence of 4 *wt*.% Au-TiO_2 photocatalysts, following pseudo first order kinetics with $k = 0.13\ h^{-1}$ and $t_{1/2} = 4.62$ h. No degradation of the pollutants was observed in the absence of the catalysts (photolysis).

Overall, engineered air-clad optical fibres that enable selective side emission of light and flexible waterproof LED strips are promising modes of light delivery for underwater photocatalysis.

7.2. Recommendations

Although major progress has been achieved in tackling the project objectives, there are limitations due to limited time and resources. Below are some of the research work which should be further exploited:

- Further investigation of parameters such as the effect of temperature, energy consumption, reactor design and the development of inexpensive catalysts should be considered.
- Visible light active photocatalysts were synthesised in this research and the next phase of work would investigate the scaling-up of the production of these doped TiO_2 materials.
- The suspended catalysts used for photodegradation (discussed in Chapter 5) showed high reusability with the separation of the catalysts from the slurry after each cycle was carried out by gravity settling followed by centrifugation. Further investigations are warranted into methods that enable easy separation of the catalysts for their commercial application. In this context, immobilised catalysts could overcome the economic issues associated with suspended catalysts.
- Photocatalysts such as TiO_2 are known to be non-selective towards target pollutants. Therefore, even EDCs present at trace levels require a large quantity of catalysts, due to TiO_2's activity towards most of the organics present in aqueous systems. Work investigating target-specific catalysts would be beneficial in this area.
- Detection, quantification and evaluation of estrogenic activity of EDCs and their intermediates at low concentration remain a major challenge. In this study

the photodegradation of estrogenic steroidal hormones was conducted under controlled conditions using relatively higher EDC concentrations than environmentally relevant; more realistic conditions should be investigated in future experiments. Selective extraction methods together with highly sensitive analytical techniques are required to fully explore the degradation mechanisms.

- A combination of novel treatment technologies should be tested for enhanced removal efficiency. For example, membrane filtration and photodegradation might be integrated by treating the concentrate from the membrane system with photodegradation for a targeted approach.
- The modified air-clad optical fibres are capable of transmitting light over long distances from LED sources. Nonetheless, the use of sunlight via solar concentrators needs to be tested.
- Flexible waterproof LED strips are useful for underwater photodegradation. However, they cannot be kept underwater for prolonged periods, hence needing the development of LEDs with excellent water-resistant capability.

Appendix

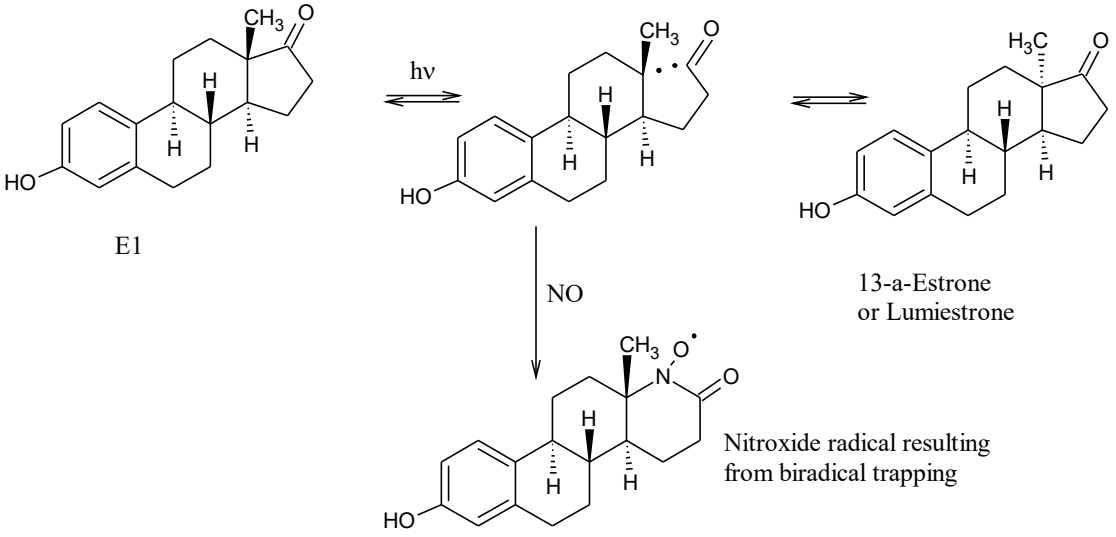

Figure A1. Proposed degradation pathway of E1 photolysis. Redrawn from Trudeau *et al.* (2011).

Bibliography

Arabatzis IM, Stergiopoulos T, Andreeva D, Kitova S, Neophytides SG, Falaras P. Characterization and photocatalytic activity of Au/TiO_2 thin films for azo-dye degradation. J. Catal. 2003; 220: 127-135.

Åslund ML, Canning J. Air-clad fibres for astronomical instrumentation: focal-ratio degradation. Exp. Astron 2009; 24: 1-7.

Atkinson SK, Marlatt VL, Kimpe LE, Lean DRS, Trudeau VL, Blais JM. Environmental factors affecting ultraviolet photodegradation rates and estrogenicity of estrone and ethinylestradiol in natural waters. Arch. Environ. Contam. Toxicol. 2011; 60: 1-7.

Ayati A, Ahmadpour A, Bamoharram FF, Tanhaei B, Mänttäri M, Sillanpää M. A review on catalytic applications of Au/TiO_2 nanoparticles in the removal of water pollutant. Chemosphere 2014; 107: 163-174.

Behnajady MA, Modirshahla N, Hamzavi R. Kinetic study on photocatalytic degradation of CI Acid Yellow 23 by ZnO photocatalyst. J. Hazard. Mater. 2006; 133: 226-232.

Belhaj D, Baccar R, Jaabiri I, Bouzid J, Kallel M, Ayadi H*, et al.* Fate of selected estrogenic hormones in an urban sewage treatment plant in Tunisia (North Africa). Sci. Total Environ. 2015; 505: 154-160.

Benotti MJ, Stanford BD, Wert EC, Snyder SA. Evaluation of a photocatalytic reactor membrane pilot system for the removal of pharmaceuticals and endocrine disrupting compounds from water. Water Res. 2009; 43: 1513-1522.

Block BP, Bailar JC. The reaction of gold(iii) with some bidentate coordinating groups. J. Am. Chem. Soc. 1951; 73: 4722-4725.

Bond GC, Thompson DT. Catalysis by gold. Catal. Rev. Sci. Eng. 1999; 41: 319-388.

Bowker M, Nuhu A, Soares J. High activity supported gold catalysts by incipient wetness impregnation. Catal. Today 2007; 122: 245-247.

Briciu RD, Kot-Wasik A, Namiesnik J. Analytical challenges and recent advances in the determination of estrogens in water environments. J. Chromatogr. Sci. 2009; 47: 127-139.

Brienza M, Ahmed MM, Escande A, Plantard G, Scrano L, Chiron S*, et al.* Relevance of a photo-Fenton like technology based on peroxymonosulphate for 17β-estradiol removal from wastewater. Chem. Eng. J. 2014; 257: 191-199.

Brzozowski AM, Pike ACW, Dauter Z, Hubbard RE, Bonn T, Engström O*, et al.* Molecular basis of agonism and antagonism in the oestrogen receptor. Nature 1997; 389: 753-758.

Canning J. Structured optical fibres and the application of their linear and non-linear properties. In: Andreone A, Cusano A, Cutolo A, Galdi V, editors. Selected topics in photonic crystals and metamaterials. World Scientific, 2011, pp. 389-452.

Canonica S, Meunier L, Von Gunten U. Phototransformation of selected pharmaceuticals during UV treatment of drinking water. Water Res. 2008; 42: 121-128.

Carballa M, Omil F, Lema JM, Llompart M, García-Jares C, Rodríguez I*, et al.* Behavior of pharmaceuticals, cosmetics and hormones in a sewage treatment plant. Water Res. 2004; 38: 2918-2926.

Carneiro JT, Yang CC, Moma JA, Moulijn JA, Mul G. How gold deposition affects anatase performance in the photo-catalytic oxidation of cyclohexane. Catal. Lett. 2009; 129: 12-19.

Caupos E, Mazellier P, Croue JP. Photodegradation of estrone enhanced by dissolved organic matter under simulated sunlight. Water Res. 2011; 45: 3341-3350.

Chalasani R, Vasudevan S. Cyclodextrin-functionalized Fe_3O_4@TiO_2: Reusable, magnetic nanoparticles for photocatalytic degradation of endocrine-disrupting chemicals in water supplies. ACS Nano 2013; 7: 4093-4104.

Chen HC, Kuo HW, Ding WH. Determination of estrogenic compounds in wastewater using liquid chromatography-tandem mass spectrometry with electrospray and atmospheric pressure photoionization following desalting extraction. Chemosphere 2009; 74: 508-514.

Chen JJ, Wu JCS, Wu PC, Tsai DP. Improved photocatalytic activity of shell-isolated plasmonic photocatalyst Au@SiO_2/TiO_2 by promoted LSPR. J. Phys. Chem. C 2012; 116: 26535-26542.

Chen PJ, Rosenfeldt EJ, Kullman SW, Hinton DE, Linden KG. Biological assessments of a mixture of endocrine disruptors at environmentally relevant concentrations in water following UV/H_2O_2 oxidation. Sci. Total Environ. 2007; 376: 18-26.

Chen Y, Zhang K, Zuo YG. Direct and indirect photodegradation of estriol in the presence of humic acid, nitrate and iron complexes in water solutions. Sci. Total Environ. 2013; 463: 802-809.

Cheneviere Y, Caps V, Tuel A. Gold-catalyzed oxidation of substituted phenols by hydrogen peroxide. Appl. Catal., A 2010; 387: 129-134.

Chowdhury RR, Charpentier P, Ray MB. Photodegradation of estrone in solar irradiation. Ind. Eng. Chem. Res. 2010; 49: 6923-6930.

Chowdhury RR, Charpentier PA, Ray MB. Photodegradation of 17β-estradiol in aquatic solution under solar irradiation: Kinetics and influencing water parameters. J. Photochem. Photobiol. A 2011; 219: 67-75.

Chusaksri S, Lomda J, Saleepochn T, Sutthivaiyakit P. Photocatalytic degradation of 3,4-dichlorophenylurea in aqueous gold nanoparticles-modified titanium dioxide suspension under simulated solar light. J. Hazard. Mater. 2011; 190: 930-937.

Clouzot L, Marrot B, Doumenq P, Roche N. 17α-ethinylestradiol: An endocrine disrupter of great concern. Analytical methods and removal processes applied to water purification. A review. Environ. Prog. 2008; 27: 383-396.

Coleman HM, Abdullah MI, Eggins BR, Palmer FL. Photocatalytic degradation of 17β-oestradiol, oestriol and 17α-ethynyloestradiol in water monitored using fluorescence spectroscopy. Appl. Catal., B 2005a; 55: 23-30.

Coleman HM, Chiang K, Amal R. Effects of Ag and Pt on photocatalytic degradation of endocrine disrupting chemicals in water. Chem. Eng. J. 2005b; 113: 65-72.

Coleman HM, Eggins BR, Byrne JA, Palmer FL, King E. Photocatalytic degradation of 17β-oestradiol on immobilised TiO_2. Appl. Catal., B 2000; 24: L1-L5.

Coleman HM, Routledge EJ, Sumpter JP, Eggins BR, Byrne JA. Rapid loss of estrogenicity of steroid estrogens by UVA photolysis and photocatalysis over an immobilised titanium dioxide catalyst. Water Res. 2004; 38: 3233-3240.

Coleman HM, Vimonses V, Leslie G, Amal R. Removal of contaminants of concern in water using advanced oxidation techniques. Water Sci. Technol. 2007; 55: 301-306.

Conley JM, Evans N, Mash H, Rosenblum L, Schenck K, Glassmeyer S*, et al.* Comparison of in vitro estrogenic activity and estrogen concentrations in source and treated waters from 25 U.S. drinking water treatment plants. Sci. Total Environ. 2017; 579: 1610-1617.

Czech B, Rubinowska K. TiO_2-assisted photocatalytic degradation of diclofenac, metoprolol, estrone and chloramphenicol as endocrine disruptors in water. Adsorption 2013; 19: 619-630.

D'Ascenzo G, Di Corcia A, Gentili A, Mancini R, Mastropasqua R, Nazzari M*, et al.* Fate of natural estrogen conjugates in municipal sewage transport and treatment facilities. Sci. Total Environ. 2003; 302: 199-209.

Damodar RA, Swaminathan T. Performance evaluation of a continuous flow immobilized rotating tube photocatalytic reactor (IRTPR) immobilized with TiO_2 catalyst for azo dye degradation. Chem. Eng. J. 2008; 144: 59-66.

de Witte B, van Langenhove H, Demeestere K, Dewulf J. Advanced oxidation of pharmaceuticals: Chemical analysis and biological assessment of degradation products. Crit. Rev. Environ. Sci. Technol. 2011; 41: 215-242.

Denny F, Scott J, Pareek V, Peng GD, Amal R. CFD modelling for a TiO_2-coated glass-bead photoreactor irradiated by optical fibres: Photocatalytic degradation of oxalic acid. Chem. Eng. Sci. 2009; 64: 1695-1706.

Desbrow C, Routledge EJ, Brighty GC, Sumpter JP, Waldock M. Identification of estrogenic chemicals in STW effluent. 1. Chemical fractionation and in vitro biological screening. Environ. Sci. Technol. 1998; 32: 1549-1558.

Dette C, Pérez-Osorio MA, Kley CS, Punke P, Patrick CE, Jacobson P*, et al.* TiO_2 anatase with a bandgap in the visible region. Nano Lett. 2014; 14: 6533-6538.

Dimitroula H, Daskalaki VM, Frontistis Z, Kondarides DI, Panagiotopoulou P, Xekoukoulotakis NP*, et al.* Solar photocatalysis for the abatement of emerging micro-contaminants in wastewater: Synthesis, characterization and testing of various TiO_2 samples. Appl. Catal., B 2012; 117: 283-291.

Directive. Directive 2013/39/EU of the European parliament and of the council of 12 August 2013 amending Directives 2000/60/EC and 2008/105/EC as regards priority substances in the field of water policy. Off. J. Eur. Union. 2013.

Dolamic I, Büergi T. In situ ATR-IR study on the photocatalytic decomposition of amino acids over Au/TiO_2 and TiO_2. J. Phys. Chem. C 2011; 115: 2228-2234.

Du P, Carneiro JT, Moulijn JA, Mul G. A novel photocatalytic monolith reactor for multiphase heterogeneous photocatalysis. Appl. Catal., A 2008; 334: 119-128.

Dzinun H, Othman MHD, Ismail AF, Puteh MH, Rahman MA, Jaafar J. Photocatalytic degradation of nonylphenol by immobilized TiO_2 in dual layer hollow fibre membranes. Chem. Eng. J. 2015; 269: 255-261.

El-Sheikh AH, Al-Degs YS, Newman AP, Lynch DE. Oxidized activated carbon as support for titanium dioxide in UV-assisted degradation of 3-chlorophenol. Sep. Purif. Technol. 2007; 54: 117-123.

Fabiyi M, Skelton R. Photocatalytic mineralisation of methylene blue using buoyant TiO_2-coated polystyrene beads. J. Photochem. Photobiol. A 2000; 132: 121-128.

Fan LF, Zhao GH, Shi HJ, Liu MC, Wang YB, Ke HY. A femtomolar level and highly selective 17β-estradiol photoelectrochemical aptasensor applied in environmental water samples analysis. Environ. Sci. Technol. 2014; 48: 5754-5761.

Feng XH, Tu JF, Ding SM, Wu F, Deng NS. Photodegradation of 17β-estradiol in water by UV-vis/Fe(III)/H_2O_2 system. J. Hazard. Mater. 2005; 127: 129-133.

Fernández-Ibáñez P, Blanco J, Malato S, de las Nieves FJ. Application of the colloidal stability of TiO_2 particles for recovery and reuse in solar photocatalysis. Water Res. 2003; 37: 3180-3188.

Fine DD, Breidenbach GP, Price TL, Hutchins SR. Quantitation of estrogens in ground water and swine lagoon samples using solid-phase extraction, pentafluorobenzyl/trimethylsilyl derivatizations and gas chromatography–negative ion chemical ionization tandem mass spectrometry. J. Chromatogr. A 2003; 1017: 167-185.

Fonseca AP, Lima DLD, Esteves VI. Degradation by solar radiation of estrogenic hormones monitored by UV-visible spectroscopy and capillary electrophoresis. Water. Air. Soil. Pollut. 2011; 215: 441-447.

Fox MA, Dulay MT. Heterogeneous photocatalysis. Chem. Rev. 1993; 93: 341-357.

Fredj SB, Nobbs J, Tizaoui C, Monser L. Removal of estrone (E1), 17β-estradiol (E2), and 17α-ethinylestradiol (EE2) from wastewater by liquid–liquid extraction. Chem. Eng. J. 2015; 262: 417-426.

Frontistis Z, Daskalaki VM, Hapeshi E, Drosou C, Fatta-Kassinos D, Xekoukoulotakis NP*, et al.* Photocatalytic (UV-A/TiO_2) degradation of 17α-ethynylestradiol in environmental matrices: Experimental studies and artificial neural network modeling. J. Photochem. Photobiol. A 2012a; 240: 33-41.

Frontistis Z, Daskalaki VM, Katsaounis A, Poulios I, Mantzavinos D. Electrochemical enhancement of solar photocatalysis: Degradation of endocrine disruptor bisphenol-A on Ti/TiO_2 films. Water Res. 2011a; 45: 2996-3004.

Frontistis Z, Drosou C, Tyrovola K, Mantzavinos D, Fatta-Kassinos D, Venieri D*, et al.* Experimental and modeling studies of the degradation of estrogen hormones in aqueous TiO_2 suspensions under simulated solar radiation. Ind. Eng. Chem. Res. 2012b; 51: 16552-16563.

Frontistis Z, Fatta-Kassinos D, Mantzavinos D, Xekoukoulotakis NP. Photocatalytic degradation of 17α-ethynylestradiol in environmental samples by ZnO under simulated solar radiation. J. Chem. Technol. Biotechnol. 2012c; 87: 1051-1058.

Frontistis Z, Kouramanos M, Moraitis S, Chatzisymeon E, Hapeshi E, Fatta-Kassinos D*, et al.* UV and simulated solar photodegradation of 17α-ethynylestradiol in secondary-treated wastewater by hydrogen peroxide or iron addition. Catal. Today 2015; 252: 84-92.

Frontistis Z, Xekoukoulotakis NP, Hapeshi E, Venieri D, Fatta-Kassinos D, Mantzavinos D. Fast degradation of estrogen hormones in environmental matrices by photo-Fenton oxidation under simulated solar radiation. Chem. Eng. J. 2011b; 178: 175-182.

Fujishima A, Zhang XT, Tryk DA. TiO_2 photocatalysis and related surface phenomena. Surf. Sci. Rep. 2008; 63: 515-582.

Gadd JB, Tremblay LA, Northcott GL. Steroid estrogens, conjugated estrogens and estrogenic activity in farm dairy shed effluents. Environ. Pollut. 2010; 158: 730-736.

Game C, Gagnon MM, Webb D, Lim R. Endocrine disruption in male mosquitofish (*Gambusia holbrooki*) inhabiting wetlands in Western Australia. Ecotoxicology 2006; 15: 665-672.

García-Reyero N, Grau E, Castillo M, De Alda MJL, Barceló D, Piña B. Monitoring of endocrine disruptors in surface waters by the yeast recombinant assay. Environ. Toxicol. Chem. 2001; 20: 1152-1158.
Grover D, Zhang Z, Readman J, Zhou J. A comparison of three analytical techniques for the measurement of steroidal estrogens in environmental water samples. Talanta 2009; 78: 1204-1210.
Grover DP, Zhou JL, Frickers PE, Readman JW. Improved removal of estrogenic and pharmaceutical compounds in sewage effluent by full scale granular activated carbon: Impact on receiving river water. J. Hazard. Mater. 2011; 185: 1005-1011.
Grzybowski W, Szydlowski J. The impact of chromophoric dissolved organic matter on the photodegradation of 17α-ethinylestradiol (EE2) in natural waters. Chemosphere 2014; 111: 13-17.
Hammer N, Kvande I, Xu X, Gunnarsson V, Tøtdal B, Chen D*, et al.* Au-TiO_2 catalysts on carbon nanotibres prepared by deposition-precipitation and from colloid solutions. Catal. Today 2007; 123: 245-256.
Han J, Liu YS, Singhal N, Wang LZ, Gao W. Comparative photocatalytic degradation of estrone in water by ZnO and TiO_2 under artificial UVA and solar irradiation. Chem. Eng. J. 2012; 213: 150-162.
Hanselman TA, Graetz DA, Wilkie AC. Manure-borne estrogens as potential environmental contaminants: A review. Environ. Sci. Technol. 2003; 37: 5471-5478.
Hansen KMS, Andersen HR. Energy effectiveness of direct UV and UV/H_2O_2 treatment of estrogenic chemicals in biologically treated sewage. Int. J. Photoenergy 2012: 9.
Haruta M. Size- and support-dependency in the catalysis of gold. Catal. Today 1997; 36: 153-166.
Haruta M, Kobayashi T, Sano H, Yamada N. Novel gold catalysts for the oxidation of carbon-monoxide at a temperature far below 0 ºC. Chem. Lett. 1987: 405-408.
Haruta M, Yamada N, Kobayashi T, Iijima S. Gold catalysts prepared by coprecipitation for low-temperature oxidation of hydrogen and of carbon-monoxide. J. Catal. 1989; 115: 301-309.
Haugen AB, Kumakiri I, Simon C, Einarsrud MA. TiO_2, TiO_2/Ag and TiO_2/Au photocatalysts prepared by spray pyrolysis. J. Eur. Ceram. Soc. 2011; 31: 291-298.
He Y, Sutton NB, Rijnaarts HH, Langenhoff AA. Degradation of pharmaceuticals in wastewater using immobilized TiO_2 photocatalysis under simulated solar irradiation. Appl. Catal., B 2016; 182: 132-141.
Hidalgo MC, Maicu M, Navío JA, Colón G. Effect of sulfate pretreatment on gold-modified TiO_2 for photocatalytic applications. J. Phys. Chem. C 2009; 113: 12840-12847.
Hidalgo MC, Murcia JJ, Navío JA, Colón G. Photodeposition of gold on titanium dioxide for photocatalytic phenol oxidation. Appl. Catal., A 2011; 397: 112-120.
Hou WB, Liu ZW, Pavaskar P, Hung WH, Cronin SB. Plasmonic enhancement of photocatalytic decomposition of methyl orange under visible light. J. Catal. 2011; 277: 149-153.

Hsiao RC, Roselin LS, Hsu H-L, Selvin R, Juang RS. Photocatalytic degradation of reactive orange 16 dye over Au-doped TiO_2 in aqueous suspension. Int. J. Mater. Eng. Innov. 2011; 2: 96-108.

Huang B, Wang B, Ren D, Jin W, Liu JL, Peng JH*, et al.* Occurrence, removal and bioaccumulation of steroid estrogens in Dianchi Lake catchment, China. Environ. Int. 2013; 59: 262-273.

Ide Y, Ogino R, Sadakane M, Sano T. Effects of Au loading and CO_2 addition on photocatalytic selective phenol oxidation over TiO_2-supported Au nanoparticles. ChemCatChem 2013; 5: 766-773.

Ifelebuegu AO. The fate and behavior of selected endocrine disrupting chemicals in full scale wastewater and sludge treatment unit processes. Int. J. Environ. Sci. Technol. 2011; 8: 245-254.

Irmak S, Erbatur O, Akgerman A. Degradation of 17β-estradiol and bisphenol A in aqueous medium by using ozone and ozone/UV techniques. J. Hazard. Mater. 2005; 126: 54-62.

Ismail AA, Hakki A, Bahnemann DW. Mesostructure Au/TiO_2 nanocomposites for highly efficient catalytic reduction of *p*-nitrophenol. J. Mol. Catal. A: Chem. 2012; 358: 145-151.

Jain PK, Huang X, El-Sayed IH, El-Sayed MA. Noble metals on the nanoscale: optical and photothermal properties and some applications in imaging, sensing, biology, and medicine. Acc. Chem. Res. 2008; 41: 1578-1586.

Jiang J, Oberdörster G, Biswas P. Characterization of size, surface charge, and agglomeration state of nanoparticle dispersions for toxicological studies. J. Nanopart. Res. 2009; 11: 77-89.

Jiang JQ, Yin Q, Zhou JL, Pearce P. Occurrence and treatment trials of endocrine disrupting chemicals (EDCs) in wastewaters. Chemosphere 2005; 61: 544-550.

Johir M, Pradhan M, Loganathan P, Kandasamy J, Vigneswaran S. Phosphate adsorption from wastewater using zirconium (IV) hydroxide: Kinetics, thermodynamics and membrane filtration adsorption hybrid system studies. J. Environ. Manage. 2016; 167: 167-174.

Johnson AC, Sumpter JP. Removal of endocrine-disrupting chemicals in activated sludge treatment works. Environ. Sci. Technol. 2001; 35: 4697-4703.

Johnson I, Harvey P. Study on the scientific evaluation of 12 substances in the context of endocrine disrupter priority list of actions. European Comission 2002; 6052.

Jovic V, Smith KE, Idriss H, Waterhouse GIN. Heterojunction synergies in titania-supported gold photocatalysts: Implications for solar hydrogen production. ChemSusChem 2015; 8: 2551-2559.

Jürgens M, Williams R, Johnson A. Fate and behaviour of steroid oestrogens in rivers: A scoping study: Environment Agency, 1999.

Karpova T, Preis S, Kallas J. Selective photocatalytic oxidation of steroid estrogens in water treatment: urea as co-pollutant. J. Hazard. Mater. 2007; 146: 465-471.

Katz A, McDonagh A, Tijing L, Shon HK. Fouling and inactivation of titanium dioxide based photocatalytic systems. Crit. Rev. Env. Sci. Technol. 2015; 45: 1880-1915.

Khan MM, Kalathil S, Lee J, Cho MH. Enhancement in the photocatalytic activity of Au@TiO_2 nanocomposites by pretreatment of TiO_2 with UV light. Bull. Korean Chem. Soc. 2012; 33: 1753-1758.

Khanal SK, Xie B, Thompson ML, Sung S, Ong S-K, Van Leeuwen J. Fate, transport, and biodegradation of natural estrogens in the environment and engineered systems. Environ. Sci. Technol. 2006; 40: 6537-6546.

Kim Y, Joo H, Her N, Yoon Y, Sohn J, Kim S*, et al.* Simultaneously photocatalytic treatment of hexavalent chromium (Cr(VI)) and endocrine disrupting compounds (EDCs) using rotating reactor under solar irradiation. J. Hazard. Mater. 2015; 288: 124-133.

King SR, Massicot J, McDonagh AM. A straightforward route to tetrachloroauric acid from gold metal and molecular chlorine for nanoparticle synthesis. Metals 2015; 5: 1454-1461.

Klein S. Health risks from exposure to endocrine disruptors. New York: Nova Biomedical Books, 2012.

Koutantou V, Kostadima M, Chatzisymeon E, Frontistis Z, Binas V, Venieri D*, et al.* Solar photocatalytic decomposition of estrogens over immobilized zinc oxide. Catal. Today 2013; 209: 66-73.

Kowalska E, Abe R, Ohtani B. Visible light-induced photocatalytic reaction of gold-modified titanium(IV) oxide particles: action spectrum analysis. Chem. Commun. 2009: 241-243.

Kowalska E, Mahaney OOP, Abe R, Ohtani B. Visible-light-induced photocatalysis through surface plasmon excitation of gold on titania surfaces. Phys. Chem. Chem. Phys. 2010; 12: 2344-2355.

Kozlowska-Tylingo K, Namieśnik J, Górecki T. Determination of estrogenic endocrine disruptors in environmental samples-A review of chromatographic methods. Crit. Rev. Anal. Chem. 2010; 40: 194-201.

Laganà A, Bacaloni A, De Leva I, Faberi A, Fago G, Marino A. Analytical methodologies for determining the occurrence of endocrine disrupting chemicals in sewage treatment plants and natural waters. Anal. Chim. Acta 2004; 501: 79-88.

Lai KM, Johnson KL, Scrimshaw MD, Lester JN. Binding of waterborne steroid estrogens to solid phases in river and estuarine systems. Environ. Sci. Technol. 2000; 34: 3890-3894.

Lea J, Adesina AA. The photo-oxidative degradation of sodium dodecyl sulphate in aerated aqueous TiO_2 suspension. J. Photochem. Photobiol. A 1998; 118: 111-122.

Leech DM, Snyder MT, Wetzel RG. Natural organic matter and sunlight accelerate the degradation of 17β-estradiol in water. Sci. Total Environ. 2009; 407: 2087-2092.

Lei P, Wang F, Gao X, Ding Y, Zhang S, Zhao J*, et al.* Immobilization of TiO_2 nanoparticles in polymeric substrates by chemical bonding for multi-cycle photodegradation of organic pollutants. J. Hazard. Mater. 2012; 227: 185-194.

Leusch FD, De Jager C, Levi Y, Lim R, Puijker L, Sacher F*, et al.* Comparison of five *in vitro* bioassays to measure estrogenic activity in environmental waters. Environ. Sci. Technol. 2010; 44: 3853-3860.

Li HX, Bian ZF, Zhu J, Huo YN, Li H, Lu YF. Mesoporous Au/TiO_2 nanocomposites with enhanced photocatalytic activity. J. Am. Chem. Soc. 2007; 129: 4538-4539.

Li J, Mailhot G, Wu F, Deng NS. Photochemical efficiency of Fe(III)-EDDS complex: (OH)-O-center dot radical production and 17β-estradiol degradation. J. Photochem. Photobiol. A 2010; 212: 1-7.

Li QS, Gao NY, Deng Y, Ma XY, Chu WH. Factors affecting UV/H_2O_2 oxidation of 17α-ethynyestradiol in water. Clean. 2013; 41: 143-147.
Li S, Sun WL. Photocatalytic degradation of 17α-ethinylestradiol in mono- and binary systems of fulvic acid and Fe(III): Application of fluorescence excitation/emission matrixes. Chem. Eng. J. 2014; 237: 101-108.
Li WC, Comotti M, Schüth F. Highly reproducible syntheses of active Au/TiO_2 catalysts for CO oxidation by deposition-precipitation or impregnation. J. Catal. 2006; 237: 190-196.
Li XZ, Li FB. Study of Au/Au^{3+}-TiO_2 photocatalysts toward visible photooxidation for water and wastewater treatment. Environ. Sci. Technol. 2001; 35: 2381-2387.
Li Y, Wang YM, Liu LH, Wang DW, Zhang WL. Ag/ZnO hollow sphere composites: reusable photocatalyst for photocatalytic degradation of 17α-ethinylestradiol. Environ. Sci. Pollut. Res. 2014; 21: 5177-5186.
Lin AYC, Reinhard M. Photodegradation of common environmental pharmaceuticals and estrogens in river water. Environ. Toxicol. Chem. 2005; 24: 1303-1309.
Lin H, Valsaraj KT. Development of an optical fiber monolith reactor for photocatalytic wastewater treatment. J. Appl. Electrochem. 2005; 35: 699-708.
Lin L, Wang H, Luo H, Xu P. Enhanced photocatalysis using side-glowing optical fibers coated with Fe-doped TiO_2 nanocomposite thin films. J. Photochem. Photobiol. A 2015a; 307: 88-98.
Lin L, Wang H, Xu P. Immobilized TiO_2-reduced graphene oxide nanocomposites on optical fibers as high performance photocatalysts for degradation of pharmaceuticals. Chem. Eng. J. 2017; 310: 389-398.
Lin ZJ, Wang XH, Liu J, Tian ZY, Dai LC, He BB*, et al.* On the role of localized surface plasmon resonance in UV-Vis light irradiated Au/TiO_2 photocatalysis systems: pros and cons. Nanoscale 2015b; 7: 4114-4123.
Liu B, Liu XL. Direct photolysis of estrogens in aqueous solutions. Sci. Total Environ. 2004; 320: 269-274.
Liu B, Wu F, Deng NS. UV-light induced photodegradation of 17α-ethynylestradiol in aqueous solutions. J. Hazard. Mater. 2003a; 98: 311-316.
Liu S, Ying GG, Zhao JL, Chen F, Yang B, Zhou LJ*, et al.* Trace analysis of 28 steroids in surface water, wastewater and sludge samples by rapid resolution liquid chromatography-electrospray ionization tandem mass spectrometry. J. Chromatogr. A 2011; 1218: 1367-1378.
Liu XL, Wu F, Deng NS. Photo degradation of 17α-ethynylestradiol in aqueous solution exposed to a high-pressure mercury lamp (250 W). Environ. Pollut. 2003b; 126: 393-398.
Liu YS, Han J, Qiu W, Gao W. Hydrogen peroxide generation and photocatalytic degradation of estrone by microstructural controlled ZnO nanorod arrays. Appl. Surf. Sci. 2012a; 263: 389-396.
Liu YY, Li Y, Li WZ, Han S, Liu CJ. Photoelectrochemical properties and photocatalytic activity of nitrogen-doped nanoporous WO_3 photoelectrodes under visible light. Appl. Surf. Sci. 2012b; 258: 5038-5045.
Liu ZH, Lu GN, Yin H, Dang Z, Rittmann B. Removal of natural estrogens and their conjugates in municipal wastewater treatment plants: A critical review. Environ. Sci. Technol. 2015; 49: 5288-5300.
Lizama C, Yeber M, Freer J, Baeza J, Mansilla H. Reactive dyes decolouration by TiO_2 photo-assisted catalysis. Water Sci. Technol. 2001; 44: 197-203.

Lopez Fernandez R, Coleman HM, Le-Clech P. Impact of operating conditions on the removal of endocrine disrupting chemicals by membrane photocatalytic reactor. Environ. Technol. 2014; 35: 2068-74.

Luo S, Xiao Y, Yang L, Liu C, Su F, Li Y*, et al.* Simultaneous detoxification of hexavalent chromium and acid orange 7 by a novel Au/TiO_2 heterojunction composite nanotube arrays. Sep. Purif. Technol. 2011; 79: 85-91.

Luttrell T, Halpegamage S, Tao JG, Kramer A, Sutter E, Batzill M. Why is anatase a better photocatalyst than rutile? - Model studies on epitaxial TiO_2 films. Sci. Rep. 2014; 4: 1-8.

Macwan DP, Dave PN, Chaturvedi S. A review on nano-TiO_2 sol-gel type syntheses and its applications. J. Mater. Sci. 2011; 46: 3669-3686.

Mai JX, Sun WL, Xiong L, Liu Y, Ni JR. Titanium dioxide mediated photocatalytic degradation of 17β-estradiol in aqueous solution. Chemosphere 2008; 73: 600-606.

Marinangeli RE, Ollis DF. Photoassisted heterogeneous catalysis with optical fibers: I. Isolated single fiber. AIChE J. 1977; 23: 415-426.

Marschall R, Wang LZ. Non-metal doping of transition metal oxides for visible-light photocatalysis. Catal. Today 2014; 225: 111-135.

Matamoros V, Duhec A, Albaigés J, Bayona JM. Photodegradation of carbamazepine, ibuprofen, ketoprofen and 17α-ethinylestradiol in fresh and seawater. Water. Air. Soil. Pollut. 2009; 196: 161-168.

Mazellier P, Méité L, De Laat J. Photodegradation of the steroid hormones 17β-estradiol (E2) and 17α-ethinylestradiol (EE2) in dilute aqueous solution. Chemosphere 2008; 73: 1216-1223.

Mboula VM, Héquet V, Andrés Y, Gru Y, Colin R, Doña-Rodríguez JM*, et al.* Photocatalytic degradation of estradiol under simulated solar light and assessment of estrogenic activity. Appl. Catal., B 2015; 162: 437-444.

McLachlan JA. Environmental signaling: What embryos and evolution teach us about endocrine disrupting chemicals. Endocr. Rev. 2001; 22: 319-341.

Min BK, Heo JE, Youn NK, Joo OS, Lee H, Kim JH*, et al.* Tuning of the photocatalytic 1,4-dioxane degradation with surface plasmon resonance of gold nanoparticles on titania. Catal. Commun. 2009; 10: 712-715.

Mizuguchi T, Sadaka S, Ogasawara C, Shimada K. Determination of the effect of hydrogen peroxide on photocatalytic degradation of estrogen using HPLC. J. Liq. Chromatogr. Relat. Technol. 2006; 29: 903-911.

Mrowetz M, Villa A, Prati L, Selli E. Effects of Au nanoparticles on TiO_2 in the photocatalytic degradation of an azo dye. Gold. Bull. 2007; 40: 154-160.

Murugananthan M, Yoshihara S, Rakuma T, Uehara N, Shirakashi T. Electrochemical degradation of 17β-estradiol (E2) at boron-doped diamond (Si/BDD) thin film electrode. Electrochim. Acta 2007; 52: 3242-3249.

Nafria R, de la Piscina PR, Homs N, Morante JR, Cabot A, Diaz U*, et al.* Embedding catalytic nanoparticles inside mesoporous structures with controlled porosity: Au@TiO_2. J. Mater. Chem. A 2013; 1: 14170-14176.

Nakashima T, Ohko Y, Kubota Y, Fujishima A. Photocatalytic decomposition of estrogens in aquatic environment by reciprocating immersion of TiO_2-modified polytetrafluoroethylene mesh sheets. J. Photochem. Photobiol. A 2003; 160: 115-120.

Nakashima T, Ohko Y, Tryk DA, Fujishima A. Decomposition of endocrine-disrupting chemicals in water by use of TiO_2 photocatalysts immobilized on

polytetrafluoroethylene mesh sheets. J. Photochem. Photobiol. A 2002; 151: 207-212.
Nakata K, Fujishima A. TiO_2 photocatalysis: Design and applications. J. Photochem. Photobiol. C. 2012; 13: 169-189.
Nasuhoglu D, Berk D, Yargeau V. Photocatalytic removal of 17α-ethinylestradiol (EE2) and levonorgestrel (LNG) from contraceptive pill manufacturing plant wastewater under UVC radiation. Chem. Eng. J. 2012; 185: 52-60.
Nguyen LQ, Salim C, Hinode H. Performance of nano-sized Au/TiO_2 for selective catalytic reduction of NO_x by propene. Appl. Catal., A 2008; 347: 94-99.
Niu MT, Huang F, Cui LF, Huang P, Yu YL, Wang YS. Hydrothermal synthesis, structural characteristics, and enhanced photocatalysis of SnO_2/α-Fe_2O_3 semiconductor nanoheterostructures. ACS Nano 2010; 4: 681-688.
Ohko Y, Iuchi KI, Niwa C, Tatsuma T, Nakashima T, Iguchi T*, et al.* 17β-estrodial degradation by TiO_2 photocatalysis as means of reducing estrogenic activity. Environ. Sci. Technol. 2002; 36: 4175-4181.
Ohsaka T, Izumi F, Fujiki Y. Raman spectrum of anatase, TiO_2. J. Raman Spectrosc. 1978; 7: 321-324.
Ohtani B. Photocatalysis A to Z-What we know and what we do not know in a scientific sense. J. Photochem. Photobiol. C. 2010; 11: 157-178.
Okumura M, Tanaka K, Ueda A, Haruta M. The reactivities of dimethylgold(III)β-diketone on the surface of TiO_2 - A novel preparation method for Au catalysts. Solid State Ion. 1997; 95: 143-149.
Oliveira HG, Ferreira LH, Bertazzoli R, Longo C. Remediation of 17α-ethinylestradiol aqueous solution by photocatalysis and electrochemically-assisted photocatalysis using TiO_2 and TiO_2/WO_3 electrodes irradiated by a solar simulator. Water Res. 2015; 72: 305-314.
Oller I, Malato S, Sánchez-Pérez JA. Combination of advanced oxidation processes and biological treatments for wastewater decontamination-A review. Sci. Total Environ. 2011; 409: 4141-4166.
Onda K, Nakamura Y, Takatoh C, Miya A, Katsu Y. The behavior of estrogenic substances in the biological treatment process of sewage. Water Sci. Technol. 2003; 47: 109-116.
Orlov A, Chan MS, Jefferson DA, Zhou D, Lynch RJ, Lambert RM. Photocatalytic degradation of water-soluble organic pollutants on TiO_2 modified with gold nanoparticles. Environ. Technol. 2006; 27: 747-752.
Orlov A, Jefferson DA, Macleod N, Lambert RM. Photocatalytic properties of TiO_2 modified with gold nanoparticles in the degradation of 4-chlorophenol in aqueous solution. Catal. Lett. 2004; 92: 41-47.
Orlov A, Jefferson DA, Tikhov M, Lambert RM. Enhancement of MTBE photocatalytic degradation by modification of TiO_2 with gold nanoparticles. Catal. Commun. 2007; 8: 821-824.
Oros-Ruiz S, Gomez R, Lopez R, Hernandez-Gordillo A, Pedraza-Avella JA, Moctezuma E*, et al.* Photocatalytic reduction of methyl orange on Au/TiO_2 semiconductors. Catal. Commun. 2012; 21: 72-76.
Oros-Ruiz S, Pedraza-Avella JA, Guzman C, Quintana M, Moctezuma E, del Angel G*, et al.* Effect of gold particle size and deposition method on the photodegradation of 4-chlorophenol by Au/TiO_2. Top. Catal. 2011; 54: 519-526.

Oros-Ruiz S, Zanella R, López R, Hernández-Gordillo A, Gómez R. Photocatalytic hydrogen production by water/methanol decomposition using Au/TiO_2 prepared by deposition–precipitation with urea. J. Hazard. Mater. 2013; 263: 2-10.

Pan Z, Stemmler EA, Cho HJ, Fan W, LeBlanc LA, Patterson HH*, et al.* Photocatalytic degradation of 17α-ethinylestradiol (EE2) in the presence of TiO_2-doped zeolite. J. Hazard. Mater. 2014; 279: 17-25.

Pany S, Naik B, Martha S, Parida K. Plasmon induced nano Au particle decorated over S,N-modified TiO_2 for exceptional photocatalytic hydrogen evolution under visible light. ACS Appl. Mater. Interfaces 2014; 6: 839-846.

Paramasivam I, Macak JM, Schmuki P. Photocatalytic activity of TiO_2-nanotube layers loaded with Ag and Au nanoparticles. Electrochem. Commun. 2008; 10: 71-75.

Peill NJ, Hoffmann MR. Chemical and physical characterization of a TiO_2-coated fiber optic cable reactor. Environ. Sci. Technol. 1996; 30: 2806-2812.

Pešoutová R, Stříteský L, Hlavínek P. A pilot scale comparison of advanced oxidation processes for estrogenic hormone removal from municipal wastewater effluent. Water Sci. Technol. 2014; 70: 70-75.

Priebe JB, Radnik J, Lennox AJJ, Pohl M-M, Karnahl M, Hollmann D*, et al.* Solar hydrogen production by plasmonic Au–TiO_2 catalysts: Impact of synthesis protocol and TiO_2 phase on charge transfer efficiency and H_2 evolution rates. ACS Catal. 2015; 5: 2137-2148.

Primo A, Corma A, García H. Titania supported gold nanoparticles as photocatalyst. Phys. Chem. Chem. Phys. 2011; 13: 886-910.

Puma GL, Puddu V, Tsang HK, Gora A, Toepfer B. Photocatalytic oxidation of multicomponent mixtures of estrogens (estrone (El), 17β-estradiol (E2), 17α-ethynylestradiol (EE2) and estriol (E3)) under UVA and UVC radiation: Photon absorption, quantum yields and rate constants independent of photon absorption. Appl. Catal., B 2010; 99: 388-397.

Qiang ZM, Nie YF, Ben WW, Qu JH, Zhang HQ. Degradation of endocrine-disrupting chemicals during activated sludge reduction by ozone. Chemosphere 2013; 91: 366-373.

Ribeiro AR, Nunes OC, Pereira MFR, Silva AMT. An overview on the advanced oxidation processes applied for the treatment of water pollutants defined in the recently launched Directive 2013/39/EU. Environ. Int. 2015; 75: 33-51.

Rincón AG, Pulgarin C. Effect of pH, inorganic ions, organic matter and H_2O_2 on E. *coli* K12 photocatalytic inactivation by TiO_2 - Implications in solar water disinfection. Appl. Catal., B 2004; 51: 283-302.

Roig B, Mnif W, Hassine AIH, Zidi I, Bayle S, Bartegi A*, et al.* Endocrine disrupting chemicals and human health risk assessment: A critical review. Crit. Rev. Environ. Sci. Technol. 2013; 43: 2297-2351.

Rosenfeldt EJ, Chen PJ, Kullman S, Linden KG. Destruction of estrogenic activity in water using UV advanced oxidation. Sci. Total Environ. 2007; 377: 105-113.

Rosenfeldt EJ, Linden KG. Degradation of endocrine disrupting chemicals bisphenol A, ethinyl estradiol, and estradiol during UV photolysis and advanced oxidation processes. Environ. Sci. Technol. 2004; 38: 5476-5483.

Rupa AV, Divakar D, Sivakumar T. Titania and noble metals deposited titania catalysts in the photodegradation of tartazine. Catal. Lett. 2009; 132: 259-267.

Rutishauser BV, Pesonen M, Escher BI, Ackermann GE, Aerni HR, Suter MJF*, et al.* Comparative analysis of estrogenic activity in sewage treatment plant effluents involving three in vitro assays and chemical analysis of steroids. Environ. Toxicol. Chem. 2004; 23: 857-864.

Sathishkumar P, Sivakumar R, Anandan S, Madhavan J, Maruthamuthu P, Ashokkumar M. Photocatalytic degradation of Acid Red 88 using Au-TiO_2 nanoparticles in aqueous solutions. Water Res. 2008; 42: 4878-4884.

Schneider J, Matsuoka M, Takeuchi M, Zhang JL, Horiuchi Y, Anpo M*, et al.* Understanding TiO_2 photocatalysis: Mechanisms and materials. Chem. Rev. 2014; 114: 9919-9986.

Scott PD, Bartkow M, Blockwell SJ, Coleman HM, Khan SJ, Lim R*, et al.* An assessment of endocrine activity in Australian rivers using chemical and in vitro analyses. Environ. Sci. Pollut. Res. 2014; 21: 12951-12967.

Serra M, Albero J, García H. Photocatalytic activity of Au/TiO_2 photocatalysts for H_2 evolution: Role of the Au nanoparticles as a function of the irradiation wavelength. Chemphyschem 2015; 16: 1842-1845.

Shan AY, Ghazi TIM, Rashid SA. Immobilisation of titanium dioxide onto supporting materials in heterogeneous photocatalysis: A review. Appl. Catal., A 2010; 389: 1-8.

Sharma M, Jain T, Singh S, Pandey OP. Photocatalytic degradation of organic dyes under UV-Visible light using capped ZnS nanoparticles. Sol. Energy 2012; 86: 626-633.

Silva CG, Juárez R, Marino T, Molinari R, García H. Influence of excitation wavelength (UV or visible light) on the photocatalytic activity of titania containing gold nanoparticles for the generation of hydrogen or oxygen from water. J. Am. Chem. Soc. 2011; 133: 595-602.

Silva CP, Lima DLD, Groth MB, Otero M, Esteves VI. Effect of natural aquatic humic substances on the photodegradation of estrone. Chemosphere 2016; 145: 249-255.

Snyder SA, Westerhoff P, Yoon Y, Sedlak DL. Pharmaceuticals, personal care products, and endocrine disruptors in water: Implications for the water industry. Environ. Eng. Sci. 2003; 20: 449-469.

So CM, Cheng MY, Yu JC, Wong PK. Degradation of azo dye Procion Red MX-5B by photocatalytic oxidation. Chemosphere 2002; 46: 905-912.

Sonawane RS, Dongare MK. Sol-gel synthesis of Au/TiO_2 thin films for photocatalytic degradation of phenol in sunlight. J. Mol. Catal. A. 2006; 243: 68-76.

Sornalingam K, McDonagh A, Zhou JL. Photodegradation of estrogenic endocrine disrupting steroidal hormones in aqueous systems: Progress and future challenges. Sci. Total Environ. 2016; 550: 209-224.

Sornalingam K, McDonagh A, Zhou JL, Johir MAH, Ahmed MB. Photocatalysis of estrone in water and wastewater: Comparison between Au-TiO_2 nanocomposite and TiO_2, and degradation by-products. Sci. Total Environ. 2018; 610: 521-530.

Su R, Tiruvalam R, He Q, Dimitratos N, Kesavan L, Hammond C*, et al.* Promotion of Phenol Photodecomposition over TiO_2 Using Au, Pd, and Au-Pd Nanoparticles. ACS Nano 2012; 6: 6284-6292.

Su WG, Zhang J, Feng ZC, Chen T, Ying PL, Li C. Surface phases of TiO_2 nanoparticles studied by UV Raman spectroscopy and FT-IR spectroscopy. J. Phys. Chem. C 2008; 112: 7710-7716.

Subash B, Krishnakumar B, Swaminathan M, Shanthi M. Highly efficient, solar active, and reusable photocatalyst: Zr-loaded Ag-ZnO for reactive red 120 dye degradation with synergistic effect and dye-sensitized mechanism. Langmuir 2013; 29: 939-949.

Sun R-D, Nakajima A, Watanabe I, Watanabe T, Hashimoto K. TiO_2-coated optical fiber bundles used as a photocatalytic filter for decomposition of gaseous organic compounds. J. Photochem. Photobiol. A 2000; 136: 111-116.

Sun WL, Li S, Mai JX, Ni JR. Initial photocatalytic degradation intermediates/pathways of 17α-ethynylestradiol: Effect of pH and methanol. Chemosphere 2010; 81: 92-99.

Suri RPS, Nayak M, Devaiah U, Helmig E. Ultrasound assisted destruction of estrogen hormones in aqueous solution: Effect of power density, power intensity and reactor configuration. J. Hazard. Mater. 2007; 146: 472-478.

Suttiponparnit K, Jiang J, Sahu M, Suvachittanont S, Charinpanitkul T, Biswas P. Role of surface area, primary particle size, and crystal phase on titanium dioxide nanoparticle dispersion properties. Nanoscale Res. Lett. 2011; 6: 27.

Tan TH, Scott J, Ng YH, Taylor RA, Aguey-Zinsou KF, Amal R. Understanding plasmon and band gap photoexcitation effects on the thermal-catalytic oxidation of ethanol by TiO_2-supported gold. ACS Catal. 2016; 6: 1870-1879.

Tanaka A, Sakaguchi S, Hashimoto K, Kominami H. Preparation of Au/TiO_2 with metal cocatalysts exhibiting strong surface plasmon resonance effective for photoinduced hydrogen formation under irradiation of visible light. ACS Catal. 2012; 3: 79-85.

Tanizaki T, Kadokami K, Shinohara R. Catalytic photodegradation of endocrine disrupting chemicals using titanium dioxide photosemiconductor thin films. Bull. Environ. Contam. Toxicol. 2002; 68: 732-739.

Tasbihi M, Ngah CR, Aziz N, Mansor A, Abdullah AZ, Teong LK*, et al.* Lifetime and regeneration studies of various supported TiO_2 photocatalysts for the degradation of phenol under UV-C light in a batch reactor. Ind. Eng. Chem. Res. 2007; 46: 9006-9014.

Tellez AA, Masson R, Robert D, Keller N, Keller V. Comparison of Hombikat UV100 and P25 TiO_2 performance in gas-phase photocatalytic oxidation reactions. J. Photochem. Photobiol. A 2012; 250: 58-65.

Thomas J, Yoon M. Facile synthesis of pure TiO_2(B) nanofibers doped with gold nanoparticles and solar photocatalytic activities. Appl. Catal., B 2012; 111: 502-508.

Tian B, Li C, Gu F, Jiang H. Synergetic effects of nitrogen doping and Au loading on enhancing the visible-light photocatalytic activity of nano-TiO_2. Catal. Commun. 2009; 10: 925-929.

Tian B, Zhang J, Tong T, Chen F. Preparation of Au/TiO_2 catalysts from Au(I)-thiosulfate complex and study of their photocatalytic activity for the degradation of methyl orange. Appl. Catal., B 2008; 79: 394-401.

Torres-Martínez CL, Kho R, Mian OI, Mehra RK. Efficient photocatalytic degradation of environmental pollutants with mass-produced ZnS nanocrystals. J. Colloid Interface Sci. 2001; 240: 525-532.

Trudeau VL, Heyne B, Blais JM, Temussi F, Atkinson SK, Pakdel F*, et al.* Lumiestrone is photochemically derived from estrone and may be released to the environment without detection. Front. Endocrinol. 2011; 2: 83.

Uraipong C, Allan RD, Li C, Kennedy IR, Wong V, Lee NA. A survey of 17α-ethinylestradiol and mestranol residues in Hawkesbury River, Australia, using a highly specific enzyme-linked immunosorbent assay (ELISA) demonstrates the levels of potential biological significance. Ecotoxicol. Environ. Saf. 2017; 144: 585-592.

Valenzuela MA, Bosch P, Jiménez-Becerrill J, Quiroz O, Páez AI. Preparation, characterization and photocatalytic activity of ZnO, Fe_2O_3 and $ZnFe_2O_4$. J. Photochem. Photobiol. A 2002; 148: 177-182.

Verma A, Prakash N, Toor A. An efficient TiO_2 coated immobilized system for the degradation studies of herbicide isoproturon: Durability studies. Chemosphere 2014; 109: 7-13.

Wang H, Faria JL, Dong S, Chang Y. Mesoporous Au/TiO_2 composites preparation, characterization, and photocatalytic properties. Mater. Sci. Eng., B 2012; 177: 913-919.

Wang JL, Xu LJ. Advanced oxidation processes for wastewater treatment: Formation of hydroxyl radical and application. Crit. Rev. Environ. Sci. Technol. 2012; 42: 251-325.

Wang LZ, Zhang FF, Liu RH, Zhang TY, Xue XY, Xu Q*, et al.* $FeCl_3$/$NaNO_2$: An efficient photocatalyst for the degradation of aquatic steroid estrogens under natural light irradiation. Environ. Sci. Technol. 2007; 41: 3747-3751.

Wang S, Xu Z, Fang G, Zhang Y, He J. Separation and determination of estrone in environmental and drinking water using molecularly imprinted solid phase extraction coupled with HPLC. J. Sep. Sci. 2008a; 31: 1181-1188.

Wang X, Mitchell DRG, Prince K, Atanacio AJ, Caruso RA. Gold nanoparticle incorporation into porous titania networks using an agarose gel templating technique for photocatalytic applications. Chem. Mater. 2008b; 20: 3917-3926.

Westerhoff P, Yoon Y, Snyder S, Wert E. Fate of endocrine-disruptor, pharmaceutical, and personal care product chemicals during simulated drinking water treatment processes. Environ. Sci. Technol. 2005; 39: 6649-6663.

Whidbey CM, Daumit KE, Nguyen TH, Ashworth DD, Davis JCC, Latch DE. Photochemical induced changes of *in vitro* estrogenic activity of steroid hormones. Water Res. 2012; 46: 5287-5296.

Windeler RS, Wagener JL, Digiovanni DJ. Silica-air microstructured fibers: Properties and applications. Optical Fiber Communication Conference, 1999, and the International Conference on Integrated Optics and Optical Fiber Communication. OFC/IOOC'99. Technical Digest. 4. IEEE, 1999, pp. 106-107.

Wolf A, Schüth F. A systematic study of the synthesis conditions for the preparation of highly active gold catalysts. Appl. Catal., A 2002; 226: 1-13.

Wongwisate P, Chavadej S, Gulari E, Sreethawong T, Rangsunvigit P. Effects of monometallic and bimetallic Au-Ag supported on sol-gel TiO_2 on photocatalytic degradation of 4-chlorophenol and its intermediates. Desalination 2011; 272: 154-163.

Wu DJ, Xu XD, Liu XJ. Electric field enhancement in bimetallic gold and silver nanoshells. Solid State Commun. 2008; 148: 163-167.

Wu SS, Cao HQ, Yin SF, Liu XW, Zhang XR. Amino acid-assisted hydrothermal synthesis and photocatalysis of SnO_2 nanocrystals. J. Phys. Chem. C 2009a; 113: 17893-17898.

Wu Y, Zhang J, Xiao L, Chen F. Preparation and characterization of TiO_2 photocatalysts by Fe^{3+} doping together with Au deposition for the degradation of organic pollutants. Appl. Catal., B 2009b; 88: 525-532.

Wu YM, Liu HB, Zhang JL, Chen F. Enhanced photocatalytic activity of nitrogen-doped titania by deposited with gold. J. Phys. Chem. C 2009c; 113: 14689-14695.

Xu H, Ouyang SX, Liu LQ, Reunchan P, Umezawa N, Ye JH. Recent advances in TiO_2-based photocatalysis. J. Mater. Chem. A 2014a; 2: 12642-12661.

Xu J, Ao Y, Fu D, Lin Y, Shen X, Yuan C*, et al.* Photocatalytic activity on TiO_2-coated side-glowing optical fiber reactor under solar light. J. Photochem. Photobiol. A 2008; 199: 165-169.

Xu SF, Lu HZ, Chen LX, Wang XC. Molecularly imprinted TiO_2 hybridized magnetic Fe_3O_4 nanoparticles for selective photocatalytic degradation and removal of estrone. RSC Adv. 2014b; 4: 45266-45274.

Yan JQ, Wu GJ, Guan NJ, Li LD. Synergetic promotion of the photocatalytic activity of TiO_2 by gold deposition under UV-visible light irradiation. Chem. Commun. 2013; 49: 11767-11769.

Ying GG, Kookana RS, Waite TD. Endocrine Disrupting Chemicals (EDCs) and Pharmaceuticals and Personal Care Products (PPCPs) in Reclaimed Water in Australia: Australian Water Conservation and Reuse Research Program, 2004.

Zainal Z, Hui LK, Hussein MZ, Taufiq-Yap YH, Abdullah AH, Ramli I. Removal of dyes using immobilized titanium dioxide illuminated by fluorescent lamps. J. Hazard. Mater. 2005; 125: 113-120.

Zanella R, Giorgio S, Henry CR, Louis C. Alternative methods for the preparation of gold nanoparticles supported on TiO_2. J. Phys. Chem. B 2002; 106: 7634-7642.

Zhang A, Li YM. Removal of phenolic endocrine disrupting compounds from waste activated sludge using UV, H_2O_2, and UV/H_2O_2 oxidation processes: Effects of reaction conditions and sludge matrix. Sci. Total Environ. 2014; 493: 307-323.

Zhang LW, Zhu YF. A review of controllable synthesis and enhancement of performances of bismuth tungstate visible-light-driven photocatalysts. Catal. Sci. Technol. 2012; 2: 694-706.

Zhang QH, Yu WW, Wang HZ. One-pot synthesis of Au supported titania composite photocatalyst and its photocatalytic activities for dye degradation. In: Ren N, Che LK, Jin B, Dong R, Su H, editors. Renewable and Sustainable Energy. 512-515. Trans Tech Publications Ltd, Stafa-Zurich, 2012a, pp. 2080-2083.

Zhang WL, Li Y, Su YL, Mao K, Wang Q. Effect of water composition on TiO_2 photocatalytic removal of endocrine disrupting compounds (EDCs) and estrogenic activity from secondary effluent. J. Hazard. Mater. 2012b; 215: 252-258.

Zhang WL, Li Y, Wu QY, Hu HY. Removal of endocrine-disrupting compounds, estrogenic activity, and escherichia coliform from secondary effluents in a TiO_2-coated photocatalytic reactor. Environ. Eng. Sci. 2012c; 29: 195-201.

Zhang Y, Zhou JL, Ning B. Photodegradation of estrone and 17β-estradiol in water. Water Res. 2007; 41: 19-26.

Zhang YC, Du ZN, Li KW, Zhang M, Dionysiou DD. High-performance visible-light-driven SnS_2/SnO_2 nanocomposite photocatalyst prepared via in situ hydrothermal oxidation of SnS_2 nanoparticles. ACS Appl. Mater. Interfaces 2011a; 3: 1528-1537.

Zhang YP, Zhou JL. Occurrence and removal of endocrine disrupting chemicals in wastewater. Chemosphere 2008; 73: 848-853.

Zhang ZH, Feng YJ, Gao P, Wang C, Ren NQ. Occurrence and removal efficiencies of eight EDCs and estrogenicity in a STP. J. Environ. Monit. 2011b; 13: 1366-1373.

Zhang ZH, Feng YJ, Liu Y, Sun QF, Gao P, Ren NQ. Kinetic degradation model and estrogenicity changes of EE2 (17α-ethinylestradiol) in aqueous solution by UV and UV/H_2O_2 technology. J. Hazard. Mater. 2010; 181: 1127-1133.

Zhao H, Chen S, Quan X, Yu H, Zhao H. Integration of microfiltration and visible-light-driven photocatalysis on g-C_3N_4 nanosheet/reduced graphene oxide membrane for enhanced water treatment. Appl. Catal., B 2016; 194: 134-140.

Zhao L, Sun Z, Ma J. Novel relationship between hydroxyl radical initiation and surface group of ceramic honeycomb supported metals for the catalytic ozonation of nitrobenzene in aqueous solution. Environ. Sci. Technol. 2009a; 43: 4157-4163.

Zhao Q, Li M, Chu J, Jiang T, Yin H. Preparation, characterization of Au (or Pt)-loaded titania nanotubes and their photocatalytic activities for degradation of methyl orange. Appl. Surf. Sci. 2009b; 255: 3773-3778.

Zhao S, Ramakrishnan G, Su D, Rieger R, Koller A, Orlov A. Novel photocatalytic applications of sub-nanometer gold particles for environmental liquid and gas phase reactions. Appl. Catal., B 2011; 104: 239-244.

Zhao YP, Hu HY. Photo-Fenton degradation of 17β-estradiol in presence of α-FeOOHR and H_2O_2. Appl. Catal., B 2008; 78: 250-258.

Zhu H, Chen X, Zheng Z, Ke X, Jaatinen E, Zhao J*, et al.* Mechanism of supported gold nanoparticles as photocatalysts under ultraviolet and visible light irradiation. Chem. Commun. 2009: 7524-7526.

Zhu SY, Liang SJ, Gu Q, Xie LY, Wang JX, Ding ZX*, et al.* Effect of Au supported TiO_2 with dominant exposed {001} facets on the visible-light photocatalytic activity. Appl. Catal., B 2012; 119: 146-155.

Zuo YG, Zhang K, Deng YW. Occurrence and photochemical degradation of 17α-ethinylestradiol in Acushnet River Estuary. Chemosphere 2006; 63: 1583-1590.

Zuo YG, Zhang K, Zhou S. Determination of estrogenic steroids and microbial and photochemical degradation of 17α-ethinylestradiol (EE2) in lake surface water, a case study. Environ. Sci.: Processes Impacts 2013; 15: 1529-1535.